A Polytopal Element Framework for Improved Solution Accuracy and Robustness

By

Brian Doran Giffin
B.S. (University of California, Davis) 2013
M.S. (University of California, Davis) 2014

Dissertation

Submitted in partial satisfaction of the requirements for the degree of

Doctor of Philosophy

in

Civil and Environmental Engineering

in the

Office of Graduate Studies

of the

University of California

Davis

Approved:

Mark M. Rashid, Chair

N. Sukumar

Boris Jeremić

Committee in Charge

2017

To Lyle . . .

for teaching me how to think deeply, to analyze new information objectively, and to appreciate the complexity and nuanced beauty in all things.

And to Nancy . . .

for inspiring me to explore my creativity, for giving me canvases to paint on, and the confidence to paint, without fear of failure.

Contents

List of Figures v
List of Tables vii
Abstract viii
Acknowledgments ix

1 Introduction **1**
1.1 Historical Development 1
1.2 Recent Developments in Polytopal Discretizations 8
1.3 Scope of the Present Work 13

2 An Overview of Computational Solid Mechanics **15**
2.1 The Lagrangian Description of Motion 16
2.2 Conservation of Linear and Angular Momentum 18
2.3 Constitutive Relations 20
2.4 Model Boundary Value Problem 22
2.5 Galerkin Approximations to the Weak Form 25
2.6 Requirements for Convergence of an Approximation Method 28

3 Partitioned Element Methods **33**
3.1 Overview 33
3.2 Definition of Polytopal Element Shape Functions 34
3.3 Shape Function Approximation Methods 37
3.4 Piecewise Polynomial Approximations to Generalized Harmonic Shape Functions 42
3.5 Partition-Based Quadrature Rules 49

4 An Implementational Framework for the DG-PEM **56**

4.1 Arbitrary Polytopal Meshes 56
4.2 Element Partitioning Schemes 61
4.3 Abstract Geometric Data Structures 63
4.4 Partition-Based Approximation Spaces 66
4.5 Linearization and Assembly of the
DG-PEM Systems of Equations 68
4.6 Numerical Conditioning of the
DG-PEM Systems of Equations 72
4.6.1 The Effect of Element Scaling 80
4.6.2 On the Choice of an Appropriate PEM Basis 80

5 A Numerical Evaluation of the PEM **81**
5.1 Convergence Analysis 81
5.2 Parameter Sensitivity Analysis 86
5.3 Computational Efficiency 86
5.3.1 Performance Comparison 86
5.4 Resistance to Locking Phenomena 86

6 Conclusions and Future Work **90**

List of Figures

2.1 A depiction of the motion of material points in a body Ω. 16

3.1 A representative polyhedral element $\Omega \subset \mathbb{R}^3$, a polygonal face $F \subset \partial\Omega$, a linear edge $E \subset \partial F$, and a node V. 35

3.2 The harmonic shape function corresponding to the indicated node V, defined hierarchially on each edge, face, and the element. 36

3.3 A representative polyhedral element $\Omega \subset \mathbb{R}^3$, and it's corresponding partition into cells, facets, segments, and verticies. 42

3.4 Polygonal element partitioning schemes, from left to right: edge-based partition, node-based partition, random voronoi partition. 44

3.5 The FE-PEM approximation to a given harmonic shape function, defined hierarchially on the element's faces and edges. 45

4.1 Canonical node numbering schemes for a linear tetrahedral element (left) and a linear hexahedral element (right). Each of these standard orderings induce corresponding nodal orderings for each triangular or quadrilateral face of the element, as well. 57

4.2 Illustration of the data necessary to describe an arbitrary polyhedral element Ω_e. The local node ID ordering for the face F_1 shown would be $\{n_i\}_{i=1}^{5} = \{14, 1, 9, 8, 13\}$. 58

4.3 Illustration of the data necessary to describe a quadratic serendipity polyhedral element Ω_e. The local node ID ordering for the face F_1 shown would be $\{n_i\}_{i=1}^{10} = \{14, 34, 1, 18, 9, 26, 8, 32, 13, 33\}$. 59

4.4 The resulting segment, facet, and cell decomposition for the proposed edge-based partitioning algorithm. 63

4.5 The resulting segment, facet, and cell decomposition for the proposed edge-based partitioning algorithm, applied to a quadratic serendipity polyhedral element. 63

4.6 A representative entity tree diagram for a 2-dimensional facet σ and its children. 64
4.7 A representative 2-dimensional sub-element $F \subset \partial\Omega$ (a polygonal face), and its corresponding sub-element tree diagram. The partition of F consists of polygonal facets $\sigma_i \in \mathcal{T}_\sigma(F)\ \forall i = 1, \ldots, 5$. 66

5.1 Infinite plate with a circular hole placed in uniaxial tension. 81
5.2 Quadrilateral meshes with varying levels of refinement. 82
5.3 L^2 error convergence plots for (a) FEM and (b) PEM formulations. . . . 85
5.4 H^1 error convergence plots for (a) FEM and (b) PEM formulations. . . . 86

List of Tables

5.1 Computed L^2 displacement error norms. 84
5.2 Computed L^2 displacement error norm convergence rates. 84
5.3 Computed H^1 energy error semi-norms. 84
5.4 Computed H^1 energy error semi-norm convergence rates. 85

Abstract

A Polytopal Element Framework for
Improved Solution Accuracy and Robustness

A high-level discussion of the fundamental problems accompanying finite element discretizations in the form of locking, addressing the scope of the work under consideration.

Acknowledgments

Many thanks to the following: Professor Amit Kanvinde who inspired much of my initial motivation for applying to graduate school; Professor N. Sukumar for exposing me to the realm of computational solid mechanics; Dr. Joseph Bishop at Sandia for being involved in my early (and continuing) development in the field of solid mechanics; Professor Mark Rashid who turned my spark of interest in the subject into a roaring fire of passion; Dr. Steven Wopschall and Mr. Omar Hafez for being my mentoring older brothers throughout my journey in graduate school; Mr. Subhajit Banerjee and Mr. Eric Chin whose fruitful discussions assisted greatly in developing a personal sense of calm and confidence prior to my qualifying examination; Professor Yannis Dafalias, Professor John Bolander, and Professor Elbridge Puckett, whose enthusiasm as lecturers and courtesy as QE examiners were indespensible; Dr. Joseph Jung, Dr. Kendall Pearson, Dr. Nathan Crane, Mr. Mark Merewether, Dr. Michael Tupek, and the whole of the Sierra Solid Mechanics Team at Sandia who introduced me to the fascinations of code development; Ms. Carly Arthur, Mr. Sam Mish, and Ms. Aimée Sylvia whose conversations as fellow class-mates and advisees were incredibly helpful and insightful; and foremost to Ms. Maha Kenawy, who has served as my primary role-model and source of inspiration for completing this thesis – I love you.

Chapter 1

Introduction

For decades, finite element methods (FEM) have been widely used by engineers and physicists in the modeling of solid continua, and numerous extensions of the method have been developed to model more complex physical processes, including nonlinear kinematic and material behavior. In spite of these advances, traditional finite element methods have been plagued by recurrent issues of numerical accuracy pertaining to locking and poor mesh quality. Various strategies have been proposed to overcome some of these issues, though few have been able to address the underlying problem of element distorsion sensitivity.

This thesis presents a novel polytopal element framework in an effort to address the aforementioned issues as a whole. The use of arbitrary polygonal and polyhedral shapes in place of canonical element shapes seeks to resolve the issue of distorsion sensitivity directly, obviating issues of meshing and mesh quality, while maintaining many of the desirable features of the FEM and its extensions.

1.1 Historical Development

According to [22], finite element methods originated in the 1950s to address engineering challenges in the design of aircraft. The method was subsequently given a more rigorous mathematical treatment by early contributors (Irons, Melosh, Strang), and its usage permeated to other fields of study (namely, structural engineering). Following the advent of the isoparametric element concept, displacement-based finite element formulations gained

widespread popularity, though most early applications considered only linear kinematic and material behavior. Subsequently, advanced solution methodologies were developed to accomodate various sources of nonlinearity, including finite deformations, nonlinear constitutive behavior, and contact.

Over half a century after its initial development, the finite element method is still widely used, and recognized as the industry standard technology for modeling complicated structural and dynamic systems. It's reigning popularity can be attributed to several desirable features of the method:

- The compact support property of the isoparametric basis functions helps to facilitate more efficient solution methodologies.

- The kronecker delta property and precise description of mesh boundaries allow for a relatively straightforward application of boundary conditions and contact constraints.

- Numerical quadrature on element domains derived from product Gauss rules balances accuracy, efficiency, and stability. Domain quadrature rules also naturally accomodate nonlinear kinematic behavior and "black box" constitutive models.

However, despite these advantageous characteristics, finite element methods have suffered from two major (related) issues:

I.) Standard element formulations are prone to the effects of numerical locking phenomena which can significantly degrade the accuracy of the method. These issues are more prevalent for low-order elements, and especially so for linear triangles and tetrahedra. Moreover, very thin or distorted elements tend to exhibit more severe pathologies.

II.) The process of meshing complex geometries is encumbered by the aforementioned concerns over locking, to the extent that it becomes difficult – if not impossible to produce quality discretizations using automated tools which do not require extensive human intervention.

Despite recent efforts to pursue automated quad-dominant [46] and hex-dominant [26] meshing algorithms which seek to optimize certain mesh quality metrics, the inherrent problem of element distorsion sensitivity still remains. Consequently, substantial efforts have been made to address the locking problem through a variety of different approaches. An overview of locking and its remedies are given in the following section.

Locking in Finite Elements

Locking, as a general phenomenon presented in [5], is characterized by a loss of solution accuracy and/or convergence for particular choices of material or discretization parameters. In mathematical terms, an approximation method is deemed *robust* (with respect to a given problem parameter) if its numerical solution converges "uniformly" to the exact solution under mesh refinement, for all values of the indicated problem parameter. Conversely, a method is said to exhibit *locking* if the accuracy of the numerical solution degenerates as the chosen problem parameter approaches some limiting value.

As a specific example, one of the most commonly discussed and addressed forms of locking in computational solid mechanics is the issue of *volumetric locking*, wherein displacement-based element formulations suffer from a marked loss of accuracy when utilized to model the deformation of nearly incompressible materials. For a linear elastic material model, the parameter dependency in question relates to the Poisson's ratio of the material. Other forms of locking may manifest as a sensitivity to geometric/discretization parameters, including: *shear locking*, which is linked to the aspect ratio of continuum elements subjected to bending-dominated deformations; *membrane locking*, which occurs in curved shell elements (see [62]); and *trapezoidal locking*, which affects the bending response of distorted four-node quadrilateral elements (see [36]).

Early efforts to address concerns over locking sought to develop more robust discretizations through the use of higher-order elements. In [4] and [54], Babuška and Suri justified the ability of high-order elements to overcome the effects of volumetric locking (for triangular discretizations). The improved convergence behavior of these elements made them an attractive option for seeking efficiency gains, as well. Nonetheless, higher-order elements were generally seen as too complex in comparison with the standard low-order

elements commonly used for commercial applications; many cite the relative difficulty of obtaining lumped mass matricies for high-order elements (for explicit dynamics applications). Moreover, the accuracy of high-order isoparametric elements can be severely degraded if the elements posess curved edges, as demonstrated in [33].

As an alternative to the standard displacement-based FEM, some have argued for the use of *mixed finite element methods* (MFEM), which provide a separate interpolation of the displacement, strain, and stress fields, utilizing a 3-field Hu-Washizu variational principle in the construction of the weak form. While these methods are generally seen as robust in the face of locking (as noted in [4] and [5]), they are nonetheless subject to potential issues of stability, i.e. the Babuška-Brezzi – or inf-sup conditions (refer to [3], [8].) Additionally, mixed methods tend to be less efficient in comparison with displacement-based FEM, and are not as flexible in their ability to handle arbitrary constitutive relationships.

In an effort to retain some of the beneficial characteristics of mixed finite element methods, *mixed assumed strain methods* (alternately the *method of incompatible modes*) were formalized for geometrically linear problems in [51], and extended to nonlinear problems in [49] and [50]. Such methods are derived from a 3-field variational principle, and rely upon energy orthogonality between the enhanced strain field and the resulting stress field to eliminate the need for an independent stress interpolation space, thereby yielding a 2-field formulation. Though the method is effective in treating a variety of geometric locking phenomena, it nonetheless leads to spurious instabilities in both linear and nonlinear problems (see [55] and [41], respectively), even for element formulations satisfying the inf-sup conditions.

Other attempts to adapt mixed formulations for more general use with arbitrary material models without relying upon an explicit interpolation of the stress or strain fields have resulted in *selective reduced integration* (SRI) and equivalent *strain projection* techniques. These methods were fairly successful in overcoming the issues of volumetric locking via the B-bar projection approach for linear problems discussed in [30], and via the F-bar approach for nonlinear problems discussed in [17]. Though these methods can be both effective and efficient, their success has been limited to the problem of volumetric locking;

they are less successful with regard to treating other forms of locking, and can lead to stability problems if the strain projection spaces are not selected carefully.

At the opposite end of the spectrum – in recognition of the inherrent issues of stability plauging mixed methods and reduced integration techniques, methodologies employing *orthogonal hourglass control* were suggested, as in [23]. These approaches consider the use of low-order quadrature rules to avoid common locking phenomena, supplemented by artificial stiffness terms to maintain stability while preserving essential convergence characteristics. While these formulations tend to be highly efficient computationally (particularly for explicit dynamic analyses), the obvious disadvantage of these approaches relates to their reliance upon user-specified artificial stiffness and viscosity parameters. Appropriate selection of these parameters is not always a trivial matter, and often warrants problem-specific investigations via sensitivity analyses.

Ultimately, the foregoing methodologies have had only limited success in resolving the full spectrum of locking problems, particularly with regard to geometric locking phenomena. Moreover, many of the proposed enhancements are limited to specific element types (typically low-order quadrilaterals or hexahedra), and are not readily generalizable to other discretizations. To a large extent, the propensity for locking in FEM is controlled by the standard isoparametric elements' sensitivity to geometric distorsion. In other words, model accuracy is too often the product of the chosen discretization. For this reason, considerable efforts have been invested in recent years towards the development of alternative discretizations and numerical methods, a few of which are discussed in the following section.

Alternative Numerical Methods and Discretizations

Driven by concerns over meshing and element quality, a wide variety of alternative approximation methods have been explored in recent decades. The general consensus is that the construction of an approximation space should be disconnected (to a variable extent) from the particular choice of discretization. In particular, isoparametric finite element basis functions are conveniently defined in terms of the discretization, but may not necessarily result in a suitable approximation space for the given problem at hand.

In direct response to these considerations, so-called *meshfree* methods were developed in an effort to construct approximation spaces that are defined independently of a chosen spatial discretization. Meshfree methods encompass a broad class of approximation schemes, including smoothed particle hydrodynamics (SPH), the element-free Galerkin (EFG) method, and the reproducing kernel particle method (RKPM), among others. A majority of these methods rely upon an a priori specification of weighting functions used to construct an associated set of polynomially reproducing basis functions. The resulting meshfree basis yields relatively smooth solutions which are less sensitive to the specific choice and distribution of weighting functions.

The departure from defining an approximation space on a structured partition of the domain presents a number of challenges, however. Specifically, meshfree methods still require the definition of a background mesh to effect numerical integration of the weak form, partially invalidating the namesake of the method. Moreover, because the meshfree basis functions tend to be non-polynomial in form (and because they are not compactly supported/overlapping on element domains), they are more challenging to accurately integrate. Chen et. al. have proposed a means of overcoming these issues in [9] through a *variationally consistent integration* scheme, though this approach is succeptible to numerical instabilities. Additionally, because the basis functions do not in general exhibit the kronecker delta property, the application of boundary conditions and contact constraints becomes less straightforward; several techniques have been proposed to address this issue, including Lagrange multiplier methods, Nitsche's method, and mesh blending at domain boundaries.

As another alternative, *discontinuous Galerkin* (DG) methods have gained recent attention due to their more flexible represention of solution fields as piece-wise polynomials over individual elements, resulting in solution discontinuities at element boundaries. To stabilize the resulting approximation space, DG methods supplement the weak form with interior penalty terms which seek to minimize these discontinuities. DG methods are advantageous in that they may accomodate arbitrary element shapes, and exhibit desireable distorsion robustness characteristics.

DG approaches are not without their own problems, however. One commonly cited issue relates to the fact that DG methods can become sensitive to the choice of penalty parameters used to weakly enforce inter-element continuity and boundary conditions; the selection of these parameters is problem dependent. Additionally, DG methods tend to suffer from poor numerical conditioning problems if the discretization does not conform with relatively stringent regularity requirements, thereby limiting the types of discretizations used with the method.

The more recent *weak Galerkin* (WG) finite element method first introduced by Wang and Ye for elliptic problems in [59], and for parabolic equations by Li and Wang in [34], considers an approximation space consisting of functions defined on polygonal element domains which are consistent with the weak gradient of functions independently defined on shared element edges. The discrete approximation spaces under consideration are typically low-order polynomials (commonly just constants) defined on elements and their edges. However, there are some non-trivial choices that must be made regarding an optimal selection of these polynomial spaces for the sake of computational efficiency (discussed in greater detail in reference [40]). The method has so-far only been applied to the solution of linear problems.

The computational accuracy of the weak Galerkin approach has been explored by Mu et. al. in [38], showing that for certain problems, the weak Galerkin method converges at rates comparable to those of the standard FEM. Lin et. al. performed a comparative study between the weak Galerkin, discontinuous Galerkin, and mixed finite element methods in [35], demonstrating some of the competitive and desirable characteristics of WG in contrast to DG or MFEMs (i.e. no need for penalty parameters, and definiteness of the resulting linear system of equations).

Mu et. al. adapted the method for use on arbitrary polytopal meshes in [39] and [40], albeit with a number of shape regularity restrictions placed on the elements. In general, the implementation of WG considers the mesh degrees of freedom as belonging to both the elements and their edges, however in [40] it is noted that the local element degrees of freedom can be expressed in terms of the bounding edge degrees of freedom alone to

improve computational efficiency. A modified approach by Wang et. al. in [60] instead chooses to express functions on edges only implicitly. Although this approach successfully eliminates the computational expense associated with edge-based degrees of freedom, it requires the inclusion of an additional interior penalty term in the weak form, similiar to a discontinuous Galerkin method.

In the wake of these investigations, it became clear that many of the desirable properties of the FEM (compact support, kronecker delta, quadrature efficiency, DoF efficiency, stability, and inter-element compatibility) were qualities worth preserving. To this end, efforts were made toward improving and generalizing existing element formulations for arbitrary element shapes – polygons and polyhedra. Rather than relying upon shape functions defined through an isoparametric transformation from a parent element domain, recent polytopal element methodologies have explored various techniques for constructing approximants directly on physical element domains. In doing so, issues regarding distorsion sensitivity of the elements are largely obviated, and new opportunities for discretizing the domain with irregular shapes are made possible. In like fashion, recent advances in meshing technologies have made polyhedral element methods a readily feasible option. Very recently, Ebeida et. al. have released VoroCrust ([21]): a robust voronoi discretization tool based on constrained Poisson disk sampling. Concurrent technologies have also advanced polyhedral mesh generation via boolean intersection of a background hexahedral mesh with a piece-wise linear boundary representation (or B-rep).

For these reasons, efficient and robust polyhedral element formulations are in high demand, leading to a proliferation of new approaches. A number of these are discussed in the following section.

1.2 Recent Developments in Polytopal Discretizations

Polytopal element methods combine many of the attractive features of FEM with the geometric flexibility afforded by arbitrary element shapes, the primary motivation for which arises from the aforementioned concerns over discretization sensitivity. Most of these methods share a few distinguishing features in common with one another: mesh

degrees of freedom are borne by nodes – the geometric verticies of (low-order) elements; nodal basis functions are compactly supported over adjoining element domains, and satisfy the kronecker delta property; basis functions are defined directly on the element's physical domain, rather than on a parent domain.

Where these methods differ is in the way that they choose to define an element's shape functions (if at all). These approaches may be loosely organized into three distinct categories: methods which explicitly define the element's basis functions via a continuous interpolation scheme; methods which define the element's shape functions only implicitly – i.e. "virtual" element methods; and methods which form a discrete representation of the element's shape functions via an approximation scheme. These three methodologies are elaborated upon in the following sections.

Continuous Interpolation on Arbitrary Polytopes

In an effort to generalize the core idea behind isoparametric element coordinates which yield a point-wise definition of the element's shape functions and their gradients within a given element domain, various efforts to explicitly define shape functions directly on arbitrary polytopal domains has led to the creation of a broad family of interpolation schemes, collectively referred to as *generalized barycentric coordinates*.

At a minimum, shape functions which fall into this category must: form a partition of unity, satisfy linear completeness, and interpolate the nodal data (i.e. satisfy the kronecker delta property). These coordinates are uniquely defined according to the standard barycentric coordinate system for simplicial domains. For arbitrary polytopal domains, numerous such coordinate systems exist, including Wachspress' coordinates [58], mean values coordinates [24], harmonic coordinates [31], and maximum entropy coordinates [53], among others.

Though generalized barycentric coordinates have been applied in the context of finite elements, their development has largely been propelled by the graphics community on account of their relatively smooth interpolatory properties. However, thier smooth (non-polynomial) character presents a challenge with regard to accurate numerical integration. Consequently, relatively high-order quadrature schemes are required to achieve reason-

able accuracy and satisfaction of patch tests. More recently, a polynomial projection scheme has been suggested in [56] to remedy these integration errors for linear problems; for general nonlinear problems, a gradient correction scheme has been proposed in [57] and [11]. These developments have illuminated new possibilities for defining more efficient quadrature rules on polytopes while still satisfying the essential requirements for convergence.

Yet in spite of these developments, many existing coordinate schemes are sill limited by moderate to severe restrictions on element shape/convexity, and produce sharp gradients in the presence of degenerate geometric features. These concerns, and a recognition of the fact that the shape functions need not be defined point-wise for finite element applications, have motivated research efforts toward discrete representations of element interpolants.

Virtual Element Methods

The *virtual element method* (VEM) summarized in [15] is a relatively new approach, and based in part upon the older concept of mimetic finite differences (MFD). Although the method supposes that continuous basis functions *exist* within arbitrary polytopal elements, the VEM never explicitly *defines* how these shape functions vary on element interiors. Instead, the VEM supposes that these "virtual" functions may be separated (via projection operators) into polynomial and non-polynomial parts, which are handled in different ways. The cornerstone of the method is the idea that the bilinear form for a given element may be decomposed into two distinct parts: a term which guarantees variational consistency (Galerkin exactness) involving the low-order polynomial part of the shape functions, and a term which provides stability involving the non-polynomial part. The consistency term must be integrated exactly, but the stability term can be evaluated approximately. Because this decomposition relies upon the linearity of the bilinear form, direct generalizations of the method to nonlinear problems are not immediately available.

VEM has been applied to three-dimensional linear elasticity problems in [25]. In [16], a VEM formulation for low-order elements which accomodates nonlinear "black-box" constitutive algorithms is presented, and in [10] an extension to finite deformations (with appropriate stabilization terms) is introduced. Given the means by which these

approaches exploit the use of a projected uniform gradient to integrate the weak form, however, it is unclear how they could be extended to accomodate higher-order elements.

Nonetheless, VEM formulations are able to tolerate geometric degeneracies and element non-convexity without encountering serious numerical difficulties, though their good behavior in the presence of these features is often governed by an ad hoc approximation of the stabilization terms. A more rigorous development of the corresponding stability terms for more complicated element domains remains to be explored.

Approximate Interpolation on Arbitrary Polytopes

In contrast with the previously described approaches, yet another strategy considers the representation of the element's shape functions in an approximate way, while enforcing a few essential requirements, namely: polynomial reproducibility, inter-element compatibility, and weak form consistency.

In [43] and [45], Rashid and co-workers explored the *variable element topology finite element method* (VETFEM), characterized by an approximate representation of the element's shape functions as low-order polynomials satisfying weak continuity requirements at element boundaries. Within this framework, the element shape functions are determined by a local minimization problem, resulting in polynomial shape functions which optimize specified continuity and smoothness objectives. This minimization procedure is constrained by the requirements of consistency and reproducibility to guarantee satisfaction of linear patch tests. Dohrmann and Rashid later extended this approach to higher-order elements in [18], instead focusing on a direct construction of shape function derivatives, rather than of the shape functions themselves.

The VETFEM may be viewed as a non-conforming finite element method, as the minimization process altogether allows for residual discontinuities at inter-element boundaries. Nonetheless, because the elements satisfy weak contunity requirements, the method exhibits proper convergence characteristics. Additionally, because the VETFEM yields a point-wise representation of the shape functions as low-order polynomials, direct integration of the weak form can be carried out using relatively efficient domain quadrature rules.

Although the VETFEM was developed to handle arbitrary polygonal elements, it was observed to suffer from sensitivity to geometric degeneracies and element non-convexity. In response to these issues, a *discrete data polyhedral finite element method* (DDPFEM) proposed in [48] was suggested to exploit the fact that for typical solid mechanics applications, it is generally only necessary to evaluate the element's shape functions (and their derivatives) at a discrete number of quadrature points. The proposed method shares several characteristics in common with the VETFEM, utilizing a similarly posed constrained minimization procedure to obtain the precise values and gradients of the shape functions at discrete points on the element's interior. One of the cited challenges with this approach pertains to the appropriate selection of an efficient quadrature rule for the elements.

Nonetheless, the initial thoughts put forward by the DDPFEM ultimately led to the development of the *partitioned element method* (PEM) presented in [44]. The PEM proceeds by partitioning an element into polygonal quadrature cells, and allowing the element's shape functions to vary according to a local polynomial defined within each of these cells, resulting in piece-wise polynomial shape functions which are discontinuous at quadrature cell boundaries. The polynomial coefficients defined in each cell are obtained by minimizing the discontinuities in the shape functions across all cell interfaces, subject to the necessary consistency and reproducibility constraints. The original presentation in [44] considers the shape functions to be approximate solutions of Laplace's equation on the partitioned element. Later developments have dispensed with this supposition, instead only penalizing discontinuities in the shape functions (and their gradients) at cell boundaries.

Subsequently, Bishop has proposed a very similar partitioned element scheme in [7], wherein the elements and their faces are subdivided into simplicies, resembling a local FE discretization of the element domain. The shape functions are obtained as the solution to Laplace's equation on this subdivision. Because this approach utilizes an FE-like discretization, the resulting shape functions are piece-wise linear and C^0 continuous, thereby avoiding the need for a penalty term to enforce continuity. However, the method still requires the use of a gradient correction scheme to account for quadrature error and recover

consistency with the weak form.

In light of these developments, we choose to recognize a new class of methods, herein collectively referred to as *partitioned element methods*. These may be viewed as a generalization of the original PEM presented in [44]. It is the subject of this thesis to further explore these methods, and to expose their particular merits and potential shortcomings.

1.3 Scope of the Present Work

In this work, we put forth a general framework for partitioned element methods – a collection of different approaches for constructing approximate representations of element shape functions on arbitrary polytopes. These methods are characterized by several distinguishing features:

(1) Elements are discretized (partitioned) into non-overlapping polygonal cells. These cells are used to inform the quadrature rule of the element.

(2) A local approximation space is defined on the partitioned element geometry.

(3) A set of BVPs and appropriate constraints are posed, whose solutions yield the shape functions of the element.

(4) A stable numerical scheme is developed to obtain approximate solutions to these BVPs using the approximation space defined in (2).

Numerous formulations are possible within this framework; a few of these are explored within the scope of this thesis.

The proposed application area of interest for these methods is in nonlinear solid mechanics. The efficacy of the methods explored will be assessed within this context, particularly with regard to their ability to naturally accomodate nonlinear kinematic and material behavior. The robustness of the resulting elements, and their performance in the face of locking phenomena will be evaluated. Additionally, several methodologies which leverage the partitioned element framework to combat certain forms of locking will be discussed.

The remainder of this dissertation is organized as follows: chapter 2 establishes the context of nonlinear computational solid mechanics, chapter 3 presents the overarching framework for partitioned element methods, chapter 4 details a particular implementational framework for the PEM, chapter 5 provides a number of numerical investigations of the PEM, and chapter 6 concludes with a discussion of opportunities for further research and development.

Chapter 2

An Overview of Computational Solid Mechanics

This chapter addresess some of the essential aspects of numerical approximation methods for modeling solid continua. The discussion herein will focus on the mathematical foundations of solid mechanics, beginning with the kinematics of motion and some common forms of constitutive relationships, followed by the expressions for conservation of momentum in both strong and weak form, and concluding with an analysis of the standard numerical methods utilized to solve these equations in an approximate sense. In the course of our discussion, we will make explicit the ensuing requirements placed upon any prospective approximation scheme. This will aid our analysis in subsequent chapters, and hopefully justify particular choices made in the construction of partitioned element methods.

2.1 The Lagrangian Description of Motion

Consider a body $\mathcal{B}_0 \subset \mathbb{R}^d$ consisting of a set of material points whose positions in some reference configuration at time $t = 0$ are denoted $\mathbf{X}$. At a later time $t > 0$, the body occupies a new configuration $\chi(\mathcal{B}_0, t) = \mathcal{B}_t \subset \mathbb{R}^d$, such that the motion of individual material points yield new spatial positions $\mathbf{x}$ according to the bijection $\chi_t : \mathbf{X} \leftrightarrow \mathbf{x}$, i.e.

$$\mathbf{x} = \chi(\mathbf{X}, t), \quad \mathbf{X} = \chi^{-1}(\mathbf{x}, t). \tag{2.1}$$

The displacement $\mathbf{u}$ of a given material point may be expressed as $\mathbf{u} = \mathbf{x} - \mathbf{X}$, and it's corresponding velocity is denoted $\mathbf{v} = \dot{\mathbf{x}} = \partial\mathbf{x}/\partial t$. Figure 2.1 provides a visual interpretation of the situation described.

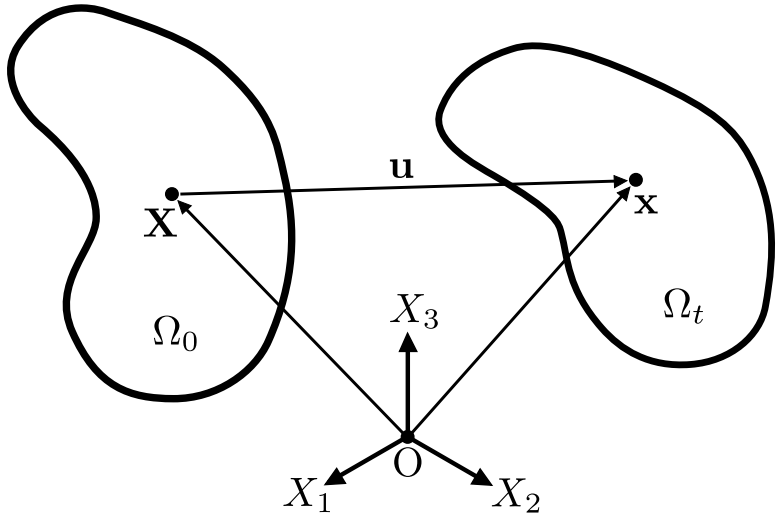

Figure 2.1. A depiction of the motion of material points in a body Ω.

At a given time t, the Jacobian of the deformation mapping χ_t yields the deformation gradient $\mathbf{F} = \nabla_X \mathbf{x}$ (a rank-2 tensor), defined as

$$\mathbf{F} = \frac{\partial \mathbf{x}}{\partial \mathbf{X}} = \mathbf{1} + \nabla_X \mathbf{u}, \tag{2.2}$$

where ∇_X denotes the gradient with respect to $\mathbf{X}$. The deformation gradient may be used to map differential line segments $d\mathbf{X}$, surface areas $d\mathbf{A}$, and volumes dV defined in the reference configuration into their corresponding transformed quantities ($d\mathbf{x}$, $d\mathbf{a}$, dv) at time t:

$$d\mathbf{x} = \mathbf{F} d\mathbf{X}, \quad d\mathbf{a} = J\mathbf{F}^{-T} d\mathbf{A}, \quad dv = J dV, \tag{2.3}$$

where $J \equiv \det \mathbf{F}$.

In like fashion, the spatial velocity gradient $\mathbf{L} = \nabla_x \mathbf{v}$ (where ∇_x denotes the gradient with respect to $\mathbf{x}$) may be expressed as

$$\mathbf{L} = \frac{\partial \mathbf{v}}{\partial \mathbf{x}} = \frac{\partial \dot{\mathbf{x}}}{\partial \mathbf{X}} \frac{\partial \mathbf{X}}{\partial \mathbf{x}} = \dot{\mathbf{F}} \mathbf{F}^{-1}, \tag{2.4}$$

which may be further decomposed into a symmetric part $\mathbf{D}$ (the rate of deformation tensor) and an anti-symmetric part $\mathbf{W}$ (the spin tensor):

$$\mathbf{D} = \frac{1}{2}(\mathbf{L} + \mathbf{L}^T), \quad \mathbf{W} = \frac{1}{2}(\mathbf{L} - \mathbf{L}^T). \tag{2.5}$$

Compatibility

Compatibility refers to the idea that a given body remains a contiguous medium following some deformation described by χ_t. In other words, χ_t must characterize a continuous mapping of material points between different configurations in time, such that the topology of body remains unchanged. Compatibilitiy is characterized by the following necessary and sufficient conditions:

$$\nabla_X \times \mathbf{F} = \mathbf{0} \quad \forall \mathbf{X} \in \mathcal{B}_0. \tag{2.6}$$

Satisfaction of the above compatibility condition implies that there exists a continuous, single-valued displacement field which gives rise to the deformation characterized by $\mathbf{F}$.

Finite Strain Measures

Consider the set of all material line segments $d\mathbf{X}$ which lie in a small neighborhood around a given material point $\mathbf{X}$. Also, consider these same material line segments $d\mathbf{x}$ in the current configuration of the body after some deformation corresponding to $\mathbf{F}(\mathbf{X}, t)$ has taken place, such that $d\mathbf{x} = \mathbf{F} d\mathbf{X}$.

At a given material point $\mathbf{X}$, the deformation gradient $\mathbf{F}(\mathbf{X}, t)$ is a linear operator, which may be decomposed into two step-wise operations: a stretching operation $\mathbf{U}$ (or $\mathbf{V}$), and a rotation $\mathbf{R}$, yielding the polar decomposition of $\mathbf{F}$:

$$\mathbf{F} = \mathbf{R}\mathbf{U} = \mathbf{V}\mathbf{R}, \tag{2.7}$$

where $\mathbf{U}$ is termed the right stretch tensor, and $\mathbf{V}$ is the left stretch tensor. There arise from $\mathbf{U}$ and $\mathbf{V}$ two primary deformation measures: the right Cauchy-Green deformation

tensor $\mathbf{C} = \mathbf{U}^2$, and the left Cauchy-Green deformation tensor $\mathbf{B} = \mathbf{V}^2$. Each of these, in turn, yield the two most commonly utilized finite strain measures: the Green-Lagrangian strain tensor $\mathbf{E} = \frac{1}{2}(\mathbf{C} - \mathbf{I})$, and the Eulerian-Almansi strain tensor $\mathbf{e} = \frac{1}{2}(\mathbf{I} - \mathbf{B}^{-1})$. It is not difficult to show that both of these strain measures reduce to the small strain tensor $\boldsymbol{\varepsilon} = \frac{1}{2}(\nabla_X \mathbf{u} + (\nabla_X \mathbf{u})^T)$ if the displacements are sufficiently small.

Another finite strain measure that has gained attention in more recent years is the Hencky (logarithmic, or "true") strain tensor $\mathbf{H} = \frac{1}{2}\log \mathbf{B}$. Because the Hencky strain tensor belongs to the Seth-Hill family of strain measures (as do the Green-Lagrangian and Eulerian-Almansi strain tensors), it likewise is seen to reduce to the small strain tensor in the limit of small displacements.

2.2 Conservation of Linear and Angular Momentum

For a given material body $\mathcal{B}_t \subset \mathbb{R}^d$, any open subset $\Omega_t \subset \mathcal{B}_t$ must satisfy Newton's second law of motion, such that the net external force which acts upon Ω_t is equal to the total change in linear momentum of the system, i.e.

$$\frac{d}{dt}\int_{\Omega_t} \rho \mathbf{v}\, dv = \int_{\Omega_t} \rho \mathbf{b}\, dv + \int_{\partial\Omega_t} \mathbf{t}\, da \quad \forall \Omega_t \subset \mathcal{B}, \tag{2.8}$$

where ρ is the mass density of the matertial, $\mathbf{v}$ is the velocity field, $\mathbf{b}$ is an applied body force per unit of mass, and $\mathbf{t}$ is the traction vector – a force per unit of area – which acts on $\partial\Omega_t$ (the boundary of Ω_t). Via the Cauchy tetrahedron argument, it is possible to express the traction vector $\mathbf{t}(\mathbf{n})$ as a linear function of the unit vector $\mathbf{n}$, which is normal to the surface upon which the traction acts:

$$\mathbf{t} = \mathbf{n} \cdot \boldsymbol{\sigma}, \tag{2.9}$$

where $\boldsymbol{\sigma}$ is referred to as the Cauchy stress tensor. Invoking the divergence theorem, we may utilize the above relation to convert the traction boundary integral into a volume integral over Ω_t:

$$\int_{\partial\Omega_t} \mathbf{t}\, da = \int_{\partial\Omega_t} \mathbf{n} \cdot \boldsymbol{\sigma}\, da = \int_{\Omega_t} \nabla_x \cdot \boldsymbol{\sigma}\, dv. \tag{2.10}$$

Moreover, utilizing Reynolds' transport theorem, conservation of mass, and a change of variables in $\mathbf{x}$ and $\mathbf{X}$, it is possible to show that

$$\frac{d}{dt}\int_{\Omega_t} \rho\mathbf{v}\, dv = \int_{\Omega_t} \rho\frac{d\mathbf{v}}{dt}\, dv, \tag{2.11}$$

which ultimately yields

$$\int_{\Omega_t} \left[\rho(\mathbf{b} - \dot{\mathbf{v}}) + \nabla_x \cdot \boldsymbol{\sigma}\right]\, dv = \mathbf{0} \quad \forall \Omega_t \subset \mathcal{B}. \tag{2.12}$$

Since we have imposed no limitations on the choice of subset Ω_t, we may invoke the localization theorem to determine a point-wise statement of equilibrium in the body $\mathcal{B}_t$:

$$\rho(\mathbf{b} - \dot{\mathbf{v}}) + \nabla_x \cdot \boldsymbol{\sigma} = \mathbf{0} \quad \forall \mathbf{x} \in \mathcal{B}_t. \tag{2.13}$$

Similarly, by formulating an expression for the conservation of angular momentum, we obtain an additional point-wise requirement on the symmetry of the Cauchy stress tensor:

$$\boldsymbol{\sigma} = \boldsymbol{\sigma}^T \quad \forall \mathbf{x} \in \mathcal{B}_t. \tag{2.14}$$

Measures of Stress

As expressed earlier, the Cauchy stress tensor $\boldsymbol{\sigma}$ relates the normal $\mathbf{n}$ of a given surface area element $d\mathbf{a} = \mathbf{n}\, da$ to the corresponding force per unit of area $\mathbf{t}$ which acts on that surface, where the surface element $d\mathbf{a}$ is defined in the current configuration of the body (at some time $t > 0$). The total force which acts on a given surface $d\mathbf{a}$ is then

$$d\mathbf{f} = \mathbf{t}\, da = \boldsymbol{\sigma}^T\, d\mathbf{a}. \tag{2.15}$$

Utilizing Nanson's formula for area transformations:

$$d\mathbf{a} = J\mathbf{F}^{-T}\, d\mathbf{A}, \tag{2.16}$$

we may consider an equivalent representation of $d\mathbf{f}$, such that

$$d\mathbf{f} = J\boldsymbol{\sigma}^T\mathbf{F}^{-T}\, d\mathbf{A} = \mathbf{P}\, d\mathbf{A} = \mathbf{p}\, dA, \tag{2.17}$$

where $\mathbf{P}$ is defined as the first Piola-Kirchhoff stress tensor (which in general is not symmetric.), and where $\mathbf{p} = \mathbf{N} \cdot \mathbf{P}^T$ is the corresponding Piola traction vector, characterizing

the distributed force which acts over a surface defined in the reference configuration with area dA and normal $\mathbf{N}$.

Another stress measure (related to the first Piola-Kirchhoff stress) is the second Piola-Kirchhoff stress tensor $\mathbf{S}$, and is commonly defined as the pull-back of the Kirchhoff stress tensor $\boldsymbol{\tau} = J\boldsymbol{\sigma}$:

$$\mathbf{S} = \mathbf{F}^{-1}\boldsymbol{\tau}\mathbf{F}^{-T}. \tag{2.18}$$

2.3 Constitutive Relations

Fundamentally, we require there to be some relationship between the forces applied to a given body, and its observed deformation. Such relationships are generally referred to as constitutive models, which characterize a macroscopic connection between stress and strain in a continuum.

Models of Elasticity

Constitutive models have variable forms, mostly notably as they relate to notions of elasticity: the tendency of a material to revert to its original undeformed configuration if the applied forces are removed. Models for elastic material behavior fall into three primary categories: hyperelasticity, Cauchy-elasticity, and hypoelasticity.

Hyperelasticity is concerned with the description of a material's state through an elastic potential function, which expresses the total stored elastic strain energy $W(\mathbf{F})$ in the material as a function of the total deformation measured from some (nominally undeformed) reference configuration. Differentiation of this potential with respect to a given deformation measure will yield an expression for the corresponding work-conjugate measure of stress, e.g.

$$\mathbf{P} = \frac{\partial W}{\partial \mathbf{F}}, \qquad \mathbf{S} = \frac{\partial W}{\partial \mathbf{E}}. \tag{2.19}$$

Some common examples of hyperelastic models include the St. Venant-Kirchhoff material model:

$$W(\mathbf{E}) = \frac{\lambda}{2}\mathrm{tr}(\mathbf{E})^2 + \mu\mathrm{tr}(\mathbf{E}^2), \tag{2.20}$$

the Hencky elasticity model:

$$W(\mathbf{H}) = \frac{\lambda}{2}\mathrm{tr}(\mathbf{H})^2 + \mu\mathrm{tr}(\mathbf{H}^2), \tag{2.21}$$

the compressible Mooney-Rivlin solid:

$$W(I_1, I_2, J) = C_{01}(J^{-4/3}I_2 - 3) + C_{10}(J^{-2/3}I_1 - 3) + D_1(J-1)^2, \tag{2.22}$$

$$I_1 = \mathrm{tr}(\mathbf{B}), \qquad I_2 = \frac{1}{2}\left[\mathrm{tr}(\mathbf{B})^2 - \mathrm{tr}(\mathbf{B}^2)\right], \qquad J = \det(\mathbf{F}), \tag{2.23}$$

$$D_1 = \frac{\kappa}{2}, \qquad (C_{01} + C_{10}) = \frac{\mu}{2}, \tag{2.24}$$

and the compressible Neo-Hookean solid (a special case of the Mooney-Rivlin solid where $C_{01} = 0$, and $C_1 = C_{10}$):

$$W(I_1, J) = C_1(J^{-2/3}I_1 - 3) + D_1(J-1)^2 \tag{2.25}$$

Cauchy-elasticity (as a terminology to describe a particular sub-class of material models) differs from hyperelasticity in the sense that the relations between particular stress and strain measures are defined directly, and do not necessarily arise from an elastic potential function. The models of linear elasticity, in particular, are generalizations of Hooke's law, namely:

$$\boldsymbol{\sigma} = \mathbf{C} : \boldsymbol{\varepsilon}, \tag{2.26}$$

and are suitable for small deformations, but are typically not applicable in the context of finite deformations. By comparison, Cauchy-elastic models are defined in terms of the deformation gradient $\mathbf{F}$, i.e.

$$\boldsymbol{\sigma} = f(\mathbf{F}), \tag{2.27}$$

and are suitable in the context of finite deformations. For such models to be considered objective under a superposed rigid rotation corresponding to $\mathbf{R}$, they must satisfy the following condition:

$$\mathbf{R}\boldsymbol{\sigma}\mathbf{R}^T = f(\mathbf{RF}). \tag{2.28}$$

Nonetheless, such models may still suffer from being non-conservative, in the sense that the total work done by the stresses acting on a body moving through an arbitrary closed

cycle of deformation does not necessarily sum to zero. For these reasons, models of hyperelasticity are generally preferred where the use of such models is deemed appropriate. Nonetheless elasticity models are still useful, particularly in the context of small deformations.

In contrast, hypoelasticity models define an evolution (rate) equation in terms of the current stress and the velocity gradient at a given material point, i.e.

$$\dot{\boldsymbol{\sigma}} = g(\boldsymbol{\sigma}, \mathbf{L}). \tag{2.29}$$

Hypoelasticity models are in general non-conservative, and moreover may not necessarily return to a state of zero stress following a closed cycle of deformation. Hypoelasticity is generally less appropriate where hyperelastic or other elastic models may be used instead. The value of hypoelasticity lies in its ability to accomodate models for plastic flow and dissipation in the material, giving rise to the common models of hypoelasto-plasticity.

One of the primary challenges of working with hypoelastic models concerns the manner in which the rate of stress transforms under superposed rigid-body rotations. These considerations have led to the formulation of co-rotational (or objective) stress rates. A multitude of such rates exist, though only a few are found to be in common usage. Most notably, the Jaumann rate of stress $\mathring{\boldsymbol{\sigma}}$ is defined as

$$\mathring{\boldsymbol{\sigma}} = g(\boldsymbol{\sigma}, \mathbf{D}) = \dot{\boldsymbol{\sigma}} + \boldsymbol{\sigma}\mathbf{W} - \mathbf{W}\boldsymbol{\sigma}, \tag{2.30}$$

where $\mathbf{D}$ and $\mathbf{W}$ specify the rate of deformation and spin at a given material point, respectively.

2.4 Model Boundary Value Problem

Up to this point, we have discussed only the essential relationships which exist between physical quantities of interest in the context of solid mechanics. Ultimately, however, we should like to determine the anticipated motion and deformation of a particular body under the action of pre-determined externally applied forces. To this end, we must turn our attention to the definition – and solution – of boundary value problems (BVPs). Such problems must be well-posed, in the sense that there exists a unique solution to the stated problem, thereby imposing certain restrictions on the choice of boundary conditions.

The Strong Form Statement of Equilibrium

In the context of solid mechanics, the solution of a given boundary value problem usually refers to a complete description of the primary field variable(s) of interest, namely the displacement field $\mathbf{u}(\mathbf{X})$ at all locations $\mathbf{X} \in \mathcal{B}_0$ within the body $\mathcal{B}_0$ in its reference configuration. Under the requirements of compatibility, we presume that the displacement field is a continuous function, whose derivatives up to second order are defined everywhere, i.e. $\mathbf{u} \in [C^2(\mathcal{B}_0)]^d$.

Now, let us examine a quasi-static solid mechanics model problem of the following form: consider an open domain $\mathcal{B}_0 \subset \mathbb{R}^d$ whose boundary $\partial\mathcal{B}_0$ consists of the partition $\left\{\Gamma_0^D, \Gamma_0^N\right\}$. Let $\mathbf{u} = \bar{\mathbf{u}}\ \forall \mathbf{X} \in \Gamma_0^D$ constitute a prescribed Dirichlet boundary condition imposed upon the displacement field, and $\mathbf{n} \cdot \boldsymbol{\sigma} = \bar{\mathbf{t}}\ \forall \mathbf{X} \in \Gamma_0^N$ be a Neumann boundary condition imposed upon the surface traction. Additionally, let us suppose that an applied body force $\mathbf{b}$ acts upon all points $\mathbf{X} \in \mathcal{B}_0$. Given these conditions, we should like to determine the displacement field $\mathbf{u} \in \mathcal{S} = \left\{\mathbf{u} \in [C^2(\mathcal{B}_0)]^d : \mathbf{u} = \bar{\mathbf{u}}\ \forall \mathbf{x} \in \Gamma_0^D\right\}$ which satisfies the equations of equilibrium in a point-wise sense:

$$\rho\mathbf{b} + \nabla_x \cdot \boldsymbol{\sigma} = \mathbf{0} \quad \forall \mathbf{x} \in \mathcal{B}_t, \tag{2.31}$$

and where we suppose that a constitutive model has been defined in order to relate some measure of the deformation (e.g. $\mathbf{F} = \mathbf{1} + \nabla_X \mathbf{u}$) to the stress (e.g. $\boldsymbol{\sigma} = f(\mathbf{F})$). Equivalently, we may write the equations of equilibrium in terms of quantities related to the reference configuration of the body:

$$\rho_0\mathbf{b} + \nabla_X \cdot \mathbf{P}^T = \mathbf{0} \quad \forall \mathbf{X} \in \mathcal{B}_0, \tag{2.32}$$

where $\rho_0 = J\rho$ is the mass density of the material at time $t = 0$. The above statement is commonly referred to as the "strong form" of the model problem, given that it requires a point-wise satisfaction of equilibrium.

It should be emphasized that the Dirichlet boundary conditions and the requirements of compatibility are satisfied implicitly, as a consequence of the deliberate choice of function space $\mathcal{S}$ for the displacement field. Such functions $\mathbf{u} \in \mathcal{S}$ are termed "admissible," as potential solutions to the boundary value problem at hand.

The Equivalent Weak Form Statement of Equilibrium

In general, solutions to the strong form problem are not easily obtained. For this reason, it proves to be much more convenient to work with the (equivalent) "weak form" statement of the boundary value problem:

Find $\mathbf{u} \in \mathcal{S} = \left\{ \mathbf{u} \in [H^1(\mathcal{B}_0)]^d : \mathbf{u} = \bar{\mathbf{u}} \ \forall \mathbf{X} \in \Gamma_0^D \right\}$ *such that*

$$\mathcal{R}(\mathbf{u}, \mathbf{v}) = \int_{\mathcal{B}_t} \rho \mathbf{b} \cdot \mathbf{v} \, dv + \int_{\Gamma_t^N} \bar{\mathbf{t}} \cdot \mathbf{v} \, da - \int_{\mathcal{B}_t} \boldsymbol{\sigma} \colon \nabla_x \mathbf{v} \, dv = 0 \quad \forall \mathbf{v} \in \mathcal{V}, \tag{2.33}$$

or equivalently

$$\mathcal{R}(\mathbf{u}, \mathbf{v}) = \int_{\mathcal{B}_0} \rho_0 \mathbf{b} \cdot \mathbf{v} \, dV + \int_{\Gamma_0^N} \bar{\mathbf{p}} \cdot \mathbf{v} \, dA - \int_{\mathcal{B}_0} \mathbf{P} \colon \nabla_X \mathbf{v} \, dV = 0 \quad \forall \mathbf{v} \in \mathcal{V}, \tag{2.34}$$

where $\mathcal{V} = \left\{ \mathbf{v} \in [H^1(\mathcal{B}_0)]^d : \mathbf{v} = \mathbf{0} \ \forall \mathbf{X} \in \Gamma_0^D \right\}$, *and*

$$H^1(\mathcal{B}_0) = \left\{ u \in L^2(\mathcal{B}_0), \, D^\alpha u \in L^2(\mathcal{B}_0) \ \forall |\alpha| \leq 1 \right\}. \tag{2.35}$$

It should be remarked that the space $\mathcal{S}$ of admissible solutions to the weak form now consists of much more general functions than those considered for the strong form. In other words, the requirements on the differentiability of functions in $\mathcal{S}$ have been "weakened."

In (2.34), the traction boundary condition has been replaced by $\mathbf{p} = \bar{\mathbf{p}} \ \forall \mathbf{X} \in \Gamma_0^N$ – i.e. a condition on the Piola (rather than Cauchy) surface traction. The function space $\mathcal{S}$ is commonly referred to as the space of admissible "trial solutions," whereas $\mathcal{V}$ is called the space of "test functions," and consists of all admissible variations such that $\mathcal{V} = T_{\mathbf{u}}\mathcal{S}$ is the tangent space to $\mathcal{S}$ (i.e. $\mathbf{u} + \mathbf{v} \in \mathcal{S} \ \forall \mathbf{u} \in \mathcal{S}, \, \mathbf{v} \in \mathcal{V}$). In words, our goal is determine the solution $\mathbf{u}$ from among all admissible trial solutions contained in $\mathcal{S}$ which satisfies equation (2.33) or (2.34) for all admissible variations $\mathbf{v} \in \mathcal{V}$.

Under the assumptions of small displacements and linear elasticity, equations (2.33) and (2.34) are equivalent, and may be more succinctly expressed in terms of a bilinear form $a \colon \mathcal{S} \times \mathcal{V} \mapsto \mathbb{R}$ and a linear form $\ell : \mathcal{V} \mapsto \mathbb{R}$ such that

$$a(\mathbf{u}, \mathbf{v}) + \ell(\mathbf{v}) = 0 \quad \forall \mathbf{v} \in \mathcal{V}. \tag{2.36}$$

2.5 Galerkin Approximations to the Weak Form

In the weak form problem statement, the trial and test spaces $\mathcal{S}$ and $\mathcal{V}$ are taken to be infinite dimensional function spaces. In a practical computational setting, however, this renders the solution of such problems infeasible. Instead, most variational methods consider approximate solutions to the weak form, where $\mathbf{u} \in \mathcal{S}$ and $\mathbf{v} \in \mathcal{V}$ are replaced by $\mathbf{u}^h \in \mathcal{S}^h \subset \mathcal{S}$ and $\mathbf{v}^h \in \mathcal{V}^h \subset \mathcal{V}$, respectively. In this context, $\{\varphi_a\}_{a=1}^N$ and $\{\phi_a\}_{a=1}^M$ denote finite dimensional bases for the sub-spaces $\mathcal{S}^h$ and $\mathcal{V}^h$, such that

$$\mathbf{u}^h(\mathbf{X}) = \sum_{a=1}^{N} \varphi_a(\mathbf{X})\mathbf{u}_a, \qquad \mathbf{v}^h(\mathbf{X}) = \sum_{a=1}^{M} \phi_a(\mathbf{X})\mathbf{v}_a. \tag{2.37}$$

This yields the Galerkin approximation to the weak form: *Find* $\mathbf{u}^h \in \mathcal{S}^h$ *such that*

$$\mathcal{R}(\mathbf{u}^h, \mathbf{v}^h) = 0 \quad \forall \mathbf{v}^h \in \mathcal{V}^h, \tag{2.38}$$

yielding the (in general, nonlinear) residual equations, in index notation:

$$R_{ia}(\mathbf{u}^h) = \int_{\mathcal{B}_0} \rho_0 b_i \phi_a \, dV + \int_{\Gamma_0^N} \bar{p}_i \phi_a \, dA - \int_{\mathcal{B}_0} P_{ij} \phi_{a,j} \, dV = 0 \quad \forall i,\, a. \tag{2.39}$$

Without loss of generality, if we suppose that $\mathcal{S} = \mathcal{V}$ (provided $\mathbf{u} = \mathbf{0}\ \forall \mathbf{X} \in \Gamma_0^D$), then we may select identical sub-spaces $\mathcal{S}^h = \mathcal{V}^h$ ($\{\varphi_a\}_{a=1}^N = \{\phi_a\}_{a=1}^M$), resulting in a symmetric (or Bubnov-) Galerkin method. Traditional finite element methods fall into this category. Such methods are advantageous in the sense that (for linear problems) they result in stable, symmetric bilinear forms satisfying the Galerkin orthgonality (or "best approximation") property – the property that the solution error $\mathbf{e} = \mathbf{u}^h - \mathbf{u}$ is orthogonal to the chosen sub-space $\mathcal{S}^h$.

Petrov-Galerkin methods consider the more general case where $\mathcal{V}^h \neq \mathcal{S}^h$, resulting in differing trial and test function spaces. Such methods must guarantee satisfaction of the LBB (inf-sup) conditions to achieve convergence. Consequently, the selection of appropriate trial and test function spaces which result in stable discretizations is not trivial. Nonetheless, Petrov-Galerkin methods allow for greater flexibility in the construction of numerical approximation schemes.

Finite Element Methods

Finite element methods (FEM) are predicated on the idea that a problem domain $\mathcal{B}_0$ can be discretized into a finite number of simpler sub-domains $\Omega_e \subset \mathcal{B}_0$, individually called elements, and collectively referred to as a "mesh." The basis functions are assumed to be low-order polynomials within each element, and are compactly supported over a given patch of elements. The traditional finite element method assumes these basis functions to be C^0 continuous at element boundaries, yielding a priori satisfaction of compatibility.

Individual FE basis functions φ_a are typically associated with the "nodes" $\mathbf{X}_a$ of the mesh (located at element verticies, along element edges, etc.), such that the kronecker delta property is satisfied, i.e. $\varphi_a(\mathbf{X}_b) = \delta_{ab}$. Consequently, the basis functions comprise a set of interpolants for discrete values of the solution defined at the nodes.

Elements consisting of regular shapes (tetrahedra, hexahedra) also provide a natural means of effecting numerical integration of the weak form through the use of the isoparametric transformation and product Gaussian quadrature rules.

Consistent Linearization of the Weak Form

In order to determine the solution $\mathbf{u}^h \in \mathcal{S}^h$ satisfying the weak form equations, we will choose to employ a Newton-Raphson algorithm:

Compute initial guess $u_{jb}^{(0)}$;
while $||R_{ia}|| < \epsilon$ **do**
  Assemble $K_{iajb} = \partial R_{ia}/\partial u_{jb}$;
  Update $u_{jb}^{(k+1)} \leftarrow u_{jb}^{(k)} - K_{jbia}^{-1} R_{ia}$;
end

Algorithm 1: Newton-Raphson Iteration

Here, R_{ia} denotes the residual (vector), and K_{iajb} denotes the stiffness matrix – the Jacobian of the residual with respect to the independent unknowns u_{jb} (the nodal displacements). The above iteration procedure is repeated until the stopping criterion $||R_{ia}|| < \epsilon$ is reached, for some specified residual measure $||\cdot||$, and tolerance ϵ.

Given the residual equations $R_{ia}(\mathbf{u}^h) = 0 \, \forall i, a$, we may express their first partial

derivatives $\partial R_{ia}/\partial u_{jb}$ with respect to the independent unknowns u_{jb} as

$$\frac{\partial R_{ia}}{\partial u_{jb}} = \int_{\Gamma_0^N} \frac{\partial \bar{p}_i}{\partial u_{jb}} \phi_a \, dA - \int_{\mathcal{B}_0} \frac{\partial P_{ik}}{\partial u_{jb}} \phi_{a,k} \, dV, \tag{2.40}$$

indicating two primary terms ($\bar{\mathbf{p}}$ and $\mathbf{P}$) which must be linearized. Subsequent discussions will focus on the linearization of the first Piola-Kirchhoff stress.

Nonlinear Deformation and Incremental Kinematics

Let us contemplate the linearization of $\partial P_{ik}/\partial u_{jb}$ by applying the chain-rule:

$$\frac{\partial P_{ik}}{\partial u_{jb}} = \frac{\partial P_{ik}}{\partial F_{lm}} \frac{\partial F_{lm}}{\partial u_{jb}}, \tag{2.41}$$

revealing the deformation "gradient operator:"

$$\frac{\partial F_{lm}}{\partial u_{jb}} = \delta_{jl} \varphi_{b,m}. \tag{2.42}$$

If an enhanced strain formulation is employed, only the gradient operator would need to be modified; the subsequent expressions pertaining to $\partial P_{ik}/\partial F_{lm}$ would remain unchanged.

Through further application of the chain-rule, and use of the following identities:

$$\frac{\partial J}{\partial F_{lm}} = J F^{-1}_{ml}, \quad \frac{\partial F^{-1}_{kj}}{\partial F_{lm}} = F^{-1}_{kl} F^{-1}_{mj}, \tag{2.43}$$

one can derive the following result:

$$\frac{\partial P_{ik}}{\partial F_{lm}} = J \sigma_{ij} (F^{-1}_{ml} F^{-1}_{kj} + F^{-1}_{kl} F^{-1}_{mj}) + J \frac{\partial \sigma_{ij}}{\partial F_{lm}} F^{-1}_{kj}. \tag{2.44}$$

If the material model allows for the Cauchy stress to be written directly as a function of the deformation gradient (i.e. $\boldsymbol{\sigma} = f(\mathbf{F})$, as is the case for Cauchy-elastic material models), then a consistent linearization for $\partial \sigma_{ij}/\partial F_{lm}$ may be obtained by direct differentiation.

Otherwise (for hypoelastic material models of the form $\dot{\boldsymbol{\sigma}} = g(\boldsymbol{\sigma}, \mathbf{L})$), we must consider the integral of the stress rate over some finite time interval $\Delta t = t_{k+1} - t_k$:

$$\boldsymbol{\sigma}_{k+1} = \boldsymbol{\sigma}_k + \int_{t_k}^{t_{k+1}} \dot{\boldsymbol{\sigma}} \, dt. \tag{2.45}$$

The corresponding increment of motion is characterized by $\hat{\mathbf{F}} = \mathbf{F}_{k+1} \mathbf{F}_k^{-1} = \hat{\mathbf{R}} \hat{\mathbf{U}}$, which is used to update the stress via the following incremental algorithm (proposed in [42]):

$$\boldsymbol{\sigma}_{k+1} = \hat{\mathbf{R}} \left[\boldsymbol{\sigma}_k + \int_{t_k}^{t_{k+1}} \mathring{\boldsymbol{\sigma}}(\mathbf{D}) \, dt \right] \hat{\mathbf{R}}^T, \tag{2.46}$$

where $\mathbf{D} = \frac{1}{\Delta t}\log\hat{\mathbf{U}}$ denotes the time-averaged rate of deformation over the time step. The resulting algorithmically consistent tangent $\partial\sigma_{ij}/\partial F_{lm}$ is computed as

$$\frac{\partial\sigma_{ij}}{\partial F_{lm}} = \frac{\partial\hat{R}_{ik}}{\partial F_{lm}}\hat{R}_{nk}\sigma_{nj} + \sigma_{in}\hat{R}_{nk}\frac{\partial\hat{R}_{jk}}{\partial F_{lm}} + \hat{R}_{ik}C_{knpq}\hat{R}_{jn}\frac{\partial D_{pq}}{\partial F_{lm}}\Delta t, \tag{2.47}$$

where $C_{knpq} \equiv \partial\mathring{\sigma}_{kn}/\partial D_{pq}$ (the material tangent modulus) is supplied by the constitutive model. The computation of $\partial\hat{R}_{ik}/\partial F_{lm}$ and $\partial D_{pq}/\partial F_{lm}$ may be accurately carried out with the aid of the following expressions:

$$\frac{\partial\hat{D}_{pq}}{\partial\hat{U}_{ij}} = \frac{1}{\Delta t}\sum_{r,s}\hat{Q}_{qr}\hat{Q}_{jr}\mathcal{H}(f,\hat{\lambda}_r,\hat{\lambda}_s)\hat{Q}_{ps}\hat{Q}_{is}; \quad f(\lambda) = \log(\lambda), \tag{2.48}$$

$$\frac{\partial\hat{U}_{ij}}{\partial\hat{B}_{kl}} = \sum_{r,s}\hat{Q}_{jr}\hat{Q}_{lr}\mathcal{H}(g,\hat{\lambda}_r^2,\hat{\lambda}_s^2)\hat{Q}_{is}\hat{Q}_{ks}; \quad g(\lambda) = \sqrt{\lambda}, \tag{2.49}$$

$$\frac{\partial\hat{B}_{kj}}{\partial F_{lm}} = F^{-1}_{mi}(\hat{F}_{ik}\hat{F}_{lj} + \hat{F}_{ij}\hat{F}_{lk}), \tag{2.50}$$

$$\frac{\partial\hat{R}_{ik}}{\partial F_{lm}} = \delta_{il}\hat{R}_{mj}F^{-1}_{jk} - \hat{R}_{in}\frac{\partial\hat{U}_{nj}}{\partial F_{lm}}\hat{U}^{-1}_{jk}, \tag{2.51}$$

where we define

$$\mathcal{H}(f,x,y) \equiv \begin{cases} f'(x), & x = y \\ \frac{f(x)-f(y)}{x-y} & x \neq y \end{cases}, \tag{2.52}$$

and $\hat{\mathbf{U}} = \hat{\mathbf{Q}}\hat{\mathbf{\Lambda}}\hat{\mathbf{Q}}^T$ represents the eigendecomposition of $\hat{\mathbf{U}}$, and $\hat{\lambda}_i$ denote the corresponding eigenvalues of $\hat{\mathbf{U}}$.

2.6 Requirements for Convergence of an Approximation Method

Because variational methods utilize finite dimensional spaces $\mathcal{S}^h$ and $\mathcal{V}^h$, they inherrently incur some error $\mathbf{e} = \mathbf{u}^h - \mathbf{u}$ in approximating the exact solution to the original boundary value problem. The approximation power of a given method is typically characterized by the rate at which a specified error measure $||\mathbf{u}^h - \mathbf{u}||$ (defined on $\mathcal{S}$) decreases as the dimension N of the approximation space $\mathcal{S}^h$ is systematically increased. For finite element methods, increasing the dimension N of the approximation space is synonymous with refining the discretization, to the extent that a specified mesh parameter h (the

diameter of the largest element in the mesh) is decreased. An approximation method will therefore yield solutions $\mathbf{u}^h$ which converge to the exact solution $\mathbf{u}$, provided

$$\lim_{N\to\infty} ||\mathbf{u}^h - \mathbf{u}|| = \lim_{h\to 0} ||\mathbf{u}^h - \mathbf{u}|| = 0. \tag{2.53}$$

Further, a method whose solution error can be bounded by an estimate

$$||\mathbf{u}^h - \mathbf{u}|| \leq Ch^\alpha ||\mathbf{u}||, \tag{2.54}$$

will converge at a rate of order α.

For an approximation method to achieve convergence, several conditions must be satisfied, namely: approximability, compatibility, stability, and quadrature consistency. These conditions are summarized in the following sections.

Approximability

To achieve α^{th}-order convergence, the approximation space $\mathcal{S}^h$ must contain $[P^k(\mathcal{B}_0)]^d$ (the space of vector-valued polynomial functions of maximal degree $k = \alpha + 1$) as a subset $\mathcal{S}^h \supset [P^k(\mathcal{B}_0)]^d$.

This property is sometimes referred to as *approximability*, reflecting a given method's ability to well-approximate the solution locally as a low-order polynomial. Alternativley, this condition is known as polynomial *reproducibility*, or *completeness*. This condition can be rationalized by the Weierstrass approximation theorem, which asserts that any smooth function can be approximated by polynomials to arbitrary precision.

Compatibility

Compatibility, in an abstract sense, imposes requirements upon the continuity of trial solutions $\mathbf{u}^h \in \mathcal{S}^h$. For conforming finite element methods, this condition is automatically satisfied, as the trial solution space consists of sufficiently continuous functions, such that $\mathcal{S}^h \subset C^0$.

By comparison, non-conforming finite element methods admit more general functions $\mathbf{u}^h \in \mathcal{S}^h \not\subset C^0$. Such spaces of functions must satisfy additional weak compatibility requirements. Namely, Stummel has proposed in [52] the necessary and sufficient conditions

for convergence of a non-conforming finite element method, necessitating passage of the *generalized patch test*:

For a given patch $\mathcal{P} \subset \overline{\mathcal{B}}_0$ and an approximating sequence of functions $u^h \in H^k(\mathcal{B}_0)$: for every $\mathbf{X} \in \mathcal{P}$ there exists an open neighborhood O in $\mathbb{R}^d$ such that

$$\lim_{h\to 0} \sum_{\forall \Omega_e} \int_{\partial\Omega_e} v\, D^\alpha u^h|_{\Omega_e} \mathbf{n}\, da = \mathbf{0} \tag{2.55}$$

for all test functions $v \in C_0^\infty(O)$, and $|\alpha| \leq k-1$.

Shi later proposed the F-E-M test in [13] as an alternative, sufficient condition for convergence, with a corresponding interface requirement (the F-test):

$$\left| \int_{\Omega_a \cap \Omega_b} [\![u^h]\!]\, da \right| \leq O(h^{d/2}) ||u^h||_{\Omega_a \cup \Omega_b} \quad \forall \Omega_a \cap \Omega_b \neq \emptyset. \tag{2.56}$$

Stability

The LBB (inf-sup) conditions (introduced in [3], [8]) pertain to potentially differing choices for $\mathcal{S}^h$ and $\mathcal{V}^h$ with appropriately defined norms. For the model problem with bilinear form $a\colon \mathcal{S} \times \mathcal{V} \to \mathbb{R}$, *uniqueness* of a given solution is contingent upon the inf-sup condition:

$$\inf_{\mathbf{u}^h \in \mathcal{S}^h} \sup_{\mathbf{v}^h \in \mathcal{V}^h} \frac{a(\mathbf{u}^h, \mathbf{v}^h)}{||\mathbf{u}^h||\, ||\mathbf{v}^h||} > 0. \tag{2.57}$$

If a is symmetric and $\mathcal{S}^h = \mathcal{V}^h$, this condition is equivalent to the requirement that a be ellipitic (coercive):

$$a(\mathbf{u}^h, \mathbf{u}^h) \geq C_c ||\mathbf{u}^h||^2 \quad \forall \mathbf{u}^h \in \mathcal{S}^h. \tag{2.58}$$

Existence of a solution further depends upon the condition that a be bounded:

$$a(\mathbf{u}^h, \mathbf{v}^h) \leq C_b ||\mathbf{u}^h||\, ||\mathbf{v}^h|| \quad \forall \mathbf{u}^h \in \mathcal{S}^h,\, \mathbf{v}^h \in \mathcal{V}^h, \tag{2.59}$$

and surjective:

$$\sup_{\mathbf{u}^h \in \mathcal{S}^h} a(\mathbf{u}^h, \mathbf{v}^h) > 0 \quad \forall \mathbf{v}^h \in \mathcal{V}^h. \tag{2.60}$$

Heuristically, these conditions require that individual element stiffness matricies be of full rank, excluding rigid body modes of deformation. This necessitates both: the specification of a stable discretization, and sufficiently accurate evaluation (numerical integration) of the weak form.

Quadrature Consistency

Considering the variational formulation of the model boundary value problem in (2.34), if the exact solution $\mathbf{u} \in \mathcal{S}$ to the weak form is contained within the chosen approximation space (i.e. if $\mathbf{u} \in \mathcal{S}^h$), we require that $\mathbf{u}$ be identified as the unique solution to the Galerkin approximation in (2.38), namely:

$$\mathcal{R}(\mathbf{u}, \mathbf{v}^h) = 0 \quad \forall \mathbf{v}^h \in \mathcal{V}^h. \tag{2.61}$$

This property is referred to as *Galerkin exactness*, and is particularly relevant to the satisfaction of finite element patch tests, which demonstrate Galerkin exactness when the exact solution is a low-order polynomial.

In particular, given a stress field $P_{ij}(\mathbf{u})$ arising from the exact solution $\mathbf{u} \in \mathcal{S}^h$, and for the given boundary conditions $\bar{p}_i = P_{ij}N_j$ and $\rho_0 b_i = -P_{ij,j}$, we may express the residual equations as

$$R_{ia} = \int_{\mathcal{B}_0} P_{ij}\phi_{a,j}\, dV + \int_{\mathcal{B}_0} P_{ij,j}\phi_a\, dV - \int_{\partial\mathcal{B}_0} P_{ij}N_j\phi_a\, dA = 0 \quad \forall i,\, a. \tag{2.62}$$

If we suppose that the exact solution is well-approximated by low-order polynomials, i.e.

$$u_i(\mathbf{X}) = \sum_{|\alpha|=0}^{k} a_{i\alpha}\mathbf{X}^\alpha, \quad P_{ij}(\mathbf{X}) = \sum_{|\alpha|=0}^{k-1} b_{ij\alpha}\mathbf{X}^\alpha, \tag{2.63}$$

then the resulting conditions for Galerkin exactness are:

$$\int_{\mathcal{B}_0} \mathbf{X}^\alpha \phi_{a,i}\, dV + \int_{\mathcal{B}_0} \mathbf{X}^\alpha_{,i}\phi_a\, dV = \int_{\partial\mathcal{B}_0} \mathbf{X}^\alpha N_i\phi_a\, dA \quad \forall i,\, a,\, |\alpha| \leq k-1. \tag{2.64}$$

The above consistency requirements are required to hold over the problem domain $\mathcal{B}_0$ as a whole, or equivalently over each individual element domain Ω_e:

$$\int_{\Omega_e} \mathbf{X}^\alpha \phi_{a,i}\, dV + \int_{\Omega_e} \mathbf{X}^\alpha_{,i}\phi_a\, dV = \int_{\partial\Omega_e} \mathbf{X}^\alpha N_i\phi_a\, dA \quad \forall i,\, a,\, |\alpha| \leq k-1,\, \Omega_e \subset \mathcal{B}_0. \tag{2.65}$$

The above conditions are sufficient for satisfaction of the Irons patch test up to k^{th} order, provided $\mathcal{S}^h \supset [P^k(\mathcal{B}_0)]^d$. It should be emphasized that these conditions apply specifically to the test functions $\phi_a \in \mathcal{V}^h$.

In most practical situations, however, the integral expressions in (2.38) are evaluated only approximately; numerical quadrature rules are defined on the elements and on their boundaries, such that

$$\int_{\Omega_e} f(\mathbf{X})dV \approx \sum_{q=1}^{N_{qp}} w_q f(\mathbf{X}_q), \quad \int_{\partial\Omega_e} f(\mathbf{X})dA \approx \sum_{b=1}^{N_{bp}} w_b f(\mathbf{X}_b). \tag{2.66}$$

This yields a discrete form of (2.65), henceforth referred to as *quadrature consistency*:

$$\sum_{q=1}^{N_{qp}} w_q \left[\mathbf{X}_q^\alpha \phi_{a,i}^{(q)} + \mathbf{X}_{q,i}^\alpha \phi_a^{(q)}\right] = \sum_{b=1}^{N_{bp}} w_b \mathbf{X}_b^\alpha N_i^{(b)} \phi_a^{(b)} \quad \forall i,\, a,\, |\alpha| \leq k-1,\, \Omega_e \subset \mathcal{B}_0. \tag{2.67}$$

These conditions effectively impose a set constraints on the accuracy of the chosen quadrature rules, and/or on the choice of test functions. Failure to satisfy the above conditions results in issues of integration error, and correspondingly, loss of convergence.

Chapter 3

Partitioned Element Methods

This chapter defines a general class of polytopal element formulations referred to as partitioned element methods (PEM). The essential characteristics and mathematical requirements placed upon these methods are formally stated, giving rise to a family of different approaches, for which some formal investigations are conducted in subsequent chapters. Several specific formulations are summarized in detail, and a number of existing methods are herein classified as particular instances of partitioned element methods.

3.1 Overview

Partitioned element methods are finite element-like methods which approach the task of constructing approximations to an arbitrary polytopal element's nodal shape functions by partitioning the element into sub-domains (quadrature cells). The element partition serves a dual purpose: it is used to establish a composite quadrature rule for the element, and to define a finite dimensional function space, from which the element's shape functions are selected as the solutions to corresponding boundary value problems, defined locally on the element.

Partitioned element methods are motivated by the idea that it is generally easier and more efficient to define complicated functions over arbitrary domains if the functions are defined in a piecewise polynomial fashion over simpler sub-domains. This is precisely the mentality which likewise motivates the finite element method and other related numerical approximation methods.

The PEM is driven by the need for establishing stable and efficient quadrature rules on arbitrary polytopes. Unlike virtual element methods which typically circumvent the use of quadrature altogether, partitioned element methods recognize the necessity of using domain quadrature rules to evaluate nonlinear residual and stiffness contributions. The use of sufficient quadrature also yields a stable integration of the weak form which does not rely upon unphysical stabilization parameters.

In contrast with traditional perspectives which regard the shape functions as being continuously defined on element domains (i.e. generalized barycentric coordinates), the PEM exploits the fact that the shape functions and their gradients only need to be evaluated at a discrete number of quadrature points. With this in mind, PEM approximation spaces are deliberately constructed around the quadrature cell partition of the element, and consequently resemble finite element approximation spaces.

The resulting approximations to the element's shape functions are altogether subject to the conditions of approximability, compatibility, stability, and quadrature consistency, as discussed in chapter 2. Together, these conditions impose a number of unique requirements upon the element's partition, it's corresponding quadrature rules, and the associated cell-based approximation spaces.

In the following sections, an abstract framework for the PEM is established, describing the shape function boundary value problems defined on an element, and their corresponding approximations. We further enumerate several specific partitioned element methods, and provide an assessment of their potential strengths and weaknesses.

3.2 Definition of Polytopal Element Shape Functions

Consider the structure of an arbitrary polyhedral element $\Omega \subset \mathbb{R}^3$, as depicted in Figure 3.1. The element's boundary $\partial\Omega$ may be subdivided into polygonal faces $F \subset \partial\Omega$, such that each face F is shared entirely with an adjacent element of the mesh, or with the mesh boundary. In turn, the boundary of each such face F may be subdivided into linear edges $E \subset \partial F$, such that each edge E is shared by one other face of the element. The end-points of each edge are called nodes, denoted V, and may be shared by multiple edges.

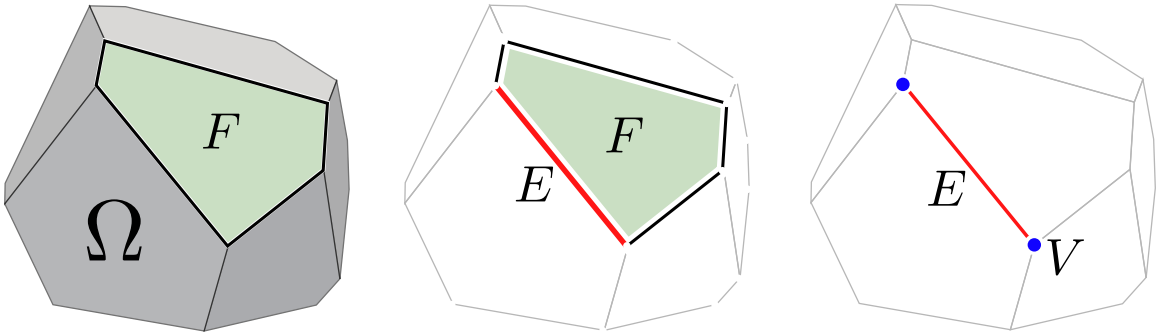

Figure 3.1. A representative polyhedral element $\Omega \subset \mathbb{R}^3$, a polygonal face $F \subset \partial\Omega$, a linear edge $E \subset \partial F$, and a node V.

The function spaces to which the element's shape functions belong are effectively broken Sobolev spaces, where a given shape function $\varphi \in \mathcal{W}_k(\overline{\Omega})$ is defined independently on the open interior of each polyhedral element $\Omega \subset \mathbb{R}^3$, and on its boundary $\partial\Omega$, such that

$$\mathcal{W}_k(\overline{\Omega}) = \left\{\varphi|_\Omega \in H^k(\Omega) : \mathcal{L}_\Omega\varphi = f_\Omega \text{ in } \Omega,\ \varphi|_F \in \mathcal{W}_k(\overline{F})\ \forall F \in \partial\Omega\right\}, \tag{3.1}$$

$$\mathcal{W}_k(\overline{F}) = \left\{\varphi|_F \in H^k(F) : \mathcal{L}_F\varphi = f_F \text{ in } F,\ \varphi|_E \in \mathcal{W}_k(\overline{E})\ \forall E \in \partial F\right\}, \tag{3.2}$$

$$\mathcal{W}_k(\overline{E}) = \left\{\varphi|_E \in H^k(E) : \mathcal{L}_E\varphi = f_E \text{ in } E,\ \varphi|_V \in \mathbb{R}\ \forall V \in \partial E\right\}. \tag{3.3}$$

In essence, a given function $\varphi|_\Omega \in H^k(\Omega)$ defined on the element's interior is related to a corresponding boundary function $\varphi|_{\partial\Omega} \equiv \bar{\varphi}$ (which itself is a broken $H^k(\partial\Omega)$ function) via a well-posed Dirichlet boundary value problem:

$$\mathcal{L}_\Omega\varphi = f_\Omega \quad \forall \mathbf{X} \in \Omega \quad \text{s.t.} \quad \varphi = \bar{\varphi} \quad \forall \mathbf{X} \in \partial\Omega, \tag{3.4}$$

where $\mathcal{L}_\Omega$ denotes a linear differential operator, and $f_\Omega \in L^2(\Omega)$ is a generic forcing function. The element's degrees of freedom are collectively accounted for in the boundary function $\bar{\varphi}$, and in the forcing function f_Ω. Consequently, the interior function $\varphi|_\Omega$ is uniquely defined, provided there exists a unique solution to (3.4). In turn, we suppose that $\varphi|_F \in H^k(F)$ is the solution to a similar (2-dimensional) boundary value problem defined on each face F, and $\varphi|_E \in H^k(E)$ is the solution to a (1-dimensional) BVP on each edge E.

The advantage of defining shape functions in this manner is that it affords a great deal of flexibility in the construction of arbitrary order interpolants (or enhancement

functions), while maintaining $C^0(\mathcal{B}_0)$ continuity at inter-element interfaces. Moreover, given that the shape functions are uniquely defined at every point $\mathbf{X} \in \Omega$, they are amenable to post-processing and visualization-related tasks.

Harmonic Shape Functions

The simplest choice of $\mathcal{L}_\Omega = -\nabla^2$ and $f_\Omega = 0$ corresponds to Laplace's equation:

$$\nabla^2 \varphi = 0 \quad \forall \mathbf{X} \in \Omega \quad \text{s.t.} \quad \varphi = \bar{\varphi} \quad \forall \mathbf{X} \in \partial\Omega, \tag{3.5}$$

whose solution φ is harmonic on Ω (and likewise on each face F and edge E – refer to Figure 3.2). Harmonic shape functions form a partition of unity, satisfy linear completeness, and arise from degrees of freedom borne only by the nodes of each element (i.e. the nodal values $\varphi|_V$); therefore, they satisfy the kronecker delta property. As such, harmonic shape functions conform to the requirements of generalized barycentric coordinates.

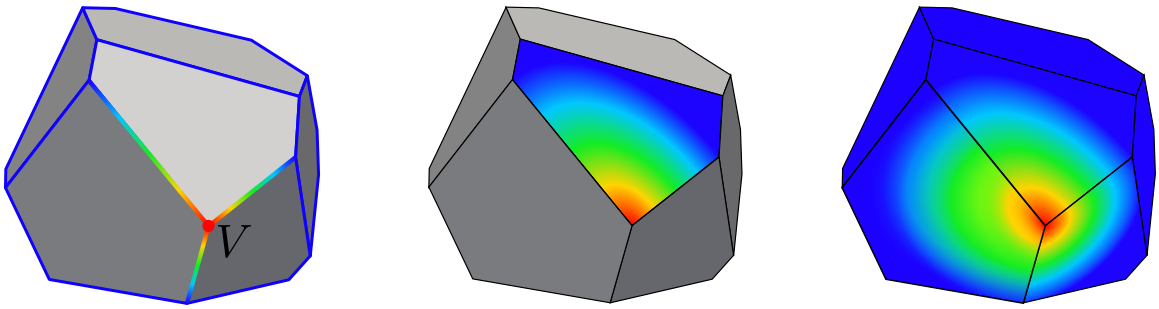

Figure 3.2. The harmonic shape function corresponding to the indicated node V, defined hierarchially on each edge, face, and the element.

If instead $f_\Omega \neq 0$ (corresponding to Poisson's equation), then

$$-\nabla^2 \varphi = f_\Omega \quad \forall \mathbf{X} \in \Omega \quad \text{s.t.} \quad \varphi = \bar{\varphi} \quad \forall \mathbf{X} \in \partial\Omega, \tag{3.6}$$

and we may introduce additional degrees of freedom through f_Ω belonging to the element (or its edges, faces). These degrees of freedom are not necessarily associated with nodal evaluations of φ, but instead may be designed to exhibit certain desirable characteristics (to recover a particular order of polynomial completeness). The corresponding solution to (3.6) is not harmonic; instead, we shall refer to functions which satisfy (3.6) as *generalized harmonic shape functions*.

Harmonic shape functions are not a new concept; Gordon and Wixom were among the first authors to propose the idea in [27], and Martin et al. later considered their application to polyhedral finite elements in [37]. However, obtaining exact solutions to (3.5) is generally infeasible for arbitrary polyhedra. In practice, approximate solutions must be considered.

In particular, Bishop has proposed a method for constructing FE approximations to harmonic shape functions in [7]. Additionally, the VETFEM ([43], [45]) and the original PEM presented in [44], may be viewed as techniques for obtaining discrete approximations to harmonic shape functions. Likewise, many virtual element methods ([10], [15], [16]) suppose that the element shape functions are harmonic over individual element domains, though they are never explicitly constructed or represented as such.

It herein becomes of interest to determine suitable approximations to harmonic shape functions on arbitrary polyhedra. A number of methods to achieve this end are subsequently discussed.

3.3 Shape Function Approximation Methods

The exact solution $\varphi \in \mathcal{U}(\Omega) = \{\varphi \in H^1(\Omega) : \varphi = \bar{\varphi}\, \forall \mathbf{X} \in \partial\Omega\}$ to Poisson's equation in (3.6) also satisfies the equivalent weak form:

$$\int_\Omega (\nabla^2 \varphi + f_\Omega)\eta \, dV = 0 \quad \forall \eta \in \mathcal{U}_0(\Omega), \tag{3.7}$$

or

$$\int_\Omega \nabla\varphi \cdot \nabla\eta \, dV - \int_{\partial\Omega} \frac{\partial\varphi}{\partial N}\eta \, dA = \int_\Omega f_\Omega \, \eta \, dV \quad \forall \eta \in \mathcal{U}_0(\Omega), \tag{3.8}$$

where $\mathcal{U}_0(\Omega) = \{\eta \in H^1(\Omega) : \eta = 0\, \forall \mathbf{X} \in \partial\Omega\}$ denotes an appropriately defined space of admissible variations – test functions.

A vast array of different variational methods may be employed to obtain an approximate solution $\varphi^h \in \mathcal{U}^h(\Omega)$ satisfying

$$\int_\Omega \nabla\varphi^h \cdot \nabla\eta^h \, dV - \int_{\partial\Omega} \frac{\partial\varphi^h}{\partial N}\eta^h \, dA = \int_\Omega f_\Omega \, \eta^h \, dV \quad \forall \eta^h \in \mathcal{U}_0^h(\Omega), \tag{3.9}$$

where $\mathcal{U}^h(\Omega)$ and $\mathcal{U}_0^h(\Omega)$ are taken to be finite-dimensional approximation spaces. Consequently, it is of interest to determine the essential requirements placed upon a given

approximation φ^h for the purposes of evaluating weak form integrals.

Specifically, for a finite element approximation to the model problem given in (2.36), consider the evaluation of an element's local bilinear form $a_\Omega(\mathbf{u}, \mathbf{v})$, where $\mathbf{u} = \sum_{a=1}^N \varphi_a \mathbf{u}_a$ and $\mathbf{v} = \sum_{a=1}^N \varphi_a \mathbf{v}_a$ are written in terms of the element's shape functions $\{\varphi_a\}_{a=1}^N$. An approximate evaluation of $a_\Omega(\mathbf{u}, \mathbf{v})$ is obtained by making the substitution $a_\Omega(\mathbf{u}^h, \mathbf{v}^h)$, where $\mathbf{u}^h = \sum_{a=1}^N \varphi_a^h \mathbf{u}_a$ and $\mathbf{v}^h = \sum_{a=1}^N \varphi_a^h \mathbf{v}_a$ are instead represented in terms of the approximations $\left\{\varphi_a^h\right\}_{a=1}^N$ to the element's shape functions.

According to the virtual element decomposition proposed in [15], we may express a given function $\mathbf{u} = \Pi_k^\Omega \mathbf{u} + (\mathbf{u} - \Pi_k^\Omega \mathbf{u})$ in terms of a low-order polynomial part $(\Pi_k^\Omega \mathbf{u})$ (up to degree k) and a non-polynomial part $(\mathbf{u} - \Pi_k^\Omega \mathbf{u})$, where $\Pi_k^\Omega : L^2(\Omega) \mapsto P^k(\Omega)$ is a corresponding polynomial projection operator satisfying $a_\Omega(\Pi_k^\Omega \mathbf{u}, \mathbf{v} - \Pi_k^\Omega \mathbf{v}) = 0 \ \forall \mathbf{u}, \mathbf{v}$, and thus

$$a_\Omega(\mathbf{u}, \mathbf{v}) = a_\Omega(\Pi_k^\Omega \mathbf{u}, \Pi_k^\Omega \mathbf{v}) + a_\Omega(\mathbf{u} - \Pi_k^\Omega \mathbf{u}, \mathbf{v} - \Pi_k^\Omega \mathbf{v}). \tag{3.10}$$

The first term appearing in the right-hand side of (3.10) accounts for the consistency of the finite element approximation, whereas the second term provides stability. To maintain consistency, the first term must be computed exactly, to the extent that

$$a_\Omega(\Pi_k^\Omega \mathbf{u}, \Pi_k^\Omega \mathbf{v}) = a_\Omega(\Pi_k^\Omega \mathbf{u}^h, \Pi_k^\Omega \mathbf{v}^h), \tag{3.11}$$

yielding the $k-$consistency property:

$$a_\Omega(\Pi_k^\Omega \mathbf{u}^h, \mathbf{v}^h) = a_\Omega(\Pi_k^\Omega \mathbf{u}, \mathbf{v}) \quad \forall \mathbf{v} \in \mathcal{V}^h(\Omega). \tag{3.12}$$

However, the second term need only be sufficiently well-approximated by

$$a_\Omega(\mathbf{u} - \Pi_k^\Omega \mathbf{u}, \mathbf{v} - \Pi_k^\Omega \mathbf{v}) \approx a_\Omega(\mathbf{u}^h - \Pi_k^\Omega \mathbf{u}^h, \mathbf{v}^h - \Pi_k^\Omega \mathbf{v}^h), \tag{3.13}$$

to the extent that the correct order of convergence is maintained, and the inf-sup condition is altogether satisfied. In [15], this is characterized by the assertion that there exist two positive constants a_* and a^* which are independent of the chosen discretization, such that the following stability condition holds:

$$a_* a_\Omega(\mathbf{v}, \mathbf{v}) \leq a_\Omega(\mathbf{v}^h, \mathbf{v}^h) \leq a^* a_\Omega(\mathbf{v}, \mathbf{v}) \quad \forall \mathbf{v} \in \mathcal{V}^h(\Omega). \tag{3.14}$$

It is argued that these conditions are necessary and sufficient to guarantee convergence of the resulting method when the local approximations $\mathbf{u}^h$ and $\mathbf{v}^h$ are used in place of $\mathbf{u}$ and $\mathbf{v}$.

It should be remarked that the evaluation of $a_\Omega(\mathbf{u}, \mathbf{v})$ will be further approximated through the use of numerical quadrature on Ω, denoted as $a^h_\Omega(\mathbf{u}, \mathbf{v})$. Incidentally, the use of low-order quadrature rules may alternatively be viewed as an exact integration of corresponding low-order approximations to $\mathbf{u}$ and $\mathbf{v}$, i.e. $a^h_\Omega(\mathbf{u}, \mathbf{v}) = a_\Omega(\mathbf{u}^h, \mathbf{v}^h)$, and is therefore subject to the conditions previously described.

With the above considerations borne in mind, we propose a set of requirements on the approximation space $\mathcal{U}^h(\Omega)$ (and $\mathcal{U}^h_0(\Omega)$):

(I) $\Pi^\Omega_k \varphi = \Pi^\Omega_k \varphi^h \ \forall \varphi \in \mathcal{U}(\Omega)$, and therefore $\mathcal{U}^h(\Omega) \supset P^k(\Omega)$.

(II) $a_* a_\Omega(\mathbf{v}, \mathbf{v}) \leq a_\Omega(\mathbf{v}^h, \mathbf{v}^h) \leq a^* a_\Omega(\mathbf{v}, \mathbf{v}) \quad \forall \mathbf{v} \in \mathcal{V}^h(\Omega)$.

An important distinction should be made regarding the requirements placed upon such approximation methods: it is not required that the approximations φ^h converge to φ as the dimension of $\mathcal{U}^h(\Omega)$ is systematically increased.

Non-conforming Galerkin Approximations to Generalized Harmonic Shape Functions

If the boundary conditions imposed upon a given shape function are relaxed to the extent that $\varphi^h \neq \bar{\varphi}$ on $\partial\Omega$, then clearly $\mathcal{U}^h(\Omega) \not\subset \mathcal{U}(\Omega)$, and one must resort to the use of non-conforming approximation methods. In such cases, the boundary conditions must be imposed in a weak sense, such that φ^h still converges to φ as the dimension of the non-conforming approximation space $\mathcal{U}^h(\Omega)$ is increased. A number of potential weak enforcement strategies are suggested in the following sections.

Weak Enforcement of Boundary Conditions via a Lagrange Multiplier Method

One possible approach would be to consider a Lagrange multiplier method, to weakly enforce the boundary condition $\varphi = \bar{\varphi}$ on $\partial\Omega$ via

$$\min_{\varphi,\, \lambda} \mathcal{L}(\varphi, \lambda), \tag{3.15}$$

$$\mathcal{L}(\varphi,\lambda) \equiv \frac{1}{2}\int_\Omega \nabla\varphi\cdot\nabla\varphi\, dV - \int_\Omega f_\Omega\,\varphi\, dV + \int_{\partial\Omega}[\varphi-\bar{\varphi}]\,\lambda\, dA, \tag{3.16}$$

involving the specification of a Lagrange multiplier field $\lambda \in \Lambda(\partial\Omega) = \{\lambda \in L^2(\partial\Omega)\}$, and it's corresponding approximation $\lambda^h \in \Lambda^h(\partial\Omega) \subset \Lambda(\partial\Omega)$. Differentiation of the Lagrangian yields two sets of equations in terms of the approximations $\varphi^h \in \mathcal{U}^h(\Omega)$ and $\lambda^h \in \Lambda^h(\partial\Omega)$:

$$\int_\Omega \nabla\varphi^h\cdot\nabla\eta^h\, dV - \int_\Omega f_\Omega\eta^h\, dV + \int_{\partial\Omega}\lambda^h\eta^h\, dA = 0 \quad \forall\eta^h \in \mathcal{U}^h(\Omega), \tag{3.17}$$

$$\int_{\partial\Omega}(\varphi^h-\bar{\varphi})\,\mu^h\, dA = 0 \quad \forall\mu^h \in \Lambda^h(\partial\Omega). \tag{3.18}$$

Suppose finite-dimensional bases are established for $\mathcal{U}^h(\Omega)$ and $\Lambda^h(\partial\Omega)$, i.e.

$$\varphi^h(\mathbf{X}) = \sum_{a=1}^{N}\psi_a(\mathbf{X})\varphi_a, \quad \lambda^h(\mathbf{X}) = \sum_{a=1}^{M}\chi_a(\mathbf{X})\lambda_a, \tag{3.19}$$

such that

$$\sum_{a=1}^{N}\left[\int_\Omega \nabla\psi_a\cdot\nabla\psi_b\, dV\right]\varphi_a + \sum_{c=1}^{M}\left[\int_{\partial\Omega}\psi_b\,\chi_c\, dA\right]\lambda_c = \int_{\partial\Omega} f_\Omega\,\psi_b\, dA \quad \forall b, \tag{3.20}$$

$$\sum_{b=1}^{N}\left[\int_{\partial\Omega}\chi_c\,\psi_b\, dA\right]\varphi_b = \int_{\partial\Omega}\bar{\varphi}\,\chi_c\, dA \quad \forall c. \tag{3.21}$$

Given an appropriate selection for the indicated bases, the determination of the unknowns (φ_a and λ_a) entails the solution of a saddle-point system of equations, written in matrix-vector format:

$$\begin{bmatrix} \mathbf{A} & \mathbf{B} \\ \mathbf{B}^T & \mathbf{0} \end{bmatrix}\begin{Bmatrix} \boldsymbol{\varphi} \\ \boldsymbol{\lambda} \end{Bmatrix} = \begin{Bmatrix} \mathbf{f} \\ \bar{\boldsymbol{\varphi}} \end{Bmatrix}, \tag{3.22}$$

where

$$A_{ab} = \int_\Omega \nabla\psi_a\cdot\nabla\psi_b\, dV, \quad B_{bc} = \int_{\partial\Omega}\psi_b\,\chi_c\, dA, \tag{3.23}$$

$$f_b = \int_{\partial\Omega} f_\Omega\,\psi_b\, dA, \quad \bar{\varphi}_c = \int_{\partial\Omega}\bar{\varphi}\,\chi_c\, dA. \tag{3.24}$$

The main advantage of this approach is that virtually any space of functions may be selected for $\mathcal{U}^h(\Omega)$, such that the resulting approximations $\varphi^h \in \mathcal{U}^h(\Omega)$ deliberately do not contain sharp gradients.

Arguably the simplest (and most efficient) choice is $\mathcal{U}^h(\Omega) = P^k(\Omega)$, resembling certain formulations of the VETFEM ([43], [45]) where the basis functions for the Lagrange multiplier field $\chi_c(\mathbf{X}) = \delta(\mathbf{X} - \mathbf{X}_c)\ \forall c = 1, \ldots, N_v$ are Dirac delta functions associated with the individual nodes of the element. A potential shortcoming of this particular choice for χ_c is that the resulting shape functions may nonetheless yield sharp gradients along short element edges.

Various other choices for the Lagrange multiplier basis are possible which may yield less spurious solutions (for instance $\Lambda^h(\partial\Omega) = P^k(\partial\Omega)$), though these may lead to ill-posedness of the saddle-point problem. More sophisticated linear solution methodologies are required in these cases.

Weak Enforcement of Boundary Conditions via Nitsche's Method

As a viable alternative to the Lagrange multiplier method presented in the previous section, one may instead consider using Nitsche's method (refer to [32]) as a means of weakly enforcing the boundary conditions for a given shape function, i.e.

$$\begin{aligned}\int_\Omega \nabla\varphi^h \cdot \nabla\eta^h \, dV - \int_{\partial\Omega} \left[\frac{\partial\varphi^h}{\partial N}\eta^h + \varphi^h\frac{\partial\eta^h}{\partial N}\right] dA + \frac{1}{\gamma|\partial\Omega|^\beta}\int_{\partial\Omega}\varphi^h\eta^h \, dA \\ = \int_\Omega f_\Omega\,\eta^h \, dV - \int_{\partial\Omega}\bar{\varphi}\frac{\partial\eta^h}{\partial N}\, dA + \frac{1}{\gamma|\partial\Omega|^\beta}\int_{\partial\Omega}\bar{\varphi}\eta^h \, dA \quad \forall\eta^h \in \mathcal{U}^h(\Omega),\end{aligned} \tag{3.25}$$

where $\gamma > 0$ is a stabilization parameter, $|\partial\Omega|$ denotes the surface area of $\partial\Omega$, and $\beta = (d-1)^{-1}$ for $\Omega \subset \mathbb{R}^d$, $d \geq 2$.

Provided the stabilization parameter γ is specified appropriately, the Galerkin approximation φ^h can be obtained as the solution to a symmetric, positive-definite system of equations: $\mathbf{A}\boldsymbol{\varphi} = \mathbf{f}$, where

$$A_{ab} = \int_\Omega \nabla\psi_a \cdot \nabla\psi_b \, dV - \int_{\partial\Omega}\left[\frac{\partial\psi_a}{\partial N}\psi_b + \psi_a\frac{\partial\psi_b}{\partial N}\right] dA + \frac{1}{\gamma|\partial\Omega|^\beta}\int_{\partial\Omega}\psi_a\,\psi_b \, dA, \tag{3.26}$$

$$f_b = \int_\Omega f_\Omega\,\psi_b \, dV - \int_{\partial\Omega}\bar{\varphi}\frac{\partial\psi_b}{\partial N}\, dA + \frac{1}{\gamma|\partial\Omega|^\beta}\int_{\partial\Omega}\bar{\varphi}\,\psi_b \, dA. \tag{3.27}$$

As discussed in the previous section, a rather natural choice for the space of approximating functions is $\mathcal{U}^h(\Omega) = P^k(\Omega)$. The resulting method yields reasonably well-conditioned stiffness matricies for convex shapes, even when the elements possess degenerate edges. However, experimental evidence suggests that for non-convex shapes, the

resulting shape function approximations may succumb to Runge's phenomenon. A more thorough investigation of this behavior is presented in chapter 5.

These considerations have led to the conclusion that approximations consisting of piecewise polynomials may yield more well-behaved solutions. The remainder of our discussion will focus upon such methods.

3.4 Piecewise Polynomial Approximations to Generalized Harmonic Shape Functions

Partitioned element methods consider the approximation to a given element's shape functions via piecewise polynomials defined over a partition of the element's domain. In this regard, the approach proposed by Bishop in [7] is properly regarded as a partitioned element method which utilizes an FE partition of the elements to approximate their shape functions; henceforth, this scheme is given the moniker FE-PEM. The eponymous partitioned element method introduced in [44] solves (3.9) by empolying an approximation scheme which closely resembles a stabilized virtual element method, hence it shall be labeled VE-PEM.

Herein we propose a novel alternative approach based upon the interior penalty discontinuous Galerkin finite element method (henceforth, the DG-PEM).

The Element Partition

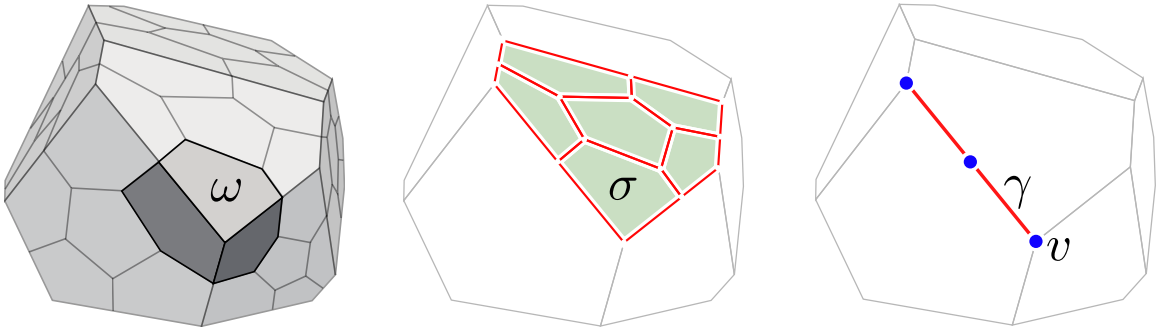

Figure 3.3. A representative polyhedral element $\Omega \subset \mathbb{R}^3$, and it's corresponding partition into cells, facets, segments, and verticies.

Consider a partition $\mathcal{T}_\omega(\Omega)$ of a given polyhedral element Ω into polyhedral cells $\omega \subset \Omega$. The boundary of each cell consists of polygonal facets $\sigma \subset \partial\omega$. Further, denote by Γ_ω the

set of all interior cell interfaces (facets) shared by two adjacent cells, such that a given polygonal facet σ belongs either to Γ_ω, or to the boundary of the element $\partial\Omega$.

In turn, let $\mathcal{T}_\sigma(F)$ denote the partition of a given face $F \subset \partial\Omega$ into polygonal facets $\sigma \subset F$. The boundary of each facet consists of linear segments $\gamma \subset \partial\sigma$. For each face F, Γ_σ shall denote the set of all interior facet interfaces (segments) shared by two facets belonging to F, such that a given linear segment γ belongs either to Γ_σ or ∂F.

Finally, $\mathcal{T}_\gamma(E)$ denotes the partition of a given edge $E \subset \partial F$ into linear segments $\gamma \subset E$. The endpoints of each segment are called verticies, denoted v. For each edge E, Γ_γ denotes the set of all interior segment interfaces (verticies) shared by two segments belonging to E, such that a given vertex v belongs either to Γ_γ or ∂E. Not all verticies are nodes, but each node is coincident with a corresponding vertex.

Several simple partitioning schemes are proposed:

- **Edge-based**: For star-convex shapes – the vertex-averaged centroid is used to sub-divide the element into triangles (in 2D) or tetrahedra (in 3D) which are associated with each linear edge of the element.

- **Node-based**: For arbitrary shapes – the element is sub-divided into quadrature cells corresponding to the tributary area surrounding each node.

- **Random Voronoi**: For arbitrary shapes – the element is sub-divided into Voronoi cells, whose corresponding voronoi sites are generated via a constrained maximal poisson-disk sampling process, as described in [20].

The aforementioned approaches are further illustrated in Figure 3.4.

We denote the volume of a given cell as $|\omega|$, the area of a facet as $|\sigma|$, and the length of a segment as $|\gamma|$. Each facet possesses an associated normal direction $\mathbf{N}_\sigma$, whose orientation is outward from Ω for all $\sigma \in \partial\Omega$. The orientation of $\mathbf{N}_\sigma$ is otherwise arbitrary for all $\sigma \in \Gamma_\omega$. Likewise,

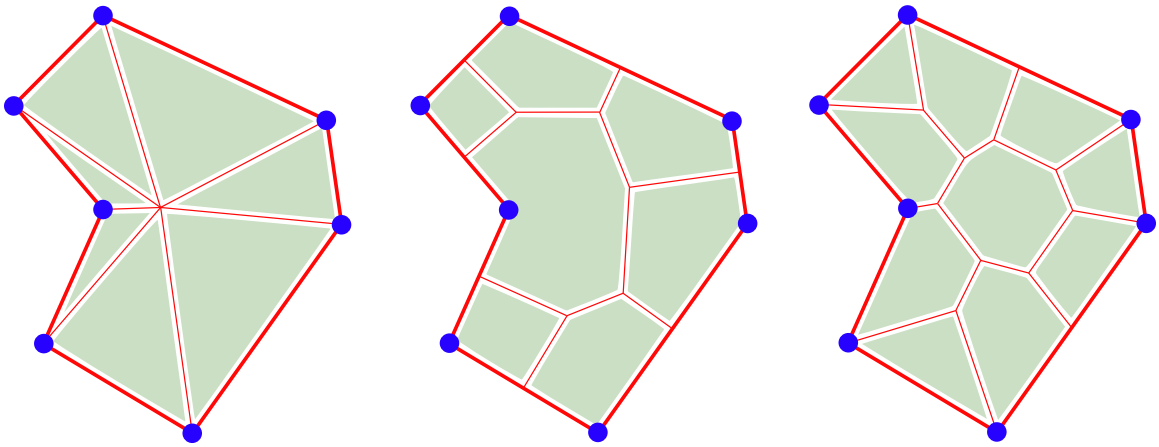

Figure 3.4. Polygonal element partitioning schemes, from left to right: edge-based partition, node-based partition, random voronoi partition.

Continuous Galerkin Approximations to Generalized Harmonic Shape Functions

Consider finite dimensional sub-spaces $\mathcal{U}^h(\Omega) \subset \mathcal{U}(\Omega)$ and $\mathcal{U}_0^h(\Omega) \subset \mathcal{U}_0(\Omega)$. The Galerkin approximation $\varphi^h \in \mathcal{U}^h(\Omega)$ to a given (generalized) harmonic shape function $\varphi \in \mathcal{U}(\Omega)$ satisfies

$$\int_\Omega \nabla\varphi^h \cdot \nabla\eta^h \, dV = \int_\Omega f_\Omega \, \eta^h \, dV \quad \forall \eta^h \in \mathcal{U}_0^h(\Omega). \tag{3.28}$$

If $f_\Omega \equiv 0$ (yielding the harmonic shape functions), we may invoke the Galerkin orthogonality property to determine that the error $e = \varphi^h - \varphi$ in approximating φ is orthogonal to $\mathcal{U}^h(\Omega)$, such that

$$\langle e, \eta^h \rangle = 0 \quad \forall \eta^h \in \mathcal{U}^h(\Omega), \tag{3.29}$$

where $\langle u, v \rangle \equiv \int_\Omega \nabla u \cdot \nabla v \, dV$. Further, it may be remarked that for any two shape functions φ_a, φ_b, we obtain

$$\langle \varphi_a, \varphi_b \rangle = \langle \varphi_a^h + e_a, \varphi_b^h + e_b \rangle = \langle \varphi_a^h, \varphi_b^h \rangle + \langle e_a, e_b \rangle, \tag{3.30}$$

owing to $\langle e_a, \varphi_b^h \rangle = \langle \varphi_a^h, e_b \rangle = 0$.

In effect, we may consider a given approximant φ^h to be the $L^2(\Omega)$ projection of φ onto $\mathcal{U}^h(\Omega)$ (a direct consequence of Galerkin orthogonality), which further implies that the evaluation of weak form integrals $a_\Omega(\mathbf{u}, \mathbf{v})$ are sufficiently well-approximated by their

counterparts $a_\Omega(\mathbf{u}^h, \mathbf{v}^h)$. Indeed, if we make the substitution

$$a_\Omega(\mathbf{u}^h, \mathbf{v}^h) = \sum_{a=1}^{N} \sum_{b=1}^{N} \mathbf{u}_a a_\Omega(\varphi_a^h, \varphi_b^h) \mathbf{v}_b, \tag{3.31}$$

we would need to verify that $a_\Omega(\varphi_a^h, \varphi_b^h)$ yields a sufficiently stable discrete operator. Satisfaction of the completeness requirements is guaranteed, so long as $\mathcal{U}^h(\Omega) \supset P^k(\Omega)$. It is not difficult to show that

$$a_\Omega(\varphi_a^h, \varphi_a^h) \leq a_\Omega(\varphi_a, \varphi_a). \tag{3.32}$$

Bishop has already explored such an approach for constructing approximations to harmonic shape functions using an FE discretization of a given polyheral element into sub-dividing tetrahedra. The corresponding shape function approximations $\varphi^h \subset C^0(\Omega)$ are obtained as the solutions to a set of local finite element problems defined on Ω (and its faces, edges – refer to Figure 3.5). Moreover, it was demonstrated in [7] that the resulting approximations preserve low-order polynomial completeness – a consequence of $\mathcal{U}^h(\Omega) \supset P^1(\Omega)$. If the elements are discretized into a sufficient number of tetrahedra, the method is observed to be both stable and consistent (provided a gradient correction scheme is employed to account for the effects of integration error).

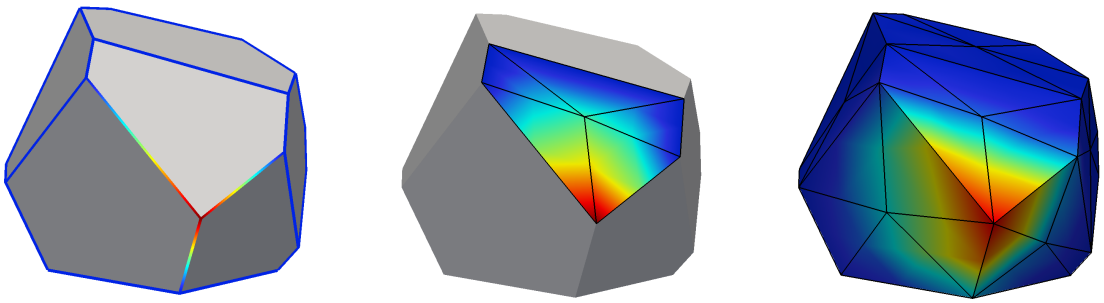

Figure 3.5. The FE-PEM approximation to a given harmonic shape function, defined hierarchially on the element's faces and edges.

This approach can become computationally expensive if the elements are subdivided into an excessively large number of tetrahedra, in the event that more accurate approximations to the shape functions are desired. However, initial numerical investigations have suggested that relatively coarse tetrahedral sub-divisions of the elements provide

sufficiently accurate results; further subdivision (tetrahedral $h-$refinement) does little to improve the overall accuracy of the approach.

A natural extension of the method proposed by Bishop to higher-order serendipity elements would be to consider $p-$refinement of an element's tetrahedral subdivision to recover higher-order polynomial completeness, i.e. to guarantee $\mathcal{U}^h(\Omega) \supset P^k(\Omega)$ for some desired polynomial order k. Unfortunately, the construction of shape functions on a given element would likely bear a much higher computational cost with increasing polynomial degree. The specification of stable and accurate numerical quadratures would present an additional challenge.

Yet another generalization would be to consider subdividing the elements into arbitrary polyhedra, and solving (3.28) by means of the virtual element method. This would allow for a more natural collocation of quadrature cells with the specified subdivision, akin to the partitioned element method proposed in [44].

However, a particular complication arises for harmonic shape functions and their corresponding $C^0(\Omega)$ approximations on irregularly shaped elements: the solution to Laplace's equation may possess extremely sharp gradients if the geometry of the element contains reflex corners or nearly degenerate features (i.e. short edges). A consequence of this is poor conditioning of the element's local stiffness matrix, leading to excessively stiff modes of deformation (locking), and issues of numerical conditioning in the linear solution process. For this reason, it becomes of interest to consider non-conforming approximations $\varphi^h \in \mathcal{U}^h(\Omega) \not\subset \mathcal{U}(\Omega)$ which have the potential to overcome these issues.

Discontinuous Galerkin Approximations to Generalized Harmonic Shape Functions

Consider the broken Sobolev space $\mathcal{D}_k^h(\Omega) = \left\{\varphi \in L^2(\Omega) : \varphi|_\omega \in P^k(\omega)\, \forall \omega \in \mathcal{T}_\omega(\Omega)\right\}$ consisting of (discontinuous) piecewise polynomials defined over the partition of the element. The interior penalty discontinuous Galerkin method described in [47] is applied to (3.8) to obtain approximations $\varphi^h \in \mathcal{D}_k^h(\Omega) \not\subset \mathcal{U}(\Omega)$ to generalized harmonic shape functions

$\varphi \in \mathcal{U}(\Omega)$, satisfying

$$\sum_{\omega\in\mathcal{T}_\omega(\Omega)}\int_\omega \nabla\varphi^h\cdot\nabla\eta^h\,dV+\sum_{\sigma\in\Gamma_\omega\cup\partial\Omega}\int_\sigma\left(\epsilon\left\{\frac{\partial\varphi^h}{\partial N_\sigma}\right\}[\![\eta^h]\!]-[\![\varphi^h]\!]\left\{\frac{\partial\eta^h}{\partial N_\sigma}\right\}\right)dA$$
$$+J_0(\varphi^h,\eta^h)+J_1(\varphi^h,\eta^h)=\int_\Omega f_\Omega\,\eta^h\,dV+\sum_{\sigma\in\partial\Omega}\int_\sigma\left(\frac{\alpha_{\sigma0}}{|\sigma|^{\beta_0}}\eta^h+\epsilon\frac{\partial\eta^h}{\partial N_\sigma}\right)\bar{\varphi}\,dA \qquad (3.33)$$

for all $\eta^h \in \mathcal{D}_k^h(\Omega)$, where

$$\{\varphi\}=\frac{1}{2}(\varphi|_{\omega_1}+\varphi|_{\omega_2}),\quad [\![\varphi]\!]=(\varphi|_{\omega_1}-\varphi|_{\omega_2})\quad \forall\sigma=\partial\omega_1\cap\partial\omega_2, \qquad (3.34)$$

$$\{\varphi\}=[\![\varphi]\!]=\varphi|_\omega\quad \forall\sigma=\partial\omega\cap\partial\Omega, \qquad (3.35)$$

and where

$$J_0(\varphi^h,\eta^h)=\sum_{\sigma\in\Gamma_\omega\cup\partial\Omega}\frac{\alpha_{\sigma0}}{|\sigma|^{\beta_0}}\int_\sigma[\![\varphi^h]\!]\,[\![\eta^h]\!]\,dA, \qquad (3.36)$$

$$J_1(\varphi^h,\eta^h)=\sum_{\sigma\in\Gamma_\omega}\frac{\alpha_{\sigma1}}{|\sigma|^{\beta_1}}\int_\sigma\left[\!\!\left[\frac{\partial\varphi^h}{\partial N_\sigma}\right]\!\!\right]\left[\!\!\left[\frac{\partial\eta^h}{\partial N_\sigma}\right]\!\!\right]dA. \qquad (3.37)$$

$J_0(\varphi^h,\eta^h)$ and $J_1(\varphi^h,\eta^h)$ are supplementary bilinear forms which penalize jumps in the indicated functions' values and their normal derivatives at cell boundaries. The parameters $\alpha_{\sigma0}$, β_0, must be appropriately specified such that $\alpha_{\sigma0} > 0$ is sufficiently large, and $\beta_0(d-1) \geq 1$ where $\Omega \subset \mathbb{R}^d$, $d \geq 2$; the specification of $\alpha_{\sigma1}$, β_1 is less strict, allowing for $\alpha_{\sigma1} \geq 0\ \forall\sigma$. The parameter $\epsilon \in \{-1,\,0,\,+1\}$ determines which interior penalty method is employed:

$\epsilon = -1$: The symmetric interior penalty Galerkin (SIPG) method.

$\epsilon = 0$: The incomplete interior penalty Galerkin (IIPG) method.

$\epsilon = +1$: The nonsymmetric interior penalty Galerkin (NIPG) method.

If one considers a non-dimensional analysis where $\mathbf{X} = h_\Omega\mathbf{X}'$, and h_Ω denotes a characteristic length scale corresponding to the diameter of the element Ω, the following quantities may be expressed in terms of their non-dimensional counterparts:

$$dV=h_\Omega^d dV',\quad dA=h_\Omega^{d-1}dA',\quad \nabla=h_\Omega^{-1}\nabla',\quad |\sigma|=h_\Omega^{d-1}|\sigma'|,\quad f_\Omega=h_\Omega^{-2}f_{\Omega'}. \qquad (3.38)$$

It is presumed that $\alpha_{\sigma 0}$, $\alpha_{\sigma 1}$ are defined independently of h_Ω. Consequently,

$$
\begin{aligned}
& h_\Omega^{d-2}\left[\sum_{\omega' \in \mathcal{T}_{\omega'}(\Omega')} \int_{\omega'} \nabla' \varphi^h \cdot \nabla' \eta^h \, dV' - \int_{\Omega'} f_{\Omega'} \, \eta^h \, dV' - \sum_{\sigma' \in \partial\Omega'} \int_{\sigma'} \epsilon \frac{\partial \eta^h}{\partial N_{\sigma'}} \, \bar{\varphi} \, dA' \right. \\
& \qquad \left. + \sum_{\sigma' \in \Gamma_{\omega'} \cup \partial\Omega'} \int_{\sigma'} \left(\epsilon \left\{ \frac{\partial \varphi^h}{\partial N_{\sigma'}} \right\} [\![\eta^h]\!] - [\![\varphi^h]\!] \left\{ \frac{\partial \eta^h}{\partial N_{\sigma'}} \right\} \right) dA' \right] \\
& + h_\Omega^{(d-1)(1-\beta_0)} \left[\sum_{\sigma' \in \Gamma_{\omega'} \cup \partial\Omega'} \frac{\alpha_{\sigma 0}}{|\sigma'|^{\beta_0}} \int_{\sigma'} [\![\varphi^h]\!] \, [\![\eta^h]\!] \, dA' - \sum_{\sigma' \in \partial\Omega'} \frac{\alpha_{\sigma 0}}{|\sigma'|^{\beta_0}} \int_{\sigma'} \eta^h \, \bar{\varphi} \, dA' \right] \\
& + h_\Omega^{(d-1)(1-\beta_1)-2} \left[\sum_{\sigma' \in \Gamma_{\omega'}} \frac{\alpha_{\sigma 1}}{|\sigma'|^{\beta_1}} \int_{\sigma'} \left[\!\!\left[\frac{\partial \varphi^h}{\partial N_{\sigma'}} \right]\!\!\right] \left[\!\!\left[\frac{\partial \eta^h}{\partial N_{\sigma'}} \right]\!\!\right] dA' \right] = 0 \quad \forall \eta^h \in \mathcal{D}_k^h(\Omega).
\end{aligned} \tag{3.39}
$$

To maintain dimensional consistency, it is suggested that β_0 and β_1 be chosen such that

$$
\beta_0 = (d-1)^{-1}, \quad \beta_1 = -(d-1)^{-1}. \tag{3.40}
$$

To ensure that the resulting linear system of equations is reasonably well-conditioned, the penalty parameters $\alpha_{\sigma 0}$, $\alpha_{\sigma 1}$ should not be made excessively large. Nonetheless, an interesting limiting case occurs when $\alpha_{\sigma 0}, \alpha_{\sigma 1} \to \infty$ proportionally:

$$
J_0(\varphi^h, \eta^h) + J_1(\varphi^h, \eta^h) = \sum_{\sigma \in \partial\Omega} \frac{\alpha_{\sigma 0}}{|\sigma|^{\beta_0}} \int_\sigma \eta^h \, \bar{\varphi} \, dA \quad \forall \eta^h \in \mathcal{D}_k^h(\Omega). \tag{3.41}
$$

Under certain conditions (for particular choices of $\mathcal{T}_\omega(\Omega)$ and $\mathcal{D}_k^h(\Omega)$), the above weak form may in fact yield a unique solution φ^h. However, the bilinear form arising from the penalty terms J_0 and J_1 alone is not guaranteed to be elliptic, in general.

The majority of our subsequent analyses will explore the family of 3-parameter methods arising from

$$
\alpha_{\sigma 0} = \alpha_0|_{\partial\Omega} \; \forall \sigma \in \partial\Omega, \quad \alpha_{\sigma 0} = \alpha_0|_{\Gamma_\omega} \; \forall \sigma \in \Gamma_\omega, \quad \alpha_{\sigma 1} = \alpha_1|_{\Gamma_\omega} \; \forall \sigma \in \Gamma_\omega, \tag{3.42}
$$

entailing a separate penalization of the boundary condition via $\alpha_0|_{\partial\Omega}$. Decreasing the value of $\alpha_0|_{\partial\Omega}$ is tantamount to relaxing the degree to which the boundary condition is enforced, the effect of which will be examined and discussed later on.

3.5 Partition-Based Quadrature Rules

If arbitrary polytopal shapes are to be used as elements in the PEM, then there arises a need for devising a means of integrating contributions to the weak form, ostensibly through the use of domain quadrature rules. Such rules must be sufficiently stable (utilizing a sufficient number of well-positioned quadrature points) and accurate (capable of exactly integrating low-order polynomials up to some specified degree).

Partitioned element methods approach this task by partitioning the elements (and their boundaries) into a sufficient number of polytopal sub-domains which are used as integration cells. Low-order (i.e. 1-point) quadrature rules are defined on each of these sub-domains, and a composite quadrature rule for the element is constructed from the resulting sets of quadrature points. In general, these rules will need to be modified to satisfy Galerkin exactness for certain low-order polynomial solutions.

Methods for partitioning the elements into sub-domains which yield stable and efficient composite quadrature rules are discussed in the following section. A discussion is given later on to the correction of these quadratures for the sake of satisfying Galerkin exactness (quadrature consistency).

Composite Quadrature Rules

Given a partition of an element into polytopal sub-domains (quadrature cells), one may utilize low order quadrature rules over each sub-domain, thereby yielding a composite quadrature rule over the element as a whole, whose overall accuracy is determined by the order of accuracy used in each sub-domain.

The simplest quadrature rule of this form is the composite mid-point scheme, where the quadrature points are located at the centroids of each sub-domain. Such a rule exactly integrates polynomials up to first order, and is reasonably accurate, otherwise. The integration points are guaranteed to be interior to each sub-domain (and the element as a whole), provided each cell is convex.

For simple sub-divisions (consisting of triangles or tetrahedra), composite quadrature rules may be extended rather naturally to obtain higher-order accuracy. For generic sub-divisions (consiting of arbitrary polytopes), the extension to high-order is not as straight-

forward. For this reason, subsequent discussions will be concerned almost exclusively with composite mid-point rules.

The weights and locations of a composite mid-point quadrature rule correspond to the volumes and geometric centroids of each cell. In general, a given quadrature cell ω may be an arbitrary polyhedron, whose volume $|\omega|$ and centroid $\bar{\mathbf{X}}$ may be computed using the 0-th and 1-st order moments of ω, i.e.

$$|\omega| = \int_\omega dV, \quad \bar{\mathbf{X}} = \frac{\int_\omega \mathbf{X}\, dV}{\int_\omega dV}. \tag{3.43}$$

Using the method proposed by Chin et al. in [12], the computation of monomial moments of arbitrary degree $|\alpha|$ may be effected via an integral over $\partial\omega$:

$$\int_\omega \mathbf{X}^\alpha\, dV = \frac{1}{d+|\alpha|} \int_{\partial\omega} (\mathbf{X}\cdot\mathbf{N})\, \mathbf{X}^\alpha\, dA, \tag{3.44}$$

for any arbitrary polytope $\omega \subset \mathbb{R}^d$. If $\partial\omega$ may be partitioned into a collection of $d-1$ dimensional facets $\sigma \subset \partial\omega$, then

$$\int_\omega \mathbf{X}^\alpha\, dV = \frac{1}{d+|\alpha|} \sum_{\sigma\in\partial\omega} \int_\sigma (\mathbf{X}\cdot\mathbf{N}_\sigma)\, \mathbf{X}^\alpha\, dA, \tag{3.45}$$

where $\mathbf{N}_\sigma$ is the outward (with respect to ω) unit normal associated with facet σ. We remark that any location $\mathbf{X}$ positioned on a given facet σ may be expressed as

$$\mathbf{X} = \mathbf{X}_\sigma + \sum_{i=1}^{d-1} X_i\, \hat{\mathbf{X}}_i, \tag{3.46}$$

where $\mathbf{X}_\sigma$ is any reference location positioned on the hyperplane which contains σ, and $\hat{\mathbf{X}}_i$ form a parameterization of the in-plane coordinates on σ. This leads to the observation $\mathbf{X}\cdot\mathbf{N}_\sigma = \mathbf{X}_\sigma\cdot\mathbf{N}_\sigma\ \forall \mathbf{X}\in\sigma$, and thus

$$\int_\omega \mathbf{X}^\alpha\, dV = \frac{1}{d+|\alpha|} \sum_{\sigma\in\partial\omega} (\mathbf{X}_\sigma\cdot\mathbf{N}_\sigma) \int_\sigma \mathbf{X}^\alpha\, dA. \tag{3.47}$$

The integral of $\mathbf{X}^\alpha$ over each facet may in turn be carried out via

$$\int_\sigma \mathbf{X}^\alpha\, dA = \frac{1}{d-1+|\alpha|} \left[\sum_{\gamma\in\partial\sigma} \left((\mathbf{X}_\gamma - \mathbf{X}_\sigma)\cdot\mathbf{N}_\gamma\right) \int_\gamma \mathbf{X}^\alpha\, dS + \mathbf{X}_\sigma \cdot \int_\sigma \nabla\mathbf{X}^\alpha\, dA \right], \tag{3.48}$$

and the integral over each segment is

$$\int_\gamma \mathbf{X}^\alpha \, dS = \frac{1}{d-2+|\alpha|} \left[\sum_{v \in \partial\gamma} \big((\mathbf{X}_v - \mathbf{X}_\gamma) \cdot \mathbf{N}_v \big) \mathbf{X}_v^\alpha + \mathbf{X}_\gamma \cdot \int_\gamma \nabla \mathbf{X}^\alpha \, dS \right]. \tag{3.49}$$

Similarly defined composite rules may be defined on each polygonal face of a given polyhedral element, or on each edge of a polygonal element. However, while composite mid-point quadrature rules are able to provide reasonable accuracy, they will not necessarily lead to quadrature consistency, as expressed in (2.67). For this reason, a gradient correction scheme (such as the one proposed by Bishop in [7], or by Talischi in [57]) must be employed, as discussed in the following section.

Gradient Correction Scheme

Consider an element $\Omega \subset \mathbb{R}^d$ upon which is specified a domain quadrature rule $\{\mathbf{X}_q,\, w_q\}_{q=1}^{N_{qp}}$ such that the integral of a scalar function $f \in L^2(\Omega)$ over Ω is approximated by

$$\int_\Omega f \, dV \approx \sum_{q=1}^{N_{qp}} w_q f(\mathbf{X}_q). \tag{3.50}$$

Additionally, suppose that each face $F \subset \partial\Omega$ possesses a quadrature rule $\big\{\mathbf{X}_b,\, w_b,\, \mathbf{N}^{(b)}\big\}_{b=1}^{N_{bp}^F}$ where $\mathbf{N}^{(b)}$ denotes the unit normal to the face F evaluated at $\mathbf{X}_b \in F$. The integral of a scalar function $f \in L^2(\partial\Omega)$ (or of a vector-valued function $f\,\mathbf{N}$) over $\partial\Omega$ is approximated by

$$\int_{\partial\Omega} f \, dA \approx \sum_{F \in \partial\Omega} \sum_{b=1}^{N_{bp}^F} w_b f(\mathbf{X}_b), \quad \int_{\partial\Omega} f\,\mathbf{N} \, dA \approx \sum_{F \in \partial\Omega} \sum_{b=1}^{N_{bp}^F} w_b f(\mathbf{X}_b) \mathbf{N}^{(b)}. \tag{3.51}$$

Suppose that the aforementioned quadrature rules (on a given polyhedral element Ω and on each of its polygonal faces $F \subset \partial\Omega$) are constructed using the composite mid-point quadrature scheme discussed in the previous section. A simple gradient correction scheme is obtained by introducing an auxiliary field $\boldsymbol{\xi} = \nabla\phi - \nabla\varphi$, such that a given trial function φ and its corresponding test function ϕ differ (minimally), to the extent that the quadrature consistency conditions hold:

$$\sum_{q=1}^{N_{qp}} w_q \left[\mathbf{X}_q^\alpha \, \nabla\phi(\mathbf{X}_q) + \nabla \mathbf{X}_q^\alpha \, \phi(\mathbf{X}_q) \right] = \sum_{F \in \partial\Omega} \sum_{b=1}^{N_{bp}^F} w_b \mathbf{X}_b^\alpha \phi(\mathbf{X}_b) \mathbf{N}^{(b)} \quad \forall |\alpha| \leq k-1, \tag{3.52}$$

for every test function ϕ, where k represents the degree of polynomial completeness exhibited by the space of trial solutions. Given the discrete conditions:

$$\phi(\mathbf{X}_b) = \varphi(\mathbf{X}_b)\,\forall b, \quad \phi(\mathbf{X}_q) = \varphi(\mathbf{X}_q)\,\forall q, \quad \nabla\phi(\mathbf{X}_q) = \nabla\varphi(\mathbf{X}_q) + \boldsymbol{\xi}(\mathbf{X}_q)\,\forall q, \tag{3.53}$$

we obtain $\boldsymbol{\xi}(\mathbf{X}_q)$ as the solution to the quadratic minimization problem:

$$\min_{\boldsymbol{\xi}} \frac{1}{2}||\boldsymbol{\xi}||^2_\Omega, \tag{3.54}$$

subject to (3.52), where $||\boldsymbol{\xi}||_\Omega$ is deliberately approximated using the element's quadrature rule, i.e.

$$||\boldsymbol{\xi}||_\Omega \approx \left[\sum_{q=1}^{N_{qp}} w_q\ [\xi_i(\mathbf{X}_q)\,\xi_i(\mathbf{X}_q)]\right]^{1/2}. \tag{3.55}$$

Suppose two adjacent elements Ω_L and Ω_R share a given face $F = \partial\Omega_L \cap \partial\Omega_R$. If the shape functions and quadrature rules defined on $F_L \subset \partial\Omega_L$ and $F_R \subset \partial\Omega_R$ (where $F_L = F_R$) are identical, then the aforementioned gradient correction scheme will automatically lead to satisfaction of finite element patch tests. However, if Ω_L and Ω_R provide separate quadrature rules on F_L and F_R (arising from different partitions of the shared face), or if the elements' shape functions are not defined identically on F_L and F_R, then we require that an additional condition be met:

$$\sum_{l=1}^{N_{bp}^{F_L}} w_l \mathbf{X}_l^\alpha \phi_l\,\mathbf{N}^{(l)} = -\sum_{r=1}^{N_{bp}^{F_R}} w_r \mathbf{X}_r^\alpha \phi_r\,\mathbf{N}^{(r)} \quad \forall\,|\alpha| \leq k-1, \tag{3.56}$$

for every shared face $\partial\Omega_L \subset F_L = F_R \subset \partial\Omega_R$.

As an alternative to using a gradient correction scheme, a novel approach to restore quadrature consistency (inspired by the virtual element method) is presented in the following section.

Selective Modal Quadrature

Consider all functions $f \in L^2(\Omega)$ represented over an arbitrary polytopal element domain $\Omega \subset \mathbb{R}^d$. Borrowing from notation typical of the VEM, consider an $L^2(\Omega)$ polynomial projection operator $\Pi_k^\Omega : L^2(\Omega) \mapsto P^k(\Omega)$ which may be used to decompose $f = f_p + f_n$ into polynomial and non-polynomial parts:

$$f_p = \Pi_k^\Omega f, \quad f_n = f - \Pi_k^\Omega f = \pi_k^\Omega f, \tag{3.57}$$

where $\pi_k^\Omega : L^2(\Omega) \mapsto L^2(\Omega) \backslash P^k(\Omega)$. Consequently, we observe that $\Pi_k^\Omega f$ is $L^2(\Omega)$ orthogonal to any $\pi_k^\Omega g$ for all $g \in L^2(\Omega)$, to the extent that

$$\int_\Omega (\Pi_k^\Omega f)(g - \Pi_k^\Omega g)\, dv = \langle \Pi_k^\Omega f, g - \Pi_k^\Omega g \rangle_\Omega = 0 \quad \forall f,\, g \in L^2(\Omega). \tag{3.58}$$

We propose a quadrature rule of the form:

$$\int_\Omega f\, dV \approx \int_\Omega f_p\, dV + \sum_{q=1}^{N_{qp}} w_q f_n(\mathbf{x}_q), \tag{3.59}$$

where it is supposed that the projection operators Π_k^Ω and π_k^Ω are well-defined on Ω, and $\int_\Omega f_p\, dV$ may be computed exactly using the methodology proposed by Chin et al. in [12]. Furthermore, if we wish to integrate the product fg where $f,\, g \in L^2(\Omega)$, we may write

$$\int_\Omega fg\, dV = \langle f, g \rangle_\Omega = \langle \Pi_k^\Omega f + \pi_k^\Omega f, \Pi_k^\Omega g + \pi_k^\Omega g \rangle_\Omega, \tag{3.60}$$

which, by the linearity of the $L^2(\Omega)$ inner product, and by the orthogonality of $\Pi_k^\Omega f$ and $\pi_k^\Omega g$ (and of $\pi_k^\Omega f$ and $\Pi_k^\Omega g$), yields

$$\int_\Omega fg\, dV = \langle \Pi_k^\Omega f, \Pi_k^\Omega g \rangle_\Omega + \langle \pi_k^\Omega f, \pi_k^\Omega g \rangle_\Omega, \tag{3.61}$$

and thus

$$\int_\Omega fg\, dV \approx \int_\Omega f_p g_p\, dV + \sum_{q=1}^{N_{qp}} w_q f_n(\mathbf{x}_q) g_n(\mathbf{x}_q). \tag{3.62}$$

This is effectively equivalent to integrating the product of all low-order polynomials exactly, while integrating the product of all non-polynomial "remainders" approximately, using a quadrature rule.

If we are only given evaluations of a function f at a set of discrete (quadrature) points $\{\mathbf{x}_q\}_{q=1}^{N_{qp}}$, then we must construct a low-order polynomial projection operator by considering the least-squares problem:

$$\min_{f_p \in P^k(\Omega)} \frac{1}{2} ||f_p - f||_\Omega^2, \tag{3.63}$$

where $||f||_\Omega = \sqrt{\langle f, f \rangle_\Omega}$ is deliberately approximated using the element's quadrature rule:

$$\langle f, f \rangle_\Omega \approx \sum_{q=1}^{N_{qp}} w_q \left[f(\mathbf{x}_q) \right]^2. \tag{3.64}$$

For a given polynomial basis $\{z_a\}_{a=1}^{K}$ which spans $P^k(\Omega)$, we may write

$$f_p(\mathbf{x}) = \sum_{a=1}^{K} z_a(\mathbf{x}) c_a = \mathbf{z}^T(\mathbf{x})\,\mathbf{c}, \tag{3.65}$$

and the solution to (3.64) satisfies

$$\sum_{a=1}^{K}\sum_{q=1}^{N_{qp}} w_q z_b(\mathbf{x}_q) z_a(\mathbf{x}_q) c_a = \sum_{q=1}^{N_{qp}} w_q z_b(\mathbf{x}_q) f(\mathbf{x}_q) \quad \forall b = 1, \ldots, K, \tag{3.66}$$

The above may be written in matrix-vector format as $\mathbf{Z}^T\mathbf{W}\mathbf{Z}\mathbf{c} = \mathbf{Z}^T\mathbf{W}\mathbf{f}$, where we denote $f_i = f(\mathbf{x}_i)$, $W_{ii} = w_i$, $W_{ij} = 0\,\forall i \neq j$, and $Z_{ij} = z_j(\mathbf{x}_i)$. The discrete polynomial projection operator $\mathbf{\Pi}_k^\Omega : \mathbb{R}^{N_{qp}} \mapsto \mathbb{R}^K$ is computed as $\mathbf{\Pi}_k^\Omega = (\mathbf{Z}^T\mathbf{W}\mathbf{Z})^{-1}\mathbf{Z}^T\mathbf{W}$, and the complement operator $\boldsymbol{\pi}_k^\Omega : \mathbb{R}^{N_{qp}} \mapsto \mathbb{R}^{N_{qp}}$ is $\boldsymbol{\pi}_k^\Omega = \mathbf{1}_{N_{qp}} - \mathbf{Z}\mathbf{\Pi}_k^\Omega$. Consequently,

$$\langle \Pi_k^\Omega f, \Pi_k^\Omega g\rangle_\Omega = \langle \mathbf{z}^T\mathbf{\Pi}_k^\Omega\mathbf{f}, \mathbf{z}^T\mathbf{\Pi}_k^\Omega\mathbf{g}\rangle_\Omega = \mathbf{f}^T\left[\mathbf{\Pi}_k^{\Omega^T}\left(\int_\Omega \mathbf{z}\otimes\mathbf{z}\,dV\right)\mathbf{\Pi}_k^\Omega\right]\mathbf{g}, \tag{3.67}$$

$$\langle \pi_k^\Omega f, \pi_k^\Omega g\rangle_\Omega \approx \sum_{q=1}^{N_{qp}} w_q f_n(\mathbf{x}_q) g_n(\mathbf{x}_q) = \mathbf{f}^T\left[\boldsymbol{\pi}_k^{\Omega^T}\mathbf{W}\boldsymbol{\pi}_k^\Omega\right]\mathbf{g}, \tag{3.68}$$

and thus

$$\int_\Omega f g\,dV \approx \mathbf{f}^T\mathbf{M}_k\mathbf{g} = \sum_{q=1}^{N_{qp}}\sum_{p=1}^{N_{qp}} M_k(\mathbf{x}_q,\mathbf{x}_p)\, f(\mathbf{x}_q)\, g(\mathbf{x}_p), \tag{3.69}$$

$$\mathbf{M}_k \equiv \left[\mathbf{\Pi}_k^{\Omega^T}\left(\int_\Omega \mathbf{z}\otimes\mathbf{z}\,dV\right)\mathbf{\Pi}_k^\Omega\right] + \left[\boldsymbol{\pi}_k^{\Omega^T}\mathbf{W}\boldsymbol{\pi}_k^\Omega\right]. \tag{3.70}$$

We shall refer to this form of integration as *selective modal quadrature*, given that the products of particular low-order polynomial modes are integrated exactly, and the products of any higher-order modes are approximated using the element's quadrature rules. The advantage of modal quadrature is that we may exactly integrate any terms which directly impact quadrature consistency. Consequently, nearly any stable numerical integration scheme (e.g. composite mid-point quadrature) may be used to integrate the higher-order products.

Rather than storing the independent quadrature weights $w_q = w(\mathbf{x}_q)$, selective modal quadrature requires the storage of a generalized quadrature weighting matrix $M_k(\mathbf{x}_q, \mathbf{x}_p)$. Alternatively, for the sake of efficiency, if the function g is known a priori (e.g. if g is a

test function for a weighted residual method), then we need only store the "augmented" test function values:

$$\tilde{g}^{(k)}(\mathbf{x}_q) = \sum_{p=1}^{N_{qp}} \frac{M_k(\mathbf{x}_q, \mathbf{x}_p)}{w_q}\, g(\mathbf{x}_p), \tag{3.71}$$

and all integrals involving f and g may be carried out via

$$\int_\Omega f g \, dV \approx \sum_{q=1}^{N_{qp}} w_q \, \tilde{g}^{(k)}(\mathbf{x}_q)\, f(\mathbf{x}_q). \tag{3.72}$$

If applied to the stress divergence integral appearing in (2.39), the resulting expression would resemble a gradient correction scheme in some respects, although it should be noted that the above procedure would need to be applied separately to each term appearing in the weak form (including boundary integrals). Specifically, the corresponding integration of the residual equations in (2.39) would be carried out via

$$\int_{\mathcal{B}_0} P_{ij}\phi_{a,j} \, dV \approx \sum_{q=1}^{N_{qp}} w_q P_{ij}(\mathbf{x}_q)\tilde{\phi}^{(k)}_{a,j}(\mathbf{x}_q), \tag{3.73}$$

$$\int_{\mathcal{B}_0} \rho_0 b_i \phi_a \, dV \approx \sum_{q=1}^{N_{qp}} w_q \rho_0(\mathbf{x}_q) b_i(\mathbf{x}_q)\tilde{\phi}^{(k-1)}_{a}(\mathbf{x}_q), \tag{3.74}$$

$$\int_{\Gamma_0^N} \bar{p}_i \phi_a \, dA \approx \sum_{b=1}^{N_{bp}} w_b \bar{p}_i(\mathbf{x}_b)\tilde{\phi}^{(k)}_{a}(\mathbf{x}_b), \tag{3.75}$$

where $\tilde{\phi}^{(k)}_a$ and $\tilde{\phi}^{(k)}_{a,j}$ denote the "augmented" test functions are their corresponding gradients, and k is the indicated order of quadrature consistency (required to pass patch tests up to order $k+1$).

Chapter 4

An Implementational Framework for the DG-PEM

The implementation of a given partitioned element method must address two primary challenges: the subdivision of an element into cells, and the solution of shape function boundary value problems by way of the chosen PEM formulation. The first of these two tasks may be accomplished by various means. However, careful attention must be paid to the stability requirements of the PEM, such that the resulting quadrature cell partition yields stable approximations to harmonic shape functions, and a stable integration rule for the element. Specifying such a discretization is not trivial for arbitrary shapes. For this reason, we will confine our attention to strictly star-convex elements, for which we propose a relatively simple (edge-based) element partitioning algorithm.

The present implementational framework is directed at obtaining DG-PEM approximations to harmonic shape functions on arbitrary polytopes – i.e. solving (3.33) on an appropriately defined partition of the element. A discussion of the pertinent data structures and solution methods is provided.

4.1 Arbitrary Polytopal Meshes

Traditional finite element methods typically permit the elements to only take the form of certain canonical shapes with fixed topology (most commonly tetrahedra or hexahedra). This yields several benefits with regard to the data and storage requirements necessary to

represent a given element in a computational setting. Frequently, it suffices to describe the geometry of a canonical shape (such as a hexahedron) by providing a list of the element's nodal coordinates, along with an ordered sequence of the element's nodal IDs, which fully determines its resulting topology according to some conventional node numbering scheme (refer to Figure 4.1 as a representative example.)

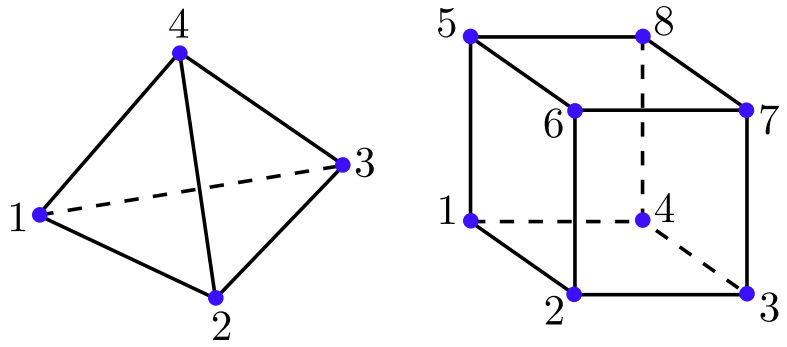

Figure 4.1. Canonical node numbering schemes for a linear tetrahedral element (left) and a linear hexahedral element (right). Each of these standard orderings induce corresponding nodal orderings for each triangular or quadrilateral face of the element, as well.

Polytopal elements with arbitrary topology (with a variable number of nodes, edges, and faces) cannot be represented in this fashion. As a consequence, more descriptive data structures are necessary to fully determine a polytopal element's nodal connectivity. A particular scheme to represent an arbitrary polyhedron in a finite element mesh is described in the following section.

Geometric Data Structures for Arbitrary Polytopes

There are multiple ways in which the geometry of a given polyhedral element Ω may be represented within a finite element code. Ideally, however, the chosen data structure should be made as compact as possible, for the sake of minimizing the storage requirements of a single element. This section describes a few basic data structures for storing arbitrary polygonal and polyhedral shapes within an unstructured finite element mesh.

The geometric data used to describe a typical finite element mesh consists of the following:

- A list of the spatial coordinates $\{\mathbf{X}_a\}_{a=1}^{N_V^{\mathcal{B}_0}}$ for all nodes in the mesh. The sub-index

$a \in 1, \ldots, N_V^{\mathcal{B}_0}$ induces a *global node ID* ascribed to each node.

- A list of all elements $\{\Omega_e\}_{e=1}^{N_\Omega^{\mathcal{B}_0}}$ where $\Omega_e \subset \mathcal{B}_0$. The sub-index $e \in 1, \ldots, N_\Omega^{\mathcal{B}_0}$ induces an associated *element ID*.
- A list of all faces $\{F_b\}_{b=1}^{N_F^{\Gamma_0^N}}$ where $F_b \subset \Gamma_0^N$ to which traction boundary conditions are assigned. Likewise, the sub-index $b \in 1, \ldots, N_F^{\Gamma_0^N}$ induces a *boundary face ID*.

In a finite element mesh consisting of arbitrary polyhedral elements, it is suggested that each element Ω_e be represented by the following data:

- A list of the global node IDs $\{a_i\}_{i=1}^{N_V^{\Omega_e}}$ comprising the set of nodes belonging to Ω_e. The sub-index $i \in 1, \ldots, N_V^{\Omega_e}$ induces a *local node ID*, particular to the element Ω_e.
- A list of the polygonal faces $\{F_j\}_{j=1}^{N_F^{\Omega_e}}$ which belong to $\partial\Omega_e$; each polygonal face F_j is in turn represented by a cycle of local node IDs denoted $\{n_i\}_{i=1}^{N_V^{F_j}}$, which further determine each face's outward orientation with respect to the element Ω_e.

An illustration of this collection of data for a given polyhedron Ω_e is provided in Figure 4.2.

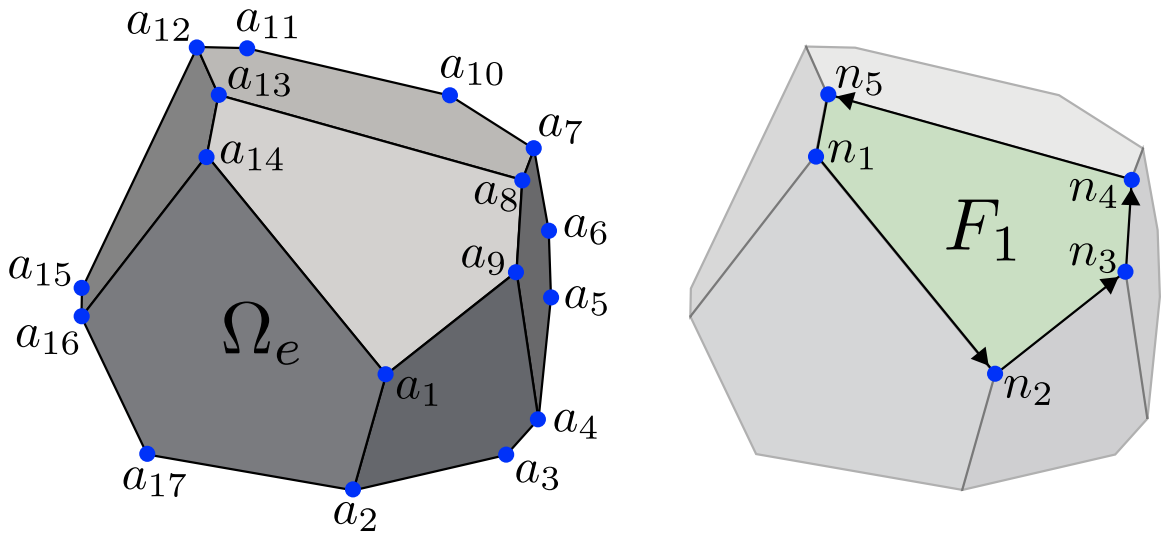

Figure 4.2. Illustration of the data necessary to describe an arbitrary polyhedral element Ω_e. The local node ID ordering for the face F_1 shown would be $\{n_i\}_{i=1}^5 = \{14, 1, 9, 8, 13\}$.

A given polygonal face $F_b \subset \Gamma_0^N$ will similarly be represented by:

- A list of the global node IDs $\{a_i\}_{i=1}^{N_V^{F_b}}$ which belong to F_b.
- A list of the linear edges $\{E_c\}_{c=1}^{N_E^{F_b}}$ which belong to ∂F_b; each linear edge E_c is in turn represented as an ordered list of local node IDs $\{n_i\}_{i=1}^{N_V^{E_c}}$.

Unlike canonical finite element shapes, the ordering of the element's nodal IDs is effectively arbitrary, and does not induce a topology. Rather, the element's topology is determined by virtue of its polygonal faces, and their respective (conventionally clockwise) local node orderings. Consequently, each edge of a given polyhedron is defined implicitly as the intersection of two adjacent faces' ordered node sets. Such a scheme may be easily generalized to accomodate serendipity elements containing additional nodes along element edges, as illustrated in Figure 4.3.

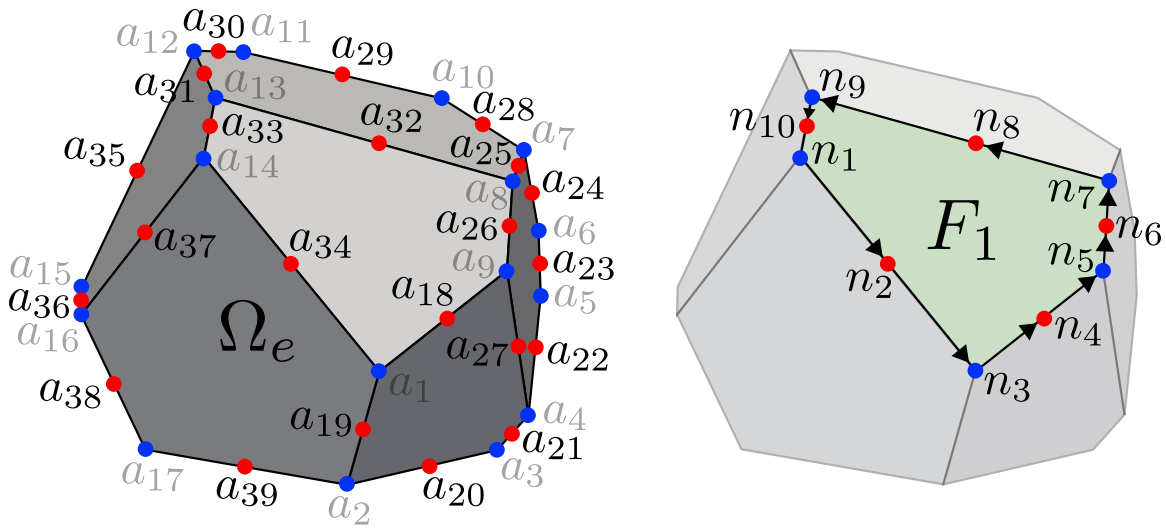

Figure 4.3. Illustration of the data necessary to describe a quadratic serendipity polyhedral element Ω_e. The local node ID ordering for the face F_1 shown would be $\{n_i\}_{i=1}^{10} = \{14, 34, 1, 18, 9, 26, 8, 32, 13, 33\}$.

Finite Element Data for Arbitrary Polytopes

Traditional Lagrangian finite element methods require each element $\Omega_e \subset \mathcal{B}_0$ to carry the following data (at a minimum) for the purposes of evaluating weak form integrals:

- A list of quadrature weights $\{w_q\}_{q=1}^{N_{qp}^{\Omega_e}}$ associated with the quadrature points of the element. The sub-index q induces a local *quadrature point ID*.

- Evaluations of the element's nodal shape functions $\{\varphi_a(\mathbf{X}_q)\}_{q=1}^{N_{qp}^{\Omega_e}} \ \forall a = 1, \ldots, N_V^{\Omega_e}$ at each quadrature point location $\mathbf{X}_q$.

- Gradients (with respect to the element's reference coordinates $\mathbf{X}$ at time $t = 0$) of the element's nodal shape functions $\{\nabla_X \varphi_a(\mathbf{X}_q)\}_{q=1}^{N_{qp}^{\Omega_e}} \ \forall a = 1, \ldots, N_V^{\Omega_e}$.

- (Optionally) if the element relies upon some form of gradient correction scheme (or more generally, if a Petrov-Galerkin method is employed): evaluations and/or gradients of the element's test functions $\{\phi_a(\mathbf{X}_q),\ \nabla_X \phi_a(\mathbf{X}_q)\}_{q=1}^{N_{qp}^{\Omega_e}} \ \forall a = 1, \ldots, N_V^{\Omega_e}$ must be stored, as well.

For solid mechanics applications, material state data (e.g. material properties, internal variables, Cauchy stress) would also need to be stored at each quadrature point location.

Similarly, each boundary face $F_b \subset \Gamma_0^N$ must carry:

- A list of quadrature weights $\{w_q\}_{q=1}^{N_{qp}^{F_b}}$ for each quadrature point of the face.

- Evaluations of the face's nodal shape functions $\{\varphi_a(\mathbf{X}_q)\}_{q=1}^{N_{qp}^{F_b}} \ \forall a = 1, \ldots, N_V^{F_b}$ at each quadrature point location $\mathbf{X}_q$.

- Gradients (with respect to the face's in-plane reference coordinates $\mathbf{X}$ at $t = 0$) of the face's nodal shape functions $\{\nabla_X \varphi_a(\mathbf{X}_q)\}_{q=1}^{N_{qp}^{F_b}} \ \forall a = 1, \ldots, N_V^{F_b}$.

- If a Petrov-Galerkin method is employed: evaluations and/or gradients of the face's test functions $\{\phi_a(\mathbf{X}_q),\ \nabla_X \phi_a(\mathbf{X}_q)\}_{q=1}^{N_{qp}^{F_b}} \ \forall a = 1, \ldots, N_V^{F_b}$.

- Outward unit normals $\{\mathbf{N}_q\}_{q=1}^{N_{qp}^{F_b}}$ to the face F_b at each quadrature point.

The data enumerated above must be determined by means of a specified formulation for how the element's (face's) shape functions and quadrature rule should be constructed. Partitioned element methods address precisely this task. Given an abstract representation for the geometry of a given polyhedral element Ω (as discussed in the previous section), a PEM formulation proceeds in a number of distinct steps:

1.) The element (and its faces, edges) are appropriately partitioned into cells (facets, segments, verticies).

2a.) Individual nodal shape functions are constructed along each edge E of the element.

2b.) Individual nodal shape functions are constructed on each face F of the element.

2c.) Individual nodal shape functions are constructed on the interior of the element Ω.

3.) The discrete finite element data (including quadrature point evaluations of the shape functions and their gradients) are computed and stored by the element.

4.) Any auxiliary data (regarding the element's partitioned geometry, etc.) is discarded.

Depending on how the chosen PEM is carried out, the above process can ammount to a relatively large computational expense. However, if a total Lagrangian approach is empolyed within the associated finite element analysis, then the above methodology would only need to be carried out once for each element, at the beginning of the simulation (prior to the first time step). Consequently, the cost of constructing element shape functions in this manner is amortized over the duration of the analysis.

The subsequent sections of this chapter are dedicated to a more detailed discussion of the aforementioned steps taken to construct a given element's partition, and its shape functions.

4.2 Element Partitioning Schemes

The process of obtaining a suitable partition for a given element constitutes the greatest challenge facing partitioned element methods. The primary complication arises from the conditions of stability: the shape function approximations, and the corresponding quadrature rules defined on the element's partition must guarantee a sufficiently stable integration of the weak form. For relatively simple shapes, a number of stable partitioning schemes exist. However, for arbitrary shapes, it becomes difficult – if not impossible – for a heuristically-driven discretization scheme to guarantee that the resulting partition will satisfy the aforementioned stabilily requirements.

For this reason, we will limit our subsequent discussion to star-convex element geometries. For such shapes, a relatively simple partitioning scheme is suggested, resembling the

decomposition used in the edge-based smoothed finite element method. In the absence of degenerate features, the resulting partition is verified to provide sufficiently stable shape function approximations and quadrature rules.

Edge-Based Partitioning for Star-Convex Elements

A star-convex shape Ω is one for which there exists some point $\mathbf{X}_0^\Omega \in \Omega$ such that the line segment connecting any point $\mathbf{X} \in \Omega$ to $\mathbf{X}_0^\Omega$ is entirely contained within Ω. If $\Omega \subset \mathbb{R}^3$ refers to a polyhedron which is star-convex, this further implies that each polygonal face $F \subset \partial\Omega$ is also star-convex with respect to some point $\mathbf{X}_0^F \in F$. Any linear edge $E \subset \partial F$ is star-convex with respect to any point $\mathbf{X} \in E$.

A simple and efficient partitioning scheme is described for polyhedral elements Ω (and their polygonal faces F_j) which are star-convex with respect to their vertex-averaged centroids $\bar{\mathbf{X}}_0^\Omega$ (or $\bar{\mathbf{X}}_0^{F_j}$), i.e.

$$\bar{\mathbf{X}}_0^\Omega = \frac{1}{N_V^\Omega} \sum_{i=1}^{N_V^\Omega} \mathbf{X}_i, \quad \text{and} \quad \bar{\mathbf{X}}_0^{F_j} = \frac{1}{N_V^{F_j}} \sum_{i=1}^{N_V^{F_j}} \mathbf{X}_i. \tag{4.1}$$

For a given polyhedral element Ω, the algorithm proceeds in several steps:

1.) Identify all edges of the polyhedron, and subdivide them into linear segements; each segment should join two adjacent nodes of a given edge.

2.) For each face, compute its vertex-averaged centroid $\bar{\mathbf{X}}_0^{F_j}$, and subdivide the face into triangular facets which emanate from $\bar{\mathbf{X}}_0^{F_j}$; each facet should share at most two segments (at least one segment) with ∂F_j.

3a.) Compute the element's vertex-averaged centroid $\bar{\mathbf{X}}_0^\Omega$, and subdivide the element into tetrahedra which emanate from $\bar{\mathbf{X}}_0^\Omega$; each tetrahedron should share a single facet with $\partial\Omega$.

3b.) Lump into cells any tetrahedra which share a segment belonging to an edge of Ω; each cell should consist of exactly two tetrahedra.

An illustration of this process is depicted in Figure 4.4. A similar agorithm may be applied to each boundary face $F_b \subset \Gamma_0^N$, entailing only the first two steps.

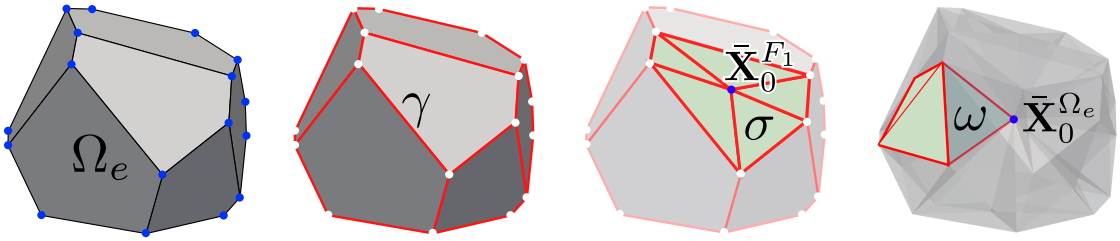

Figure 4.4. The resulting segment, facet, and cell decomposition for the proposed edge-based partitioning algorithm.

The algorithm can also be naturally extended to accomodate serendipity polyhedral elements, with additional nodes belonging to element edges, as depicted in Figure 4.5.

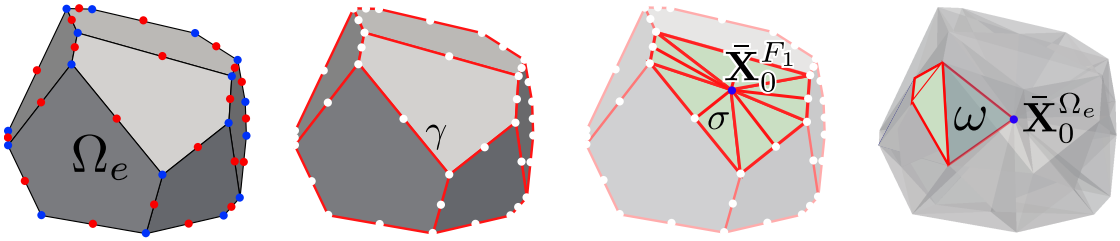

Figure 4.5. The resulting segment, facet, and cell decomposition for the proposed edge-based partitioning algorithm, applied to a quadratic serendipity polyhedral element.

4.3 Abstract Geometric Data Structures

Because partitioned element methods consist of solving a set of 1D, 2D, and 3D problems on each edge, face, and element, there arise a number of similarities between these problems of variable dimension. Namely, the geometric data describing each cell, facet, segment and vertex may be abstracted through the use of generic parent-child (tree-based) data structures. Instead of requiring a separate implementation for the solution of each 1D, 2D, 3D problem, generic programming paradigms are exploited to facilitate a single, unified implementation which is agnostic to the dimensionality of the problem being solved. The proposed organization shares many similarities with the generic programming approaches presented in [14]. A number of definitions for the abstract data structures used henceforth are given in the following sections.

Geometric Entities

Geometric entities (or simply *entities*) are defined as the atomic units of the element's geometric partition. An entity may be: a polyhedral cell, a polygonal facet, a linear segment, or a vertex. Entities are defined in terms of their relationship to other geometric entities. Specifically, a 3−dimensional entity (a polyhedral cell ω) is uniquely defined in terms of its 2-dimensional facets $\sigma \subset \partial\omega$ (termed the "children" of ω). Each facet σ is in turn considered a 2-dimensional entity, defined in terms of its 1-dimensional children (its bounding segements $\gamma \subset \partial\sigma$). An entity of dimension 0 (a vertex) is identified as having no children.

Each geometric entity may be viewed as a "node" in a corresponding tree diagram, as illustrated in Figure 4.6, where the height of a given entity within the tree structure indicates its dimensionality d.

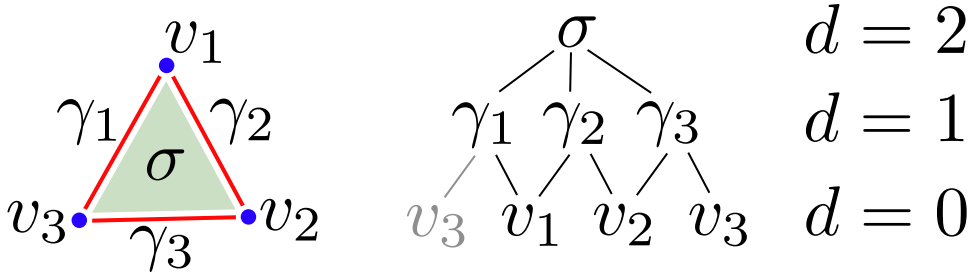

Figure 4.6. A representative entity tree diagram for a 2-dimensional facet σ and its children.

Henceforth, we denote by ε any generic d−dimensional entity, and by ζ any $(d-1)$-dimensional child of ε (such that $\zeta \subset \partial\varepsilon$). The data stored on a given entity ε consists of:

- Information (pointers or entity IDs) refering to the $(d-1)$-dimensional children of ε, and/or information (pointers or entity IDs) refering to the $(d+1)$-dimensional parents of ε.
- An (optional) orientation/unit direction $\mathbf{N}_\varepsilon$.
- A quadrature rule $\{\mathbf{X}_q, w_q\}_{q=1}^{N_{qp}^\varepsilon}$ defined on ε, or pre-computed monomial integrals $\int_\varepsilon \mathbf{X}^\alpha \, d\varepsilon$ for all $|\alpha| \leq k$ (alternatively, the shifted monomial moments $\int_\varepsilon (\mathbf{X} - \mathbf{X}_\varepsilon)^\alpha \, d\varepsilon$

may be computed and stored, instead.)

- A list of the DG-PEM basis function IDs which are associated with ε.

If quadrature rules are to be defined on each geometric entity, we may exploit the particular choice made regarding the element's edge-based partition, noting that every polygonal facet will be a triangle, and every polyhedral cell will consist of two adjoining tetrahedra, allowing for the use of standard Dunavant [19] and Grundmann-Möller [28] quadrature rules for triangles and tetrahedra, respectively. Standard Gaussian quadrature rules may be specified on each linear segment.

The advantage of defining entities in this fashion is that it affords greater flexibility in solving the DG-PEM problem (3.33) on elements with arbitrary dimensionality.

Sub-Elements

Herein, a *sub-element* (generically denoted as $\mathcal{E}$) is defined as a $d-$dimensional polytope (a polyhedral element, a polygonal face, a linear edge, or a node) upon which nodal shape functions are locally constructed and defined as the solution to a $d-$dimensional boundary value problem. Sub-elements consist of a partition $\mathcal{T}_\varepsilon(\mathcal{E})$ of $\mathcal{E}$ into $d-$dimensional entities ε. The boundary of each sub-element $\mathcal{E}$ is comprised of $(d-1)-$dimensional sub-elements, denoted $e \subset \partial\mathcal{E}$ (called the "children" of $\mathcal{E}$, in analog to the terminology used for geometric entities). A sub-element of dimension 0 (a node) refers to a single vertex, and possesses no children.

As a representative example, consider the face $F \subset \partial\Omega$ shown in Figure 4.7, which is classified as a $2-$dimensional sub-element, whose partition $\mathcal{T}_\sigma(F)$ consists of $2-$dimensional facets $\sigma \subset F$. The children of F are comprised of $1-$dimensional sub-elements – edges $E \subset \partial F$; in turn, the children of each edge E are the nodes of the element. As with geometric entities, the parent-child relationships between different sub-elements induces a tree-like data stucture, where the height of a given sub-element within the tree corresponds to its dimensionality d.

The data stored for a given sub-element $\mathcal{E}$ consists of:

- Information (pointers or entity IDs) refering to the d-dimensional entities $\varepsilon \in \mathcal{T}_\varepsilon(\mathcal{E})$

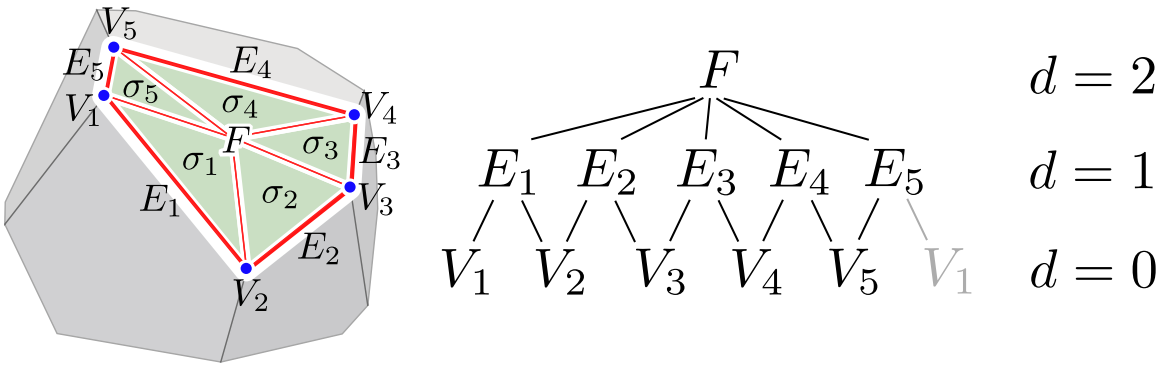

Figure 4.7. A representative 2-dimensional sub-element $F \subset \partial\Omega$ (a polygonal face), and its corresponding sub-element tree diagram. The partition of F consists of polygonal facets $\sigma_i \in \mathcal{T}_\sigma(F)\ \forall i = 1, \ldots, 5$.

belonging to the partition of $\mathcal{E}$.

- Information (pointers or sub-element IDs) refering to the $(d-1)$-dimensional children of $\mathcal{E}$ (the sub-elements $e \subset \partial\mathcal{E}$ which constitute the boundary of $\mathcal{E}$).

- A list of the DG-PEM basis function IDs which are defined on $\mathcal{T}_\varepsilon(\mathcal{E})$.

A more through discussion is dedicated to the subject of DG-PEM basis functions in the following section.

4.4 Partition-Based Approximation Spaces

As discussed in chapter 3, partitioned element methods consider a weak formulation of a given PDE (e.g. Laplace's equation), whose solution is approximated through the specification of a finite dimensional function space $\mathcal{U}^h(\mathcal{E})$ defined on the partition $\mathcal{T}_\varepsilon(\mathcal{E})$ of a given sub-element $\mathcal{E}$. The (sub-)element's shape functions are selected as the "best approximations" to (harmonic) functions which are contained within the chosen approximation space $\mathcal{U}^h(\mathcal{E})$.

Herein, we consider $\mathcal{U}^h(\mathcal{E})$ to be spanned by a set of basis functions $\{\psi_A\}_{A=1}^{N_{bf}^{\mathcal{E}}}$, such that each basis function $\psi \in \mathcal{U}^h(\mathcal{E})$ is compactly supported over a given geometric entity $\varepsilon \in \mathcal{T}_\varepsilon(\mathcal{E})$ (or patch of entities).

Any function $\varphi^h \in \mathcal{U}^h(\mathcal{E})$ may be written as a linear combination of the basis functions

which span $\mathcal{U}^h(\mathcal{E})$, i.e.

$$\varphi^h(\mathbf{X}) = \sum_{A=1}^{N_{bf}^{\mathcal{E}}} \psi_A(\mathbf{X})\, \varphi_A \quad \forall \mathbf{X} \in \mathcal{E}. \tag{4.2}$$

The restriction of φ^h to a given geometric entity ε may be written in terms of only those basis functions $\{\psi_a^\varepsilon\}_{a=1}^{N_{bf}^\varepsilon} \subset \mathcal{U}^h(\Omega)$ which possess compact support over ε, such that

$$\varphi^h|_\varepsilon(\mathbf{X}) = \sum_{a=1}^{N_{bf}^\varepsilon} \psi_a^\varepsilon(\mathbf{X})\, \varphi_a \quad \forall \mathbf{X} \in \varepsilon. \tag{4.3}$$

To guarantee $P^k(\mathcal{E}) \subset \mathcal{U}^h(\mathcal{E})$ for some desired degree of polynomial completeness k, it is necessary for a given entity's local basis $\{\psi_a^\varepsilon\}_{a=1}^{N_{bf}^\varepsilon}$ to span $P^k(\varepsilon)$. Arguably the simplest such basis consists of the monomials through order k defined on each entity $\varepsilon \in \mathcal{T}_\varepsilon(\mathcal{E})$. However, the use of (unscaled) monomial bases can lead to ill-conditioning of the DG-PEM problem, particularly as the maximal polynomial degree k is increased. This fact has been well-established in the literature pertaining to discontinuous Galerkin methods (see for example [29].) An exploration of the condition number for the resulting DG-PEM systems of equations is presented at the end of this chapter. For this reason, other (well-scaled) polynomial bases are recommended, such as the Lagrange polynomials defined on each entity (for linear segments and triangular facets), or the orthogonal polynomials obtained via the methodology proposed in [6].

Regardless of the chosen basis, each basis function $\psi(\mathbf{X})$ may be expressed as a low-order polynomial (of maximal degree k) via a linear combination of (possibly shifted) monomials:

$$\psi(\mathbf{X}) = \sum_{|\alpha| \leq k} c_\alpha (\mathbf{X} - \mathbf{X}_0)^\alpha, \tag{4.4}$$

where $\alpha = \alpha_1, \ldots, \alpha_d$ is a multi-index, such that $|\alpha| = \alpha_1 + \ldots + \alpha_2$ and $\mathbf{X}^\alpha = X_1^{\alpha_1} \cdots X_d^{\alpha_d}$. Consequently, a given basis function is uniquely defined in terms of its shifted coordinate $\mathbf{X}_0$, and its monomial coefficients c_α. The gradient of a given basis function $\nabla\psi(\mathbf{X})$ may in turn be computed via

$$\frac{\partial \psi(\mathbf{X})}{\partial X_i} = \sum_{|\alpha| \leq k} \alpha_i c_\alpha (\mathbf{X} - \mathbf{X}_0)^{\alpha_1, \ldots, (\alpha_i - 1), \ldots, \alpha_d}. \tag{4.5}$$

4.5 Linearization and Assembly of the DG-PEM Systems of Equations

The DG-PEM problem of (3.33) may be written as a linear system of equations arising from the chosen basis $\{\psi_A\}_{A=1}^{N_{bf}^{\mathcal{E}}}$ for $\mathcal{U}^h(\mathcal{E})$, such that the basis function coefficients $\varphi_A \; \forall A = 1, \ldots, N_{bf}^{\mathcal{E}}$ representing a given shape function $\varphi^h(\mathbf{X}) = \sum_{A=1}^{N_{bf}^{\mathcal{E}}} \psi_A(\mathbf{X})\, \varphi_A$ may be determined as the solution to:

$$\sum_{A=1}^{N_{bf}^{\mathcal{E}}} J_{AB}\, \varphi_A = F_B \quad \forall B = 1, \ldots, N_{bf}^{\mathcal{E}}, \tag{4.6}$$

where J_{AB} and F_B are computed via an entity-wise assembly process (akin to the methodology employed for assembling finite element systems of equations). However, in addition to assembling local contributions J_{ab}^{ε} and F_b^{ε} to J_{AB} and F_B from all d-dimensional entities $\varepsilon \in \mathcal{T}_{\varepsilon}(\mathcal{E})$, here it is also necessary to assemble appropriate contributions from all $(d-1)$-dimensional interfaces $\zeta \in \Gamma_{\varepsilon} \cup \partial\mathcal{E}$, as well.

Specifically, each d-dimensional entity $\varepsilon \in \mathcal{T}_{\varepsilon}(\mathcal{E})$ contributes the following local arrays:

$$J_{ab}^{\varepsilon} = \int_{\varepsilon} \nabla\psi_a^{\varepsilon} \cdot \nabla\psi_b^{\varepsilon}\, d\varepsilon, \quad \forall a,\, b = 1, \ldots, N_{bf}^{\varepsilon}, \tag{4.7}$$

$$F_b^{\varepsilon} = \int_{\varepsilon} f_{\mathcal{E}}\, \psi_b^{\varepsilon}\, d\varepsilon \quad \forall b = 1, \ldots, N_{bf}^{\varepsilon}, \tag{4.8}$$

each $\zeta \in \partial\mathcal{E}$ (which borders a single d-dimensional entity ε) contributes:

$$J_{ab}^{\varepsilon} = \int_{\zeta} \left(\epsilon\, \mathbf{N}_{\zeta} \cdot \nabla\psi_a^{\varepsilon}\, \psi_b^{\varepsilon} - \psi_a^{\varepsilon}\, \nabla\psi_b^{\varepsilon} \cdot \mathbf{N}_{\zeta} \right) d\zeta + \frac{\alpha_{\zeta 0}}{|\zeta|^{\beta_0}} \int_{\zeta} \psi_a^{\varepsilon}\, \psi_b^{\varepsilon}\, d\zeta \quad \forall a,\, b = 1, \ldots, N_{bf}^{\varepsilon}, \tag{4.9}$$

$$F_b^{\varepsilon} = \int_{\zeta} \epsilon\, \bar{\varphi}\, \nabla\psi_b^{\varepsilon} \cdot \mathbf{N}_{\zeta}\, d\zeta + \frac{\alpha_{\zeta 0}}{|\zeta|^{\beta_0}} \int_{\zeta} \bar{\varphi}\, \psi_b^{\varepsilon}\, d\zeta \quad \forall b = 1, \ldots, N_{bf}^{\varepsilon}, \tag{4.10}$$

and each $\zeta \in \Gamma_{\varepsilon}$ (which borders two d-dimensional entities, ε_1 and ε_2) contributes:

$$J_{ab}^{\varepsilon_i \varepsilon_j} = -\frac{1}{2} \int_{\zeta} \left((-1)^j\, \epsilon\, \mathbf{N}_{\zeta} \cdot \nabla\psi_a^{\varepsilon_i}\, \psi_b^{\varepsilon_j} - (-1)^i \psi_a^{\varepsilon_i}\, \nabla\psi_b^{\varepsilon_j} \cdot \mathbf{N}_{\zeta} \right) d\zeta \tag{4.11}$$

$$+ (-1)^{|i-j|} \frac{\alpha_{\zeta 0}}{|\zeta|^{\beta_0}} \int_{\zeta} \psi_a^{\varepsilon_i}\, \psi_b^{\varepsilon_j}\, d\zeta \tag{4.12}$$

$$+ (-1)^{|i-j|} \frac{\alpha_{\zeta 1}}{|\zeta|^{\beta_1}} \int_{\zeta} \nabla\psi_a^{\varepsilon_i} \cdot (\mathbf{N}_{\zeta} \otimes \mathbf{N}_{\zeta}) \cdot \nabla\psi_b^{\varepsilon_j}\, d\zeta \tag{4.13}$$

for all $i,\ j = 1,\ 2$, and $a = 1, \ldots, N_{bf}^{\varepsilon_i}$, $b = 1, \ldots, N_{bf}^{\varepsilon_j}$. For the remainder of our discussions, we will consider only the case where $f_{\mathcal{E}} \equiv 0$ for all sub-elements $\mathcal{E} \subset \Omega$.

For a given d-dimensional sub-element $\mathcal{E}$, the assembly of the above terms entails an entity-wise integration of products between basis functions (and their gradients) over d-dimensional entities $\varepsilon \in \mathcal{T}_{\varepsilon}(\mathcal{E})$ and their $(d-1)$-dimensional children $\zeta \in \Gamma_{\varepsilon} \cup \partial\mathcal{E}$. This may be effected through the use of appropriately defined quadrature rules on each entity, or by pre-computing the monomial integrals over each entity up to some sufficiently high degree (nominally $2k$).

Additionally, it is remarked that the boundary condition $\bar{\varphi}$ is defined independently on every $(d-1)$-dimensional sub-element $e \subset \partial\mathcal{E}$, such that its restriction $\bar{\varphi}|_{\zeta}$ may be written in terms of the local basis functions $\left\{\psi_c^{\zeta}\right\}_{c=1}^{N_{bf}^{\zeta}}$ belonging to a given boundary entity $\zeta \in \mathcal{T}_{\zeta}(e)$, i.e.

$$\bar{\varphi}|_{\zeta}(\mathbf{X}) = \sum_{c=1}^{N_{bf}^{\zeta}} \psi_c^{\zeta}(\mathbf{X})\, \bar{\varphi}_c. \tag{4.14}$$

For a given $\zeta \in \partial\mathcal{E}$, this yields:

$$F_b^{\varepsilon} = \sum_{c=1}^{N_{bf}^{\zeta}} \bar{J}_{bc}^{\varepsilon}\, \bar{\varphi}_c \quad \forall b = 1, \ldots, N_{bf}^{\varepsilon}, \tag{4.15}$$

which may be used in lieu of (4.10), where

$$\bar{J}_{bc}^{\varepsilon} = \int_{\zeta} \epsilon\, \psi_c^{\zeta}\, \nabla\psi_b^{\varepsilon} \cdot \mathbf{N}_{\zeta}\, d\zeta + \frac{\alpha_{\zeta 0}}{|\zeta|^{\beta_0}} \int_{\zeta} \psi_c^{\zeta}\, \psi_b^{\varepsilon}\, d\zeta \quad \forall b = 1, \ldots, N_{bf}^{\varepsilon},\ c = 1, \ldots, N_{bf}^{\zeta}. \tag{4.16}$$

Consequently, we may re-write the right-hand side of (4.6) as a linear mapping from the basis coefficients $\bar{\varphi}_C$ which determine the boundary function $\bar{\varphi}(\mathbf{X}) = \sum_{C=1}^{N_{bf}^{\partial\mathcal{E}}} \psi_C(\mathbf{X})\, \bar{\varphi}_C$:

$$\sum_{A=1}^{N_{bf}^{\mathcal{E}}} J_{AB}\, \varphi_A = \sum_{C=1}^{N_{bf}^{\partial\mathcal{E}}} \bar{J}_{BC}\, \bar{\varphi}_C \quad \forall B = 1, \ldots, N_{bf}^{\mathcal{E}}, \tag{4.17}$$

which may alternatively be written in matrix-vector format:

$$\mathbf{J}\, \boldsymbol{\varphi} = \bar{\mathbf{J}}\, \bar{\boldsymbol{\varphi}}. \tag{4.18}$$

The above system of equations can be solved to obtain a linear mapping from $\bar{\boldsymbol{\varphi}}$ to $\boldsymbol{\varphi}$, denoted $\mathbf{M}^{\partial\mathcal{E}\mapsto\mathcal{E}} = \mathbf{J}^{-1}\bar{\mathbf{J}} : \mathbb{R}^{N_{bf}^{\partial\mathcal{E}}} \mapsto \mathbb{R}^{N_{bf}^{\mathcal{E}}}$. This mapping may be utilized to define the shape

functions in a recursive fashion (over the children of each sub-element, in succession), ultimately yielding a representation for the shape functions on $\mathcal{E}$ in terms of only nodal evaluations $\varphi|_V$. This process is discussed in greater detail in the following section.

Hierarchial Construction of Shape Functions

For a given polyhedral element $\Omega \subset \mathbb{R}^d$, we presume that each shape function φ_A is associated with a particular node V_A of the element, such that

$$\varphi_A|_{V_B} = \delta_{AB} \quad \forall A,\, B = 1, \ldots, N_V. \tag{4.19}$$

Additionally, for the sake of simplicity (and computational efficiency), it is suggested that the shape functions along each linear edge E be constructed from the Lagrange polynomials which interpolate the nodal values of that edge, i.e.

$$\varphi_A|_E(\mathbf{X}) = \sum_{b=1}^{N_V^E} \psi_b(\mathbf{X})\, \varphi_A|_{V_b}. \tag{4.20}$$

For each polygonal face F, linear mappings $\mathbf{M}^{\partial F \mapsto F} : \mathbb{R}^{N_V^F} \mapsto \mathbb{R}^{N_{bf}^F}$ may be constructed according to the process described in the previous section, yielding

$$\varphi_A|_F(\mathbf{X}) = \sum_{b=1}^{N_{bf}^F} \sum_{c=1}^{N_V^F} \psi_b(\mathbf{X})\, M_{bc}^{\partial F \mapsto F} \varphi_A|_{V_c}. \tag{4.21}$$

Subsequently, a mapping $\mathbf{M}^{\partial\Omega \mapsto \Omega} : \mathbb{R}^{N_{bf}^{\partial\Omega}} \mapsto \mathbb{R}^{N_{bf}^{\Omega}}$ is constructed to determine the representation for the shape functions on the interior of the element, which may be composed with the mappings $\mathbf{M}^{\partial F \mapsto F}$ for each face to determine a final mapping $\mathbf{M}^{V \mapsto \Omega} : \mathbb{R}^{N_V^\Omega} \mapsto \mathbb{R}^{N_{bf}^\Omega}$ which yields

$$\varphi_A|_\Omega(\mathbf{X}) = \sum_{b=1}^{N_{bf}^\Omega} \sum_{c=1}^{N_V^\Omega} \psi_b(\mathbf{X})\, M_{bc}^{V \mapsto \Omega} \varphi_A|_{V_c}. \tag{4.22}$$

Once the above representations for the element's have been obtained, the discrete data for the element (evaluations of the shape functions and their gradients at a discrete number of quadrature points $\{\mathbf{X}_q\}_{q=1}^{N_{qp}}$ can be obtained directly from

$$\varphi_A|_\Omega(\mathbf{X}_q) = \sum_{b=1}^{N_{bf}^\Omega} \sum_{c=1}^{N_V^\Omega} \psi_b(\mathbf{X}_q)\, M_{bc}^{V \mapsto \Omega} \varphi_A|_{V_c}, \tag{4.23}$$

and

$$\nabla\varphi_A|_\Omega(\mathbf{X}_q) = \sum_{b=1}^{N_{bf}^\Omega} \sum_{c=1}^{N_V^\Omega} \nabla\psi_b(\mathbf{X}_q)\, M_{bc}^{V\mapsto\Omega} \varphi_A|_{V_c}. \tag{4.24}$$

Once the discrete quadrature point evaluations for the shape functions have been obtained, there is no need to retain any information regarding the DG-PEM basis functions, or the transitional mappings; these objects and their corresponding data structures may therefore be discarded.

The specification of the element's quadrature rule is discussed in the following section.

Construction of Quadrature Rules

The quadrature rule for an element $\{\mathbf{X}_q,\, w_q\}_{q=1}^{N_{qp}}$ nominally consists of quadrature points $\mathbf{X}_q$ located at the centroids of each cell $\omega \in \mathcal{T}_\omega(\Omega)$, whose corresponding quadrature weights w_q are equal to the volumes of each respective cell $|\omega|$. This results in the composite mid-point rule discussed in chapter 3.

As presviously discussed, the volumes $|\omega|$ and centroids $\bar{\mathbf{X}}_\omega$ of each cell may be obtained via the exact integration formulas provided by Chin et al. in [12]. Alternatively, we may exploit the geometric simplicity of the chosen edge-based partitioning to compute these quantities more easily, by considering the fact that each edge-centered cell ω consists of two tetrahedral sub-domains (i.e. $T_1 \cup T_2 = \omega$). Volumes and centroids for each tetrahedron can be easily computed using standard formulas, and the resulting quantities of interest may be expressed as

$$|\omega| = |T_1| + |T_2|, \quad \bar{\mathbf{X}}_\omega = \frac{|T_1|\bar{\mathbf{X}}_{T_1} + |T_2|\bar{\mathbf{X}}_{T_2}}{|\omega|}. \tag{4.25}$$

Straightforward integration rules $\{\mathbf{X}_q,\, w_q\}_{q=1}^{N_{qp}^F}$ for each face $F \subset \partial\Omega$ are more more easily obtained by considering the corresponding areas $|\sigma|$ and centroids $\bar{\mathbf{X}}_\sigma$ of each (strictly triangular) facet $\sigma \in \mathcal{T}_\sigma(F)$. Outward unit normals $\mathbf{N}_\sigma$ to each facet may also be readily computed and stored, as needed.

With these quantities in hand, the element's shape functions (and their gradients) may be evaluated at the quadrature points of the element and it's faces. Subsequently, a consistent integration scheme (as discussed in 3) may be constructed from the discrete

data stored at the element's quadrature points. If a gradient correction scheme is adopted, the corrected test function gradients $\nabla\phi_A(\mathbf{X}_q)$ at all quadrature points may be computed and stored according to the methodology previously described.

4.6 Numerical Conditioning of the DG-PEM Systems of Equations

As a representative example, consider a given sub-element $\mathcal{E} \subset \mathbb{R}^d$ and its corresponding partition into $d-$dimensional entities $\varepsilon \subset \mathcal{T}_\varepsilon(\mathcal{E})$. Recall that the representation of a given shape function $\varphi \in \mathcal{U}^h(\mathcal{E})$ is piecewise polynomial in each entity, i.e. $\varphi|_\varepsilon \in P^k(\varepsilon)$.

A reasonable estimate for the condition number $\kappa(\mathbf{J})$ of the SPD matrix $\mathbf{J}$ appearing in (4.18) may be obtained via

$$\frac{\max_a |J^\varepsilon_{aa}|}{\min_a |J^\varepsilon_{aa}|} \leq \kappa(\mathbf{J}), \tag{4.26}$$

where

$$\begin{aligned} J^\varepsilon_{aa} = &\int_\varepsilon \nabla\psi^\varepsilon_a \cdot \nabla\psi^\varepsilon_a \, d\varepsilon + (\epsilon - 1) \sum_{\zeta \in \partial\varepsilon \cap \partial\mathcal{E}} \int_\zeta (\psi^\varepsilon_a) \left(\mathbf{N}_\zeta \cdot \nabla\psi^\varepsilon_a\right) \, d\zeta \\ &+ \frac{1}{2}(\epsilon - 1) \sum_{\zeta \in \partial\varepsilon \cap \Gamma_\varepsilon} \int_\zeta (\psi^\varepsilon_a) \left(\mathbf{N}_\zeta \cdot \nabla\psi^\varepsilon_a\right) \, d\zeta \\ &+ \sum_{\zeta \in \partial\varepsilon} \frac{\alpha_{\zeta 0}}{|\zeta|^{\beta_0}} \int_\zeta (\psi^\varepsilon_a)^2 \, d\zeta + \sum_{\zeta \in \partial\varepsilon \cap \Gamma_\varepsilon} \frac{\alpha_{\zeta 1}}{|\zeta|^{\beta_1}} \int_\zeta \left(\mathbf{N}_\zeta \cdot \nabla\psi^\varepsilon_a\right)^2 \, d\zeta. \end{aligned} \tag{4.27}$$

A brief remark should be made regarding the positivity of J^ε_{aa}, and its relation to the particular choice of DG method (i.e. whether the SIPG, NIPG, or IIPG is chosen). As discussed in [47], the NIPG method with $\epsilon = +1$ will yield strictly positive diagonal entries provided $\alpha_{\zeta 0} > 0$, resulting in the coercivity of $\mathbf{J}$. If the SIPG ($\epsilon = -1$) or IIPG ($\epsilon = 0$) methods are employed, then the penalty parameters must be made sufficiently large enough to guarantee coercivity, stability.

The subsequent discussion examines the case where $\epsilon = +1$, yielding:

$$J^\varepsilon_{aa} = \int_\varepsilon \nabla\psi^\varepsilon_a \cdot \nabla\psi^\varepsilon_a \, d\varepsilon + \sum_{\zeta \in \partial\varepsilon} \frac{\alpha_{\zeta 0}}{|\zeta|^{\beta_0}} \int_\zeta (\psi^\varepsilon_a)^2 \, d\zeta + \sum_{\zeta \in \partial\varepsilon \cap \Gamma_\varepsilon} \frac{\alpha_{\zeta 1}}{|\zeta|^{\beta_1}} \int_\zeta \left(\mathbf{N}_\zeta \cdot \nabla\psi^\varepsilon_a\right)^2 \, d\zeta. \tag{4.28}$$

Let h_ε denote the diameter of ε, such that

$$h_\varepsilon = \sup_{\mathbf{X},\mathbf{Y} \in \varepsilon} ||\mathbf{X} - \mathbf{Y}||_2. \tag{4.29}$$

Using the following trace inequalities:

$$\int_{\zeta} (\psi_a^{\varepsilon})^2 \, d\zeta \leq C h_{\varepsilon}^{-1/2} \int_{\varepsilon} (\psi_a^{\varepsilon})^2 \, d\varepsilon \quad \forall \zeta \subset \partial\varepsilon, \tag{4.30}$$

$$\int_{\zeta} (\mathbf{N}_{\zeta} \cdot \nabla \psi_a^{\varepsilon})^2 \, d\zeta \leq C h_{\varepsilon}^{-1/2} \int_{\varepsilon} \nabla \psi_a^{\varepsilon} \cdot \nabla \psi_a^{\varepsilon} \, d\varepsilon \quad \forall \zeta \subset \partial\varepsilon, \tag{4.31}$$

and observing $|\zeta|^{\beta_0} \leq h_{\varepsilon}$, $|\zeta|^{\beta_1} \geq h_{\varepsilon}^{-1}$ if $\beta_0 = (d-1)^{-1}$, $\beta_1 = -(d-1)^{-1}$ (assuming $h_{\varepsilon} \geq 1$, without loss of generality), then

$$J_{aa}^{\varepsilon} \leq (1 + C_1 h_{\varepsilon}^{1/2}) \int_{\varepsilon} \nabla \psi_a^{\varepsilon} \cdot \nabla \psi_a^{\varepsilon} \, d\varepsilon + C_2 h_{\varepsilon}^{-3/2} \int_{\varepsilon} (\psi_a^{\varepsilon})^2 \, d\varepsilon. \tag{4.32}$$

If $\varphi|_{\varepsilon}$ is represented in terms of the (unshifted and unscaled) monomial basis (i.e. $\{\varphi_a^{\varepsilon}\}_{a=1}^{N_{bf}^{\varepsilon}} = \{\mathbf{X}^{\alpha}\}_{|\alpha| \leq k}$), then by application of the min-max inequality:

$$\int_{\varepsilon} \mathbf{X}^{2\alpha} \, d\varepsilon \leq h_{\varepsilon}^d \max_{\mathbf{X} \in \varepsilon} \{\mathbf{X}^{2\alpha}\} \leq h_{\varepsilon}^d R_{\varepsilon}^{2|\alpha|}, \tag{4.33}$$

$$\int_{\varepsilon} \nabla \mathbf{X}^{\alpha} \cdot \nabla \mathbf{X}^{\alpha} \, d\varepsilon \leq h_{\varepsilon}^d \max_{\mathbf{X} \in \varepsilon} \{\nabla \mathbf{X}^{\alpha} \cdot \nabla \mathbf{X}^{\alpha}\} \leq h_{\varepsilon}^d R_{\varepsilon}^{2\langle |\alpha| - 1 \rangle}, \tag{4.34}$$

where

$$R_{\varepsilon} = \max_{\mathbf{X} \in \varepsilon} ||\mathbf{X}||_2. \tag{4.35}$$

Without loss of generality, if $R_{\varepsilon} \geq 1$, it becomes clear that

$$C \left[(h_{\varepsilon}^d + C_1 h_{\varepsilon}^{d+1/2}) + C_2 h_{\varepsilon}^{d-3/2} \right] \leq J_{aa}^{\varepsilon} \leq (h_{\varepsilon}^d + C_1 h_{\varepsilon}^{d+1/2}) R_{\varepsilon}^{2\langle k-1 \rangle} + C_2 h_{\varepsilon}^{d-3/2} R_{\varepsilon}^{2k}. \tag{4.36}$$

If the penalty parameter $\alpha_{\gamma 0}$ is sufficiently small, we obtain the estimate $\kappa(\mathbf{J}) \approx O(R_{\max}^{2\langle k-1 \rangle})$, where $R_{\max} = \max_{\varepsilon \in \mathcal{E}} R_{\varepsilon}$. Otherwise, if $\alpha_{\gamma 0}$ is sufficiently large, then $\kappa(\mathbf{J}) \approx O(R_{\max}^{2k})$; a similar estimate may be obtained for the SIPG and IIPG methods.

Clearly, the condition number of $\mathbf{J}$ under these circumstances may become unacceptably large for increasing values of k and $R_{\max}$, leading to numerical inaccuracies in the resulting shape functions, which ultimately degrades the degree of precision by which finite element patch tests are satisfied.

To mitigate this issue, the (sub-)element's shape functions may be computed with respect to a shifted and scaled coordinate system, i.e. $\mathbf{X}' = h_{\mathcal{E}}^{-1}(\mathbf{X} - \bar{\mathbf{X}}_0^{\mathcal{E}})$. This assists in limiting the worst-case value of $R_{\max}$ appearing in the previous estimate, yielding a

somewhat improved bound on the condition number: $\kappa(\mathbf{J}) \approx O(\rho^{2k})$, where $\rho = h_{\mathcal{E}}/h_{\min}$, and where

$$h_{\min} = \inf_{\varepsilon \in \mathcal{T}_\varepsilon(\mathcal{E})} \sup_{B_r(\mathbf{X}_B) \subset \varepsilon} |2r| \tag{4.37}$$

denotes the smallest diameter of the largest closed ball $B_r(\mathbf{X}_B) = \left\{ \mathbf{X} \in \mathbb{R}^d : ||\mathbf{X} - \mathbf{X}_B||_2 \leq r \right\}$ fully contained within any single entity $\varepsilon \in \mathcal{T}_\varepsilon(\mathcal{E})$. Nonetheless, the condition number of $\mathbf{J}$ can become large if: a relatively refined partition of the element is utilized; if the aspect ratio of the element becomes large; or if the element's partition contains "sliver cells" (i.e. if an edge-based partition is employed on an element with nearly degenerate geometric features – short edges.)

Significant improvements in obtaining more well-conditioned systems can be had by considering the DG basis described in [6].

Further, consider an individual interface ζ which separates two entities, ε_1 and ε_2. Note that

$$\int_\zeta [\![\varphi]\!]^2 \, ds = (\mathbf{c}^{\varepsilon_1} - \mathbf{c}^{\varepsilon_2}) \cdot \left[\int_\zeta \mathbf{m} \otimes \mathbf{m} \, d\zeta \right] (\mathbf{c}^{\varepsilon_1} - \mathbf{c}^{\varepsilon_2}), \tag{4.38}$$

and

$$h_b^2 \int_\zeta [\![\mathbf{N} \cdot \nabla \varphi]\!]^2 \, d\zeta = (\mathbf{c}^{\varepsilon_1} - \mathbf{c}^{\varepsilon_2}) \cdot \left[h_b^2 \int_\zeta \frac{\partial \mathbf{m}}{\partial N} \otimes \frac{\partial \mathbf{m}}{\partial N} \, d\zeta \right] (\mathbf{c}^{\varepsilon_1} - \mathbf{c}^{\varepsilon_2}), \tag{4.39}$$

where we prescribe $h_b = (|\sigma_{b1}| + |\sigma_{b2}|)/|\gamma_b|$ to obtain a proportional scaling of the two integral contributions to $\mathcal{G}$. If we define moment matrices $\mathbf{M}_{0b}$ and $\mathbf{M}_{1b}$ as

$$\mathbf{M}_{0b} \equiv \int_{\gamma_b} \mathbf{m} \otimes \mathbf{m} \, ds \tag{4.40}$$

$$\mathbf{M}_{1b} \equiv h_b^2 \int_{\gamma_b} \frac{\partial \mathbf{m}}{\partial n} \otimes \frac{\partial \mathbf{m}}{\partial n} \, ds \tag{4.41}$$

then we may express the local contribution from segment γ_b to $\mathcal{G}$ as

$$\mathcal{G}_b = \frac{1}{2} \left\{ \begin{array}{c} \mathbf{a}_{\sigma_{b1}} \\ \mathbf{a}_{\sigma_{b2}} \end{array} \right\} \cdot \left(\beta_0 \left[\begin{array}{cc} \mathbf{M}_{0b} & -\mathbf{M}_{0b} \\ -\mathbf{M}_{0b} & \mathbf{M}_{0b} \end{array} \right] + \beta_1 \left[\begin{array}{cc} \mathbf{M}_{1b} & -\mathbf{M}_{1b} \\ -\mathbf{M}_{1b} & \mathbf{M}_{1b} \end{array} \right] \right) \left\{ \begin{array}{c} \mathbf{a}_{\sigma_{b1}} \\ \mathbf{a}_{\sigma_{b2}} \end{array} \right\}, \tag{4.42}$$

or more concisely:

$$\mathcal{G}_b = \frac{1}{2} \mathbf{a}_{\sigma_{b_{1,2}}} \cdot \mathbf{J}_b \mathbf{a}_{\sigma_{b_{1,2}}}. \tag{4.43}$$

The matrix $\mathbf{J}_b$ expressed in the above equation constitutes a local contribution from segment γ_b to the Jacobian of $\partial \mathcal{G}/\partial \mathbf{a}_{\sigma_c}$ (i.e. to $\mathbf{J} = \partial^2 \mathcal{G}/\partial \mathbf{a}_{\sigma_c} \partial \mathbf{a}_{\sigma_d}$, which will ultimately be

inverted when we solve for the unknown monomial coefficients in each cell). Consequently, it becomes of interest to investigate the condition number for the Jacobian of $\partial\mathcal{G}/\partial\mathbf{a}_{\sigma_c}$ in terms of our choice of polynomial basis.

We proceed in obtaining a rough approximation to $\kappa(\mathbf{J})$ by examining a particular element whose partition contains only one cell σ. For this simple case, we have

$$\mathbf{J} = \beta_0 \int_{\partial\sigma} \mathbf{m} \otimes \mathbf{m}\, ds = \beta_0 \sum_{\forall b} \mathbf{M}_{0b}. \tag{4.44}$$

Let us approximate the bounds for each monomial integral. By application of the triangle inequality to the Riemann integral of the monomials over $\partial\sigma$, we obtain

$$\left| \int_{\partial\sigma} m_i m_j \, ds \right| \leq \int_{\partial\sigma} |m_i m_j| \, ds, \tag{4.45}$$

and by the max-min inequality, we find

$$\int_{\partial\sigma} |m_i m_j| \, ds \leq \max_{\mathbf{x}\in\partial\sigma}\{|m_i m_j|\} \int_{\partial\sigma} ds. \tag{4.46}$$

Since the monomials are continuous functions on $\partial\sigma$, by the mean-value theorem we have

$$m_i^* m_j^* \int_{\partial\sigma} ds = \int_{\partial\sigma} m_i m_j \, ds \tag{4.47}$$

and by extension

$$|m_i^* m_j^*| \int_{\partial\sigma} ds = \left| \int_{\partial\sigma} m_i m_j \, ds \right| \tag{4.48}$$

for some $m_i^* m_j^*$ evaluated at a particular $\mathbf{x}^* \in \partial\sigma$. By the extreme value theorem and the continuity of $|m_i m_j|$,

$$\min_{\mathbf{x}\in\partial\sigma}\{|m_i m_j|\} \leq |m_i^* m_j^*| \leq \max_{\mathbf{x}\in\partial\sigma}\{|m_i m_j|\}. \tag{4.49}$$

Therefore,

$$\min_{\mathbf{x}\in\partial\sigma}\{|m_i m_j|\} \int_{\partial\sigma} ds \leq |m_i^* m_j^*| \int_{\partial\sigma} ds = \left| \int_{\partial\sigma} m_i m_j \, ds \right|, \tag{4.50}$$

and our bounds are thus,

$$\min_{\mathbf{x}\in\partial\sigma}\{|m_i m_j|\} \int_{\partial\sigma} ds \leq \left| \int_{\partial\sigma} m_i m_j \, ds \right| \leq \max_{\mathbf{x}\in\partial\sigma}\{|m_i m_j|\} \int_{\partial\sigma} ds. \tag{4.51}$$

These bounds are approximate, and in particular, the lower bound may be equal to zero in some cases. For our analysis of the condition number, these bounds prove to be insufficient. Indeed, the monomials of odd degree may well be equal to zero, but those of even degree are guaranteed to be non-zero for any cell σ with finite area. It suffices to consider the projection $\mathcal{P}(\sigma)$ of the domain of σ onto any linear subspace of dimension 1 which yields a characteristic minimum dimension $d_{\min}$:

$$d_{\min} = \inf_{\mathcal{P}(\sigma)} \{ \sup_{x,y \in \mathcal{P}(\sigma)} \{|x - y|\}\}. \tag{4.52}$$

Intuitively, $d_{\min}$ is the smallest possible dimension of any bounding box which contains σ. It is not difficult to see that the integral of any monomial of even degree $2p$ will be bounded from below by a finite term of order $O(d_{\min}^{2p})$. This remark will find significance later on.

Returning to the Jacobian $\mathbf{J}$, its entries J_{ij} correspond to

$$J_{ij} = \beta_0 \int_{\partial\sigma} m_i m_j \, ds. \tag{4.53}$$

By Gershgorin's theorem, we may determine approximate bounds for every eigenvalue λ of $\mathbf{J}$, such that

$$|\lambda - J_{ii}| \leq \sum_{j \neq i} |J_{ij}| \quad \forall i, \tag{4.54}$$

and consequently

$$c_i - d_i \leq \lambda \leq c_i + d_i \quad \forall i, \tag{4.55}$$

where

$$c_i = \beta_0 \int_{\partial\sigma} m_i m_i \, ds, \tag{4.56}$$

$$d_i = \sum_{j \neq i} \left| \beta_0 \int_{\partial\sigma} m_i m_j \, ds \right|. \tag{4.57}$$

The condition number of $\mathbf{J}$ is then bounded by

$$\kappa(\mathbf{J}) \leq \frac{\max_i\{|c_i + d_i|\}}{\min_i\{|c_i - d_i|\}}. \tag{4.58}$$

By the triangle inequality

$$|c_i + d_i| \leq |c_i| + |d_i| = \sum_j \left| \beta_0 \int_{\partial\sigma} m_i m_j \, ds \right|, \tag{4.59}$$

such that

$$\kappa(\mathbf{J}) \leq \frac{\max_i\{|c_i + d_i|\}}{\min_i\{|c_i - d_i|\}} \leq \frac{\max_i\{|c_i| + |d_i|\}}{\min_i\{|c_i - d_i|\}}. \tag{4.60}$$

where

$$\max_i\{|c_i| + |d_i|\} = \max_i \left\{ \sum_j \left| \beta_0 \int_{\partial\sigma} m_i m_j \, ds \right| \right\}. \tag{4.61}$$

Provided $\beta_0 > 0$,

$$\max_i\{|c_i| + |d_i|\} \leq \beta_0 \max_i \left\{ \sum_j \max_{\mathbf{x}\in\partial\sigma}\{|m_i m_j|\} \right\} \int_{\partial\sigma} ds. \tag{4.62}$$

Since $\mathbf{J}$ is assumed to be positive definite, $c_i > 0$ and $c_i - |d_i| > 0$, and we may write (approximately)

$$\min_i\{|c_i - d_i|\} \approx \min_i\{|c_i|\} \geq \beta_0 \min_i \left\{ \beta_0 \int_{\partial\sigma} m_i m_i \, ds \right\}. \tag{4.63}$$

Suppose there exist some maximum and minimum radii $r_{\max}$ and $r_{\min}$ such that $r_{\min} \leq ||\mathbf{x}||_2 \leq r_{\max} \, \forall \mathbf{x} \in \partial\sigma$ and $r_{\max} > r_{\min} \geq 0$. Note that if $r_{\max} > 1$, then

$$\max_i \left\{ \sum_j \max_{\mathbf{x}\in\partial\sigma}\{|m_i m_j|\} \right\} = O(r_{\max}^{2k}), \tag{4.64}$$

and if $r_{\max} < 1$, then

$$\max_i \left\{ \sum_j \max_{\mathbf{x}\in\partial\sigma}\{|m_i m_j|\} \right\} = O(1). \tag{4.65}$$

Separately, if $r_{\min} > 1$, then

$$\min_i \left\{ \int_{\partial\sigma} m_i m_i \, ds \right\} \geq \min_i \left\{ \min_{\mathbf{x}\in\partial\sigma}\{|m_i m_i|\} \right\} \int_{\partial\sigma} ds = O(1), \tag{4.66}$$

and if $r_{\min} < 1$, then

$$\min_i \left\{ \int_{\partial\sigma} m_i m_i \, ds \right\} \geq \min_i \left\{ \min_{\mathbf{x}\in\partial\sigma}\{|m_i m_i|\} \right\} \int_{\partial\sigma} ds = O(r_{\min}^{-2k}). \tag{4.67}$$

If $r_{\min} = 0$ (or when $d_{\min} > 2r_{\min}$), we invoke our alternative lower bound for the monomial integrals of even degree, such that

$$\min_i \left\{ \int_{\partial\sigma} m_i m_i \, ds \right\} = O(d_{\min}^{-2k}). \tag{4.68}$$

Now, define a characteristic dimension h satisfying

$$h = \frac{\max\{r_{\max},\, 1\}}{\min\{\max\{d_{\min}/2,\, r_{\min}\},\, 1\}}. \tag{4.69}$$

The approximate condition number of $\mathbf{J}$ for a given cell σ with characteristic dimension h using a monomial basis up to order k is then

$$\kappa(\mathbf{J}) \approx O(h^{2k}). \tag{4.70}$$

Following a number of numerical experiments, it was determined that the estimate in (4.74) is quite accurate, and illuminates a number of key points:

(I.) The condition number depends upon the dimensions of the element, and more specifically, upon the dimensions of its partition.

a. Isotropically scaling an element will change the condition number of the resulting PEM linear systems, for better or for worse. This would seem to justify the idea of rescaling PEM elements into a corresponding "parent" domain – ideally one which minimizes h. Shape functions and gradients would then be computed in the parent configuration, and subsequently mapped back into the element's physical configuration.

b. Choosing the element's reference coordinate system poorly may subtly impact the conditioning of the PEM linear systems. This further justifies the idea that the element's local coordinate system should be shifted in such a way as to minimize h. However, certain choices of reference coordinate may be preferable/optimal for the different tope-level minimum problems. Namely, recent numerical experiments have revealed that the solution inaccuracies caused by nearly planar faces can be effectively mitigated when the element's reference coordinate is chosen to lie on or near the warped face(s). This finding may warrant the reconsideration of a local coordinate system being used for every cell (or at the very least, for every tope) of the element.

c. Elements with unequal dimensions (i.e. thin elements) will unavoidably suffer from issues of poor conditioning due to a larger relative value of h (regardless

of isotropic scaling). The natural temptation would be to scale the element anisotropically in an effort to achieve better conditioning. However, this would need to be done with care; every tope of the element would need to be scaled independently, according to a given tope's dimensions alone. This condition is necessary to guarantee inter-face compatibility between elements, as two anisotropically scaled elements would not, in general, produce identical shape functions on their shared face.

(II.) The condition number becomes drastically worse when higher order monomials are used.

a. This explains a great deal about why the quadratic PEM elements have performed so poorly in convergence studies up to this point: not only does h become worse under mesh refinement, but the condition number scales as $O(h^4)$ for quadratic elements, leading to significant inaccuracies in the shape function computations, and subsequent losses in solution accuracy.

b. Unfortunately, this makes thin quadratic elements even more sensitive to the relative scaling of h. It is unclear whether or not anisotropically rescaling the elements will sufficiently improve matters.

(III.) Perhaps most importantly: the strong dependence of the condition number upon h and k is largely a consequence of our specific choice of polynomial basis (i.e. the monomial basis).

a. Because the solution unknowns that we seek are monomial coefficients, it is to be expected that the constant, gradient (and curvature) coefficients may differ by orders of magnitude, depending on the relative scale of the element in physical space.

b. A more robust solution to the aforementioned issues of conditioning might be obtained through the selection of a different polynomial basis for $P_k(\Omega)$ (other than the monomial basis). In particular, the use of an orthonormal polynomial

basis (with respect to an appropriately defined norm on an arbitrary element domain) could entirely circumvent the problem of poor conditioning. To prove this, we would need to illustrate that the resulting condition number of $\mathbf{J}$ using an orthonormal polynomial basis is less sensitive to both h and k.

4.6.1 The Effect of Element Scaling

4.6.2 On the Choice of an Appropriate PEM Basis

Chapter 5

A Numerical Evaluation of the PEM

5.1 Convergence Analysis

Infinite Elastic Plate in Far-Field Tension

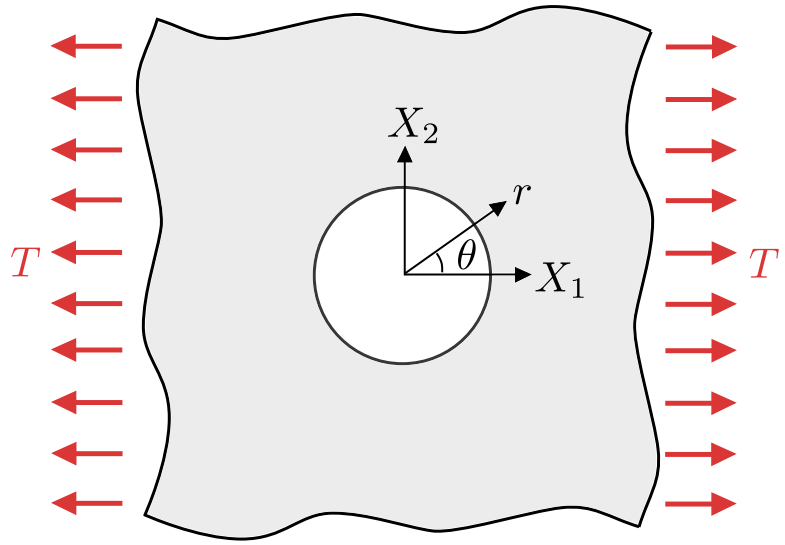

Figure 5.1. Infinite plate with a circular hole placed in uniaxial tension.

To demonstrate optimal convergence of the PEM for higher-order elements, we will choose to investigate the 2D elastostatics problem of an infinite plate with a circular hole in uniaxial tension (depicted in figure 5.1), for which there exist analytical solutions of the resulting displacement and stress fields (obtained from reference [61]):

$$u_1(r,\theta) = \frac{Ta}{8\mu}\left[\frac{r}{a}(\kappa+1)\cos\theta + \frac{2a}{r}((1+\kappa)\cos\theta + \cos 3\theta) - \frac{2a^3}{r^3}\cos 3\theta\right] \tag{5.1}$$

$$u_2(r,\theta) = \frac{Ta}{8\mu}\left[\frac{r}{a}(\kappa-3)\sin\theta + \frac{2a}{r}((1-\kappa)\sin\theta + \sin 3\theta) - \frac{2a^3}{r^3}\sin 3\theta\right] \tag{5.2}$$

$$\sigma_{11}(r,\theta) = T - T\frac{a^2}{r^2}\left(\frac{3}{2}\cos 2\theta + \cos 4\theta\right) + T\frac{3a^4}{2r^4}\cos 4\theta \tag{5.3}$$

$$\sigma_{22}(r,\theta) = -T\frac{a^2}{r^2}\left(\frac{1}{2}\cos 2\theta - \cos 4\theta\right) - T\frac{3a^4}{2r^4}\cos 4\theta \tag{5.4}$$

$$\sigma_{12}(r,\theta) = -T\frac{a^2}{r^2}\left(\frac{1}{2}\sin 2\theta + \sin 4\theta\right) + T\frac{3a^4}{2r^4}\sin 4\theta \tag{5.5}$$

where T is the far-field value of the applied tensile stress, a is the radius of the circular hole centered at $r = 0$, $\kappa = 4 - 3\nu$ (under plane-strain conditions), and ν and μ are the the Poisson's ratio and shear modulus of the material, respectively.

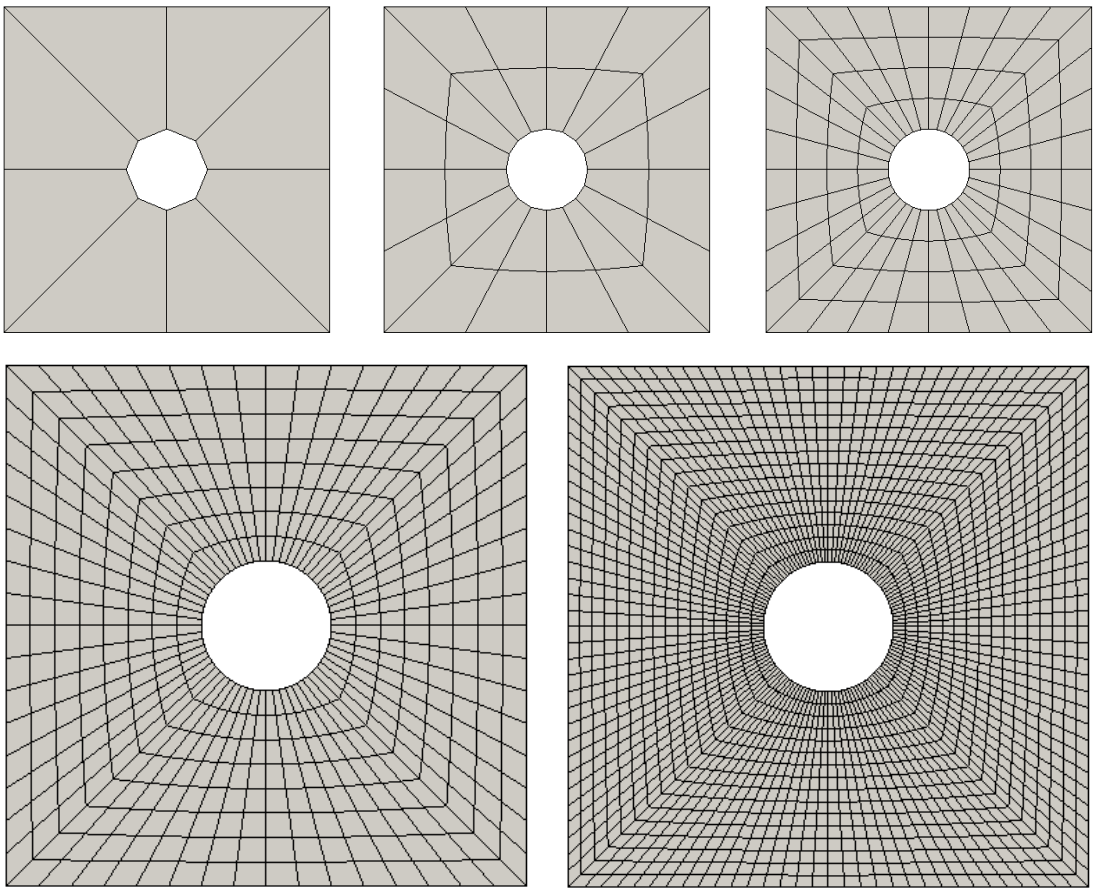

Figure 5.2. Quadrilateral meshes with varying levels of refinement.

A convergence study was carried out using a series of quadrilateral meshes with varying levels of refinement discretizing the restricted problem domain $X_i \in [-1, +1]$ (see

figure 5.2.) The meshes consisted of either 4-node quadrilateral or 8-node serendipity quadrilateral elements, and employed either an isoparametric formulation, or a sufficiently high-order PEM formulation (i.e. $k = 1$ for 4-node quadrilaterals, and $k = 2$ for 8-node quadrilaterals.) Displacement boundary conditions were prescribed to be consistent with the exact solution on the restricted boundary. L^2 displacement error norms and H^1 energy error semi-norms were computed with reference to the exact solution, with the numerical results summarized in tables 5.1-5.4. The convergence rates in the L^2 and H^1 error norms are depicted in figures 5.3 and 5.4, respectively.

h	4-node FEM	4-node PEM	8-node FEM	8-node PEM
1.2500	1.3133E-006	1.4901E-006	9.8369E-007	2.9990E-006
0.8006	6.9557E-007	9.8453E-007	4.8165E-007	1.3918E-006
0.4488	2.8755E-007	4.2859E-007	2.2034E-007	3.3673E-007
0.2371	1.0460E-007	1.3672E-007	8.1971E-008	4.8942E-008
0.1218	3.1430E-008	3.7296E-008	2.4628E-008	6.7201E-009
0.0617	8.3877E-009	9.5661E-009	6.5479E-009	1.6002E-009

Table 5.1. Computed L^2 displacement error norms.

h	4-node FEM	4-node PEM	8-node FEM	8-node PEM
1.2500	-	-	-	-
0.8006	1.4265	0.9302	1.6028	1.7230
0.4488	1.5262	1.4369	1.3512	2.4518
0.2371	1.5848	1.7906	1.5496	3.0225
0.1218	1.8051	1.9502	1.8053	2.9808
0.0617	1.9424	2.0007	1.9479	2.1100

Table 5.2. Computed L^2 displacement error norm convergence rates.

h	4-node FEM	4-node PEM	8-node FEM	8-node PEM
1.2500	2.1468E-001	2.8913E-001	1.8275E-001	5.3700E-001
0.8006	1.8622E-001	2.5620E-001	1.5959E-001	3.0529E-001
0.4488	1.3786E-001	1.7930E-001	1.2495E-001	1.5310E-001
0.2371	9.2075E-002	1.1251E-001	7.9144E-002	5.8671E-002
0.1218	5.2124E-002	6.2223E-002	4.2868E-002	1.5541E-002
0.0617	2.7048E-002	3.2135E-002	2.1789E-002	3.3672E-003

Table 5.3. Computed H^1 energy error semi-norms.

A number of observations should be made regarding the resulting data. In particular, it is worthwhile to note that part of the incurred solution error may be attributable to the inexact representation of the problem geometry, especially for the coarse meshes. This may in part explain why the observed convergence rates are lower at coarser levels of refinement, but approach the expected rates as the mesh is further refined.

h	4-node FEM	4-node PEM	8-node FEM	8-node PEM
1.2500	-	-	-	-
0.8006	0.3192	0.2714	0.3042	1.2675
0.4488	0.5195	0.6166	0.4228	1.1924
0.2371	0.6326	0.7303	0.7156	1.5031
0.1218	0.8542	0.8892	0.9205	1.9944
0.0617	0.9646	0.9716	0.9950	2.2488

Table 5.4. Computed H^1 energy error semi-norm convergence rates.

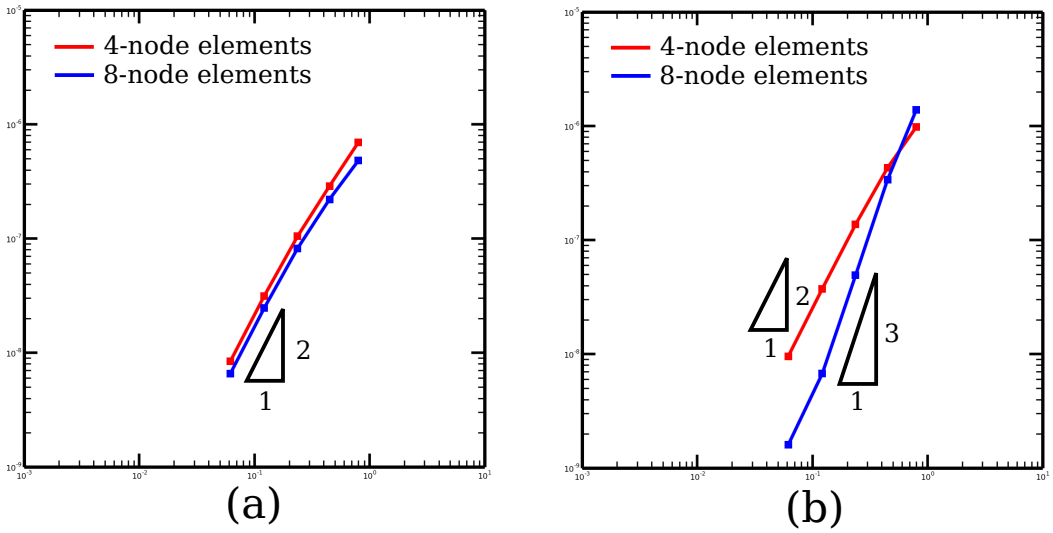

Figure 5.3. L^2 error convergence plots for (a) FEM and (b) PEM formulations.

Additionally, we remark that isoparametric serendipity quadrilateral elements converge at sub-optimal rates if the elements are distorted in a non-affine fashion (as is the case for our meshes). This is an altogether expected result, and has been discussed in references [2] and [1].

Conversely, we observe that the PEM quadrilateral elements converge at the optimal rates in both the L^2 and H^1 error norms, as we would hope.

Further work will seek to investigate the measured error and convergence rates of the PEM when the elements take on arbitrary shape, and for a variety of different formulations and penalization parameter settings.

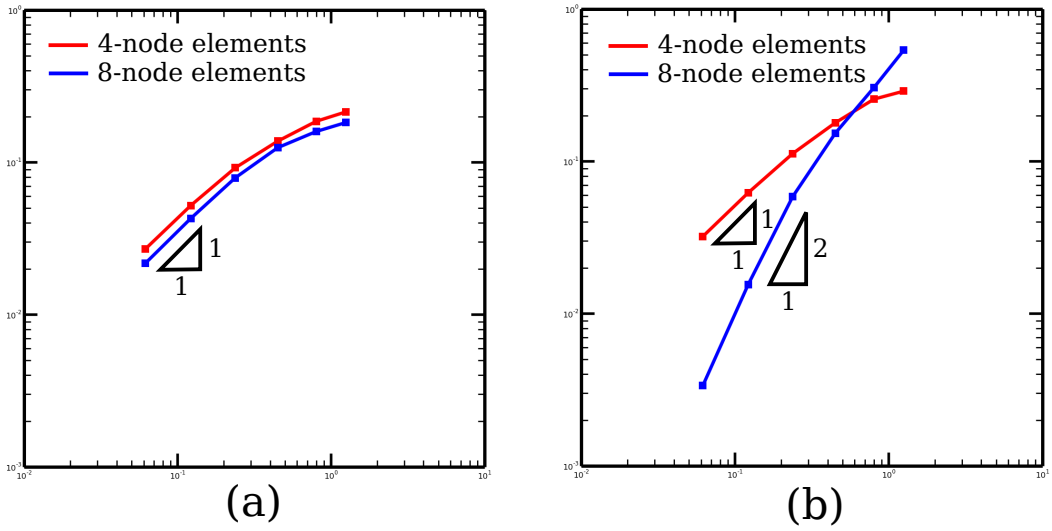

Figure 5.4. H^1 error convergence plots for (a) FEM and (b) PEM formulations.

5.2 Parameter Sensitivity Analysis

5.3 Computational Efficiency

5.3.1 Performance Comparison

5.4 Resistance to Locking Phenomena

Twisting Annulus

Consider an incompressible elastic annulus whose inner radius at $r = R_i$ is fixed, and whose outer radius $r = R_o$ rigidly rotates at an angular velocity of Φ. The radially symmetric displacement boundary conditions for this motion are described by

$$u_r(R_i, t) = u_r(R_o, t) = 0, \quad u_z(R_i, t) = u_z(R_o, t) = 0, \tag{5.6}$$

$$u_\theta(R_i, t) = 0, \quad u_\theta(R_o, t) = R_o \, \Phi \, t, \tag{5.7}$$

for all $t \geq 0$.

The elastic material is characterized by a linear hypoelastic material model of grade zero, obeying

$$\dot{\boldsymbol{\sigma}} = \mathbb{C} : \mathbf{D} + \mathbf{W}\boldsymbol{\sigma} - \boldsymbol{\sigma}\mathbf{W}, \tag{5.8}$$

Exact Solution

An exact solution for the aforementioned problem may be obtained by considering the stress divergence equations in cylindrical polar coordinates:

$$\nabla \cdot \boldsymbol{\sigma} = \left\{ \begin{array}{c} \frac{\partial \sigma_{rr}}{\partial r} + \frac{\sigma_{rr}}{r} + \frac{1}{r}\frac{\partial \sigma_{\theta r}}{\partial \theta} + \frac{\partial \sigma_{zr}}{\partial z} - \frac{\sigma_{\theta\theta}}{r} \\ \frac{1}{r}\frac{\partial \sigma_{\theta\theta}}{\partial \theta} + \frac{\partial \sigma_{r\theta}}{\partial r} + \frac{\sigma_{r\theta}}{r} + \frac{\sigma_{\theta r}}{r} + \frac{\partial \sigma_{z\theta}}{\partial z} \\ \frac{\partial \sigma_{zz}}{\partial z} + \frac{\partial \sigma_{rz}}{\partial r} + \frac{\sigma_{rz}}{r} + \frac{1}{r}\frac{\partial \sigma_{\theta z}}{\partial \theta} \end{array} \right\} = \mathbf{0}. \tag{5.9}$$

By the assumptions of plane strain and axisymmetry, we rationalize that $\boldsymbol{\sigma}(r)$ is a function of r, alone, and therefore,

$$\nabla \cdot \boldsymbol{\sigma} = \left\{ \begin{array}{c} \frac{\partial \sigma_{rr}}{\partial r} + \frac{\sigma_{rr} - \sigma_{\theta\theta}}{r} \\ \frac{\partial \sigma_{r\theta}}{\partial r} + \frac{2\sigma_{r\theta}}{r} \\ \frac{\partial \sigma_{rz}}{\partial r} + \frac{\sigma_{rz}}{r} \end{array} \right\} = \mathbf{0}. \tag{5.10}$$

Furthermore, by the assumptions of plane strain, we observe that $\sigma_{rz} = 0$ and $\sigma_{\theta z} = 0$. Additionally, if we impose the incompressibility condition $\nabla \cdot \mathbf{v} = \mathrm{tr}(\mathbf{D}) = 0$, we find that

$$\mathrm{tr}(\dot{\boldsymbol{\sigma}}) = 0 \;\Rightarrow\; \mathrm{tr}(\boldsymbol{\sigma}) = 0 \, \forall t. \tag{5.11}$$

The deformation necessitates that $\sigma_{zz} = 0$, and therefore $\sigma_{\theta\theta} = -\sigma_{rr}$. Consequently, we are left with 2 governing differential equations for σ_{rr} and $\sigma_{r\theta}$:

$$\frac{\partial \sigma_{rr}}{\partial r} + \frac{2\sigma_{rr}}{r} = 0, \quad \frac{\partial \sigma_{r\theta}}{\partial r} + \frac{2\sigma_{r\theta}}{r} = 0, \tag{5.12}$$

whose solutions are of the form

$$\sigma_{rr} = \frac{a}{r^2}, \quad \sigma_{r\theta} = \frac{b}{r^2}. \tag{5.13}$$

Consequently,

$$\left\{ \begin{array}{c} \sigma_{rr} \\ \sigma_{\theta\theta} \\ \sigma_{r\theta} \end{array} \right\} = r^{-2} \left\{ \begin{array}{c} +a \\ -a \\ b \end{array} \right\}. \tag{5.14}$$

Under the assumption of incompressibility, we may characterize the deformation via the velocity field $v_r = 0$, $v_z = 0$, and $v_\theta(r) = r\dot{\phi}(r)$, yielding the velocity gradient (in

cylindrical polar coordinates):

$$\mathbf{L} = \nabla \mathbf{v} = \begin{bmatrix} v_{r,r} & v_{r,\theta}/r - v_\theta/r & v_{r,z} \\ v_{\theta,r} & v_{\theta,\theta}/r + v_r/r & v_{\theta,z} \\ v_{z,r} & v_{z,\theta}/r & v_{z,z} \end{bmatrix} = \begin{bmatrix} 0 & -\dot{\phi} & 0 \\ \dot{\phi} + r\dot{\phi}_{,r} & 0 & 0 \\ 0 & 0 & 0 \end{bmatrix}, \tag{5.15}$$

and the corresponding rate of deformation and spin tensors:

$$\mathbf{D} = \frac{r\dot{\phi}_{,r}}{2} \begin{bmatrix} 0 & 1 & 0 \\ 1 & 0 & 0 \\ 0 & 0 & 0 \end{bmatrix}, \quad \mathbf{W} = \frac{2\dot{\phi} + r\dot{\phi}_{,r}}{2} \begin{bmatrix} 0 & -1 & 0 \\ 1 & 0 & 0 \\ 0 & 0 & 0 \end{bmatrix}. \tag{5.16}$$

The resulting stress rate equations are

$$\begin{Bmatrix} \dot{\sigma}_{rr} \\ \dot{\sigma}_{\theta\theta} \\ \dot{\sigma}_{r\theta} \end{Bmatrix} = \begin{Bmatrix} 0 \\ 0 \\ \mu r\dot{\phi}_{,r} \end{Bmatrix} + (2\dot{\phi} + r\dot{\phi}_{,r}) \begin{Bmatrix} -\sigma_{r\theta} \\ \sigma_{r\theta} \\ \sigma_{rr} \end{Bmatrix}, \tag{5.17}$$

or

$$\begin{Bmatrix} \dot{a} \\ \dot{b} \end{Bmatrix} = \begin{Bmatrix} 0 \\ \mu r^3 \dot{\phi}_{,r} \end{Bmatrix} + (2\dot{\phi} + r\dot{\phi}_{,r}) \begin{bmatrix} 0 & -1 \\ 1 & 0 \end{bmatrix} \begin{Bmatrix} a \\ b \end{Bmatrix}, \tag{5.18}$$

which must be valid $\forall r$, t. If we assume that $\dot{\phi} = f(r)$ is a function of r (and not of t), then we obtain the condition

$$3f_{,r} + rf_{,rr} = 0, \tag{5.19}$$

implying $f_{,r} = Br^{-3}$, and $\phi(r,t) = (A - Br^{-2}/2)t$, thus

$$\begin{Bmatrix} \dot{a} \\ \dot{b} \end{Bmatrix} = \begin{Bmatrix} 0 \\ \mu B \end{Bmatrix} + 2A \begin{bmatrix} 0 & -1 \\ 1 & 0 \end{bmatrix} \begin{Bmatrix} a \\ b \end{Bmatrix}, \tag{5.20}$$

and

$$a(t) = -\frac{\mu B}{2A} - C_2 \sin(2At) + C_1 \cos(2At), \tag{5.21}$$

$$b(t) = C_1 \sin(2At) + C_2 \cos(2At). \tag{5.22}$$

Imposing the initial conditions $a(0) = b(0) = 0$ results in:

$$a(t) = \frac{\mu B}{2A} \left[\cos(2At) - 1\right], \quad b(t) = \frac{\mu B}{2A} \sin(2At). \tag{5.23}$$

Imposing the boundary conditions $\phi(R_i, t) = 0\ \forall t$, $\phi(R_o, t) = \Phi\, t\ \forall t$ yields:

$$A = \frac{\Phi R_i^{-2}}{R_i^{-2} - R_o^{-2}}, \quad B = \frac{2\Phi}{R_i^{-2} - R_o^{-2}}. \tag{5.24}$$

The final analytical solution for the displacement and stress fields is presented below:

$$u_r = 0, \quad u_\theta = r\Phi \frac{R_i^{-2} - r^{-2}}{R_i^{-2} - R_o^{-2}} t, \quad u_z = 0, \tag{5.25}$$

$$\sigma_{rr} = -\sigma_{\theta\theta} = \mu \frac{r^{-2}}{R_i^{-2}} \left[\cos\left(2 \frac{\Phi R_i^{-2}}{R_i^{-2} - R_o^{-2}} t \right) - 1 \right], \tag{5.26}$$

$$\sigma_{r\theta} = \mu \frac{r^{-2}}{R_i^{-2}} \sin\left(2 \frac{\Phi R_i^{-2}}{R_i^{-2} - R_o^{-2}} t \right). \tag{5.27}$$

Chapter 6

Conclusions and Future Work

Evaluate the efficacy of the proposed formulations within the presented context. Assess whether there really is a silver bullet to the locking problem, or if we can expect for locking to be an inherrent issue with any numerical approximation method.

Describe the nature of future work that will be done in this area of research.

References

[1] D. N. Arnold, D. Boffi, and R. S. Falk. Approximation by quadrilateral finite elements. *Mathematics of Computation*, 71(239):909–922, 2002.

[2] D. N. Arnold, D. Boffi, R. S. Falk, and L. Gastaldi. Finite element approximation on quadrilateral meshes. *Communications in Numerical Methods in Engineering*, 17(11):805–812, 2001.

[3] Ivo Babuška. Error-bounds for finite element method. *Numerische Mathematik*, 16:322–333, 1971.

[4] Ivo Babuška and Manil Suri. Locking effects in the finite element approximation of elasticity problems. *Numerische Mathematik*, 62:439–463, 1992.

[5] Ivo Babuška and Manil Suri. On locking and robustness in the finite element method. *SIAM Journal on Numerical Analysis*, 29(5):1261–1293, 1992.

[6] F. Bassi, L. Botti, A. Colombo, D.A. Di Pietro, and P. Tesini. On the flexibility of agglomeration based physical space discontinuous galerkin discretizations. *Journal of Computational Physics*, 231(1):45 – 65, 2012.

[7] J. E. Bishop. A displacement-based finite element formulation for general polyhedra using harmonic shape functions. *International Journal for Numerical Methods in Engineering*, 97:1–31, 2014.

[8] Franco Brezzi. On the existence, uniqueness and approximation of saddle-point problems arising from lagrangian multipliers. *ESAIM: Mathematical Modelling and Numerical Analysis - Modlisation Mathmatique et Analyse Numrique*, 8:129–151, 1974.

[9] Jiun-Shyan Chen, Michael Hillman, and Marcus Rüter. An arbitrary order variationally consistent integration for galerkin meshfree methods. *International Journal for Numerical Methods in Engineering*, 95:387–418, 2013.

[10] H. Chi, L. Beirão da Veiga, and G. H. Paulino. Some basic formulations of the virtual element method (vem) for finite deformations. *Computer Methods in Applied Mechanics and Engineering*, 318:148–192, 2017.

[11] Heng Chi, Cameron Talischi, Oscar Lopez-Pamies, and Glaucio H. Paulino. A paradigm for higher-order polygonal elements in finite elasticity using a gradient correction scheme. *Computer Methods in Applied Mechanics and Engineering*, 306:216–251, 2016.

[12] Eric B. Chin, Jean B. Lasserre, and N. Sukumar. Numerical integration of homogeneous functions on convex and nonconvex polygons and polyhedra. *Computational Mechanics*, 56:967–981, 2015.

[13] Zhong ci Shi. The f-e-m-test for convergence of nonconforming finite elements. *Mathematics of Computation*, 49(180):391–405, 1987.

[14] M. Cicuttin, D.A. Di Pietro, and A. Ern. Implementation of discontinuous skeletal methods on arbitrary-dimensional, polytopal meshes using generic programming. *Journal of Computational and Applied Mathematics*, 2017.

[15] L. Beirão da Veiga, F. Brezzi, A. Cangiani, G. Manzini, L. D. Marini, and A. Russo. Basic principles of virtual element methods. *Computer Methods in Applied Mechanics and Engineering*, 23:199–214, 2013.

[16] L. Beirão da Veiga, C. Lovadina, and D. Mora. A virtual element method for elastic and inelastic problems on polytope meshes. *Computer Methods in Applied Mechanics and Engineering*, 295:327–346, 2015.

[17] E. A. de Souza Neto, D. Perić, M. Dukto, and D. R. J. Owen. Design of simple low order finite elements for large strain analysis of nearly incompressible solids. *International Journal of Solids and Structures*, 33:3277–3296, 1996.

[18] C. R. Dohrmann and M. M. Rashid. Polynomial approximation of shape function gradients from element geometries. *International Journal for Numerical Methods in Engineering*, 53:945–958, 2002.

[19] D. A. Dunavant. High degree efficient symmetrical gaussian quadrature rules for the triangle. *International Journal for Numerical Methods in Engineering*, 21(6):1129–1148, 1985.

[20] Mohamed S. Ebeida and Scott A. Mitchell. Uniform random voronoi meshes. *Proceedings of the 20th International Meshing Roundtable*, pages 273–290, 2011.

[21] Mohamed Salah Ebeida. Vorocrust v. 1.0, Jul 2017.

[22] Carlos A. Felippa. *Introduction to Finite Element Methods*. University of Colorado, Boulder, 2004.

[23] D. P. Flanagan and T. Belytschko. A uniform strain hexahedron and quadrilateral with orthogonal hourglass control. *International Journal for Numerical Methods in Engineering*, 17:679–706, 1981.

[24] Michael S. Floater. Mean value coordinates. *Computer Aided Geometric Design*, 20:19–27, 2003.

[25] Arun Gain, Cameron Talischi, and Glaucio H. Paulino. On the virtual element method for three-dimensional elasticity problems on arbitrary polyhedral meshes. *Computer Methods in Applied Mechanics and Engineering*, 282, 11 2013.

[26] Xifeng Gao, Wenzel Jakob, Marco Tarini, and Daniele Panozzo. Robust hex-dominant mesh generation using field-guided polyhedral agglomeration. *ACM Transactions on Graphics*, 36, 2017.

[27] William J. Gordon and James A. Wixom. Pseudo-harmonic interpolation on convex domains. *SIAM Journal on Numerical Analysis*, 11(5):909–933, 1974.

[28] Axel Grundmann and H. M. Möller. Invariant integration formulas for the n-simplex by combinatorial methods. *SIAM Journal on Numerical Analysis*, 15(2):282–290, 1978.

[29] Jan S. Hesthaven and Tim Warburton. *Nodal Discontinuous Galerkin Methods: Algorithms, Analysis, and Applications*. Springer Publishing Company, Incorporated, 1st edition, 2010.

[30] Thomas J. R. Hughes. *The Finite Element Method–Linear Static and Dynamic Finite Element Analysis*. Dover Publications, 2000.

[31] Pushkar Joshi, Mark Meyer, Tony DeRose, Brian Green, and Tom Sanocki. Harmonic coordinates for character articulation. *ACM Transactions on Graphics*, 26, 2007.

[32] Mika Juntunen and Rolf Stenberg. Nitsche's method for general boundary conditions. *Mechanics of Computation*, 78(267):1353–1374, 2009.

[33] Nam-Sua Lee and Klaus-Jürgen Bathe. Effects of element distortions on the performance of isoparametric elements. *International Journal for Numerical Methods in Engineering*, 36:3553–3576, 1993.

[34] Qiaoluan H. Li and Junping Wang. Weak galerkin finite element methods for parabolic equations. *Numerical Methods for Partial Differential Equations*, 29:2004–2024, 2013.

[35] Guang Lin, Jiangguo Liu, and Farrah Sadre-Marandi. A comparative study on the weak galerkin, discontinuous galerkin, and mixed finite element methods. *Journal of Computational and Applied Mathematics*, 273:346–362, 2015.

[36] Richard H. MacNeal. A theorem regarding the locking of tapered four-noded membrane elements. *International Journal for Numerical Methods in Engineering*, 24:1793–1799, 1987.

[37] Sebastian Martin, Peter Kaufmann, Mario Botsch, Martin Wicke, and Markus Gross. Polyhedral finite elements using harmonic basis functions. *Eurographics Symposium on Geometry Processing 2008*, 27(5), 2008.

[38] L. Mu, J. Wang, and Y. Wang. A computational study of the weak galerkin method for second-order elliptic equations. *Numerical Algorithms*, 63:753, 2013.

[39] L. Mu, J. Wang, and X. Ye. Weak galerkin finite element method for second-order elliptic problems on polytopal meshes. *International Journal of Numerical Analysis and Modeling*, 12:31–53, 2015.

[40] Lin Mu, Junping Wang, and Xiu Ye. A weak galerkin finite element method with polynomial reduction. *Journal of Computational and Applied Mathematics*, 285:45–58, 2015.

[41] Daniel Pantuso and Klaus-Jürgen Bathe. On the stability of mixed finite elements in large strain analysis of incompressible solids. *Finite Elements in Analysis and Design*, 28:83–104, 1997.

[42] M. M. Rashid. Incremental kinematics for finite element applications. *International Journal for Numerical Methods in Engineering*, 36:3937–3956, 1993.

[43] M. M. Rashid and P. M. Gullett. On a finite element method with variable element topology. *Computer Methods in Applied Mechanics and Engineering*, 190:1509–1527, 2000.

[44] M. M. Rashid and A. Sadri. The partitioned element method in computational solid mechanics. *Computer Methods in Applied Mechanics and Engineering*, 237–240:152–165, 2012.

[45] M. M. Rashid and M. Selimotić. A three-dimensional finite element method with arbitrary polyhedral elements. *International Journal for Numerical Methods in Engineering*, 67:226–252, 2006.

[46] J.-F. Remacle, J. Lambrechts, B. Seny, E. Marchandise, A. Johnen, and C. Geuzainet. Blossom-quad: a non-uniform quadrilateral mesh generator using a minimum cost perfect matching algorithm. *International Journal for Numerical Methods in Engineering*, 89:1102–1119, 2012.

[47] Béatrice Rivière. *Discontinuous Galerkin Methods for Solving Elliptic and Parabolic Equations: Theory and Implementation*. Society for Industrial and Applied Mathematics, 3600 Market Street, 6th Floor, Philadelphia, PA 19104-2688 USA, 2008.

[48] Mili Selimotić. *Polyhedral Finite-Element Approximants in 3D Solid Mechanics*. PhD thesis, University of California, Davis, 2008.

[49] J. C. Simo and F. Armero. Geometrically non-linear enhanced strain mixed methods and the method of incompatible modes. *International Journal for Numerical Methods in Engineering*, 33:1413–1449, 1992.

[50] J. C. Simo, F. Armero, and R. L. Taylor. Improved versions of assumed enhanced strain tri-linear elements for 3d finite deformation problems. *Computer Methods in Applied Mechanics and Engineering*, 110:359–386, 1993.

[51] J. C. Simo and M. S. Rifai. A class of mixed assumed strain methods and the method of incompatible modes. *International Journal for Numerical Methods in Engineering*, 29:1595–1638, 1990.

[52] Friedrich Stummel. The generalized patch test. *SIAM Journal on Numerical Analysis*, 16(3):449–471, 1979.

[53] N. Sukumar. Construction of polygonal interpolants: a maximum entropy approach. *International Journal for Numerical Methods in Engineering*, 61:2159–2181, 2004.

[54] Manil Suri. On the robustness of the h- and p-versions of the finite-element method. *Journal of Computational and Applied Mathematics*, 35:303–310, 1991.

[55] Theodore Sussman and Klaus-Jürgen Bathe. Spurious modes in geometrically nonlinear small displacement finite elements with incompatible modes. *Computers & Structures*, 140:14–22, 2014.

[56] Cameron Talischi and Glaucio H. Paulino. Addressing integration error for polygonal finite elements through polynomial projections: A patch test connection. *Mathematical Models and Methods in Applied Sciences*, 24:1701–1727, 2014.

[57] Cameron Talischi, Anderson Pereira, Ivan F. M. Menezes, and Glaucio H. Paulino. Gradient correction for polygonal and polyhedral finite elements. *International Journal for Numerical Methods in Engineering*, 102:728–747, 2015.

[58] Eugene L. Wachspress. *A Rational Finite Element Basis*. Academic Press, 1975.

[59] J. Wang and X. Ye. A weak galerkin finite element method for second-order elliptic problems. *Journal of Computational and Applied Mathematics*, 241:103–115, 2013.

[60] X. Wang, N.S. Malluwawadu, F. Gao, and T.C. McMillan. A modified weak galerkin finite element method. *Journal of Computational and Applied Mathematics*, 271:319–329, 2014.

[61] Wikiversity. Introduction to elasticity/plate with hole in tension, 2017.

[62] Robert Winkler. Comments on membrane locking. *Proceedings in Applied Mathematics and Mechanics*, 10:229–230, 2010.

Brian Doran Giffin
December 2017
Civil and Environmental Engineering

A Polytopal Element Framework for Improved Solution Accuracy and Robustness

Abstract

The abstract that is submitted to UMI must be formatted as shown in the example here. The body of the abstract cannot exceed 350 words. It should be in typewritten form, double-spaced, and on bond paper. It is important to write an abstract that gives a clear description of the content and major divisions of the dissertation, since UMI will publish the abstract exactly as submitted. Students completing their requirements under Plan A should provide extra copies of the typed summary for use by the dissertation committee during the examination.

The abstract that is submitted to UMI must be formatted as shown in the example here. The body of the abstract cannot exceed 350 words. It should be in typewritten form, double-spaced, and on bond paper. It is important to write an abstract that gives a clear description of the content and major divisions of the dissertation, since UMI will publish the abstract exactly as submitted. Students completing their requirements under Plan A should provide extra copies of the typed summary for use by the dissertation committee during the examination.

The abstract that is submitted to UMI must be formatted as shown in the example here. The body of the abstract cannot exceed 350 words. It should be in typewritten form, double-spaced, and on bond paper. It is important to write an abstract that gives a clear description of the content and major divisions of the dissertation, since UMI will publish the abstract exactly as submitted. Students completing their requirements under Plan A should provide extra copies of the typed summary for use by the dissertation committee during the examination.

The abstract that is submitted to UMI must be formatted as shown in the example here. The body of the abstract cannot exceed 350 words. It should be in typewritten form,

form, double-spaced, and on bond paper. It is important to write an abstract that gives a clear description of the content and major divisions of the dissertation, since UMI will publish the abstract exactly as submitted. Students completing their requirements under Plan A should provide extra copies of the typed summary for use by the dissertation committee during the examination.